Supplementary Information for

Two-Coordinated Au(I) Complex Photoredoxcatalyst: Highly Efficient Catalysis in C–C Cross-coupling Reactions and the Underlying Mechanism

Byung Hak Jhun[1], Jihoon Jang,[2] Shinae Lee,[1] Eun Jin Cho,[2*] and Youngmin You[1*]

[1]*Department of Chemical and Biomolecular Engineering, Yonsei University, Seoul 03722, Republic of Korea.*

[2]*Department of Chemistry, Chung-Ang University, Seoul 06974, Republic of Korea.*

CONTENTS

Supplementary Methods

General procedures. Commercially available chemicals, including substrates and anhydrous dimethyl sulfoxide were purchased from Sigma-Aldrich, Thermo Fisher Scientific, or Tokyo Chemical Industry and used without further purification. 2-Chloro-5-(trifluoromethyl)pyridine (>97%), 3,4-dichlorobenzotrifluoride (97%), methyl 4-bromobenzoate (99%), methyl 5-bromo-2-iodobenzoate (97%), 3,5-bis(trifluoromethyl)bromobenzene (99%), bromopentafluorobenzene (99%), *N*-methylpyrrole (99%), *N*,*N*,*N*′,*N*′-tetramethylethylenediamine (TMEDA, 99%), potassium carbonate (99%), potassium phosphate tribasic (≥98%), dimethyl sulfoxide (DMSO, ≥99.9%), *N*,*N*-dimethylacetamide (DMA, 99.8%), tetrahydrofuran (THF, ≥99.9%), dichloromethane (DCM, ≥99.9%), and acetonitrile (99.8%), were purchased from Sigma Aldrich. 2-Chloroquinoline (99%), 1-chloroisoquinoline (95%), 4-bromoacetophenone (98%), 4-bromobenzaldehyde (99%), 2-bromopyridine (99%), 4-bromobenzotrifluoride (>98%), 4-iodobenzotrifluoride (98%), 1-methylindole (98%), 3-methylindole (99%), triethylamine (99%), 1,8-diazabicyclo[5,4,0]undec-7-ene (99%), sodium acetate (99%), potassium acetate (99%), and trifluoroethanol (TFE, 99+%) were purchased from Alfa Aesar. 2-Chloronaphthalene (>98%), 1-bromo-4-iodobenzene (>98%), *N*,*N*-diisopropylethylamine (DIPEA, >99%), were purchased from Tokyo Chemical Industry. 3-Bromoquinoline (98%), 8-bromoquinoline (98%), and 4-bromoisoquinoline (97%) were purchased from Combi-blocks. 4-Chlorobenzonitrile (99%) was purchased from Acros Organics. Sodium bicarbonate (>99%) was purchased from Duksan General Science. The synthetic procedures of the Au(I) complexes, except for [Au(^{Dipp}I)(Cz)], were reported in our previous study.[1]

Steady-State UV–Vis Absorption Measurements. UV−Vis absorption spectra were collected on an Agilent, Cary 300 spectrophotometer at 298 K. Sample solutions were prepared prior to measurements at a concentration of 50 μM [Au(BZI)(TMCz)] dissolved in Ar-saturated DMSO and toluene, unless otherwise stated. The solution was delivered into a quartz cell (Hellma, beam path length = 1.0 cm).

Steady-State Photoluminescence Measurements. Photoluminescence spectra were obtained at 298 K using a Photon Technology International, Quanta Master 400 scanning spectrofluorometer. The solutions used for the steady-state UV−Vis absorption studies were also used for the photoluminescence measurements. The excitation wavelength for the solution of [Au(BZI)(TMCz)] were 380 nm, unless otherwise stated. All the solutions were deaerated by bubbling Ar for 10 min prior to the measurements. A quartz cell (Hellma, beam path length = 1.0 cm) was used for solution samples.

Determination of Photoluminescence Lifetime. Photoluminescence decay traces were acquired

on the basis of time-correlated single-photon counting (TCSPC) techniques, using a PicoQuant, FluoTime 200 instrument after 377 nm pulsed laser excitation (pulse duration = 25 ps). A pico-second pulsed diode laser that produced 377 nm (PicoQuant, LDH375) was driven by a PDL800-D driver (PicoQuant). Transient photon signals were collected at the peak emission wavelength for [Au(BZI)(TMCz)] through an automated motorized monochromator. The photon acquisition was terminated when the accumulated photon count reached 10^4. Photoluminescence decay traces were fitted to a mono- or bi-exponential decay models embedded in the OriginLab, OriginPro 2022 software.

Determination of Relative Photoluminescence Quantum Yield. The photoluminescence quantum yield (Φ) was determined for 50 μM [Au(BZI)(TMCz)] dissolved in Ar-saturated DMSO and toluene. The Φ was calculated using the equation $\Phi = \Phi_{ref} \times (I/I_{ref}) \times (A_{ref}/A) \times (n/n_{ref})^2$, where A, I, and n are the absorbance at the excitation wavelength, the integrated photoluminescence intensity, and the refractive index of the solvent, respectively. 9,10-Diphenylanthracene (Φ_{ref} = 1.00, toluene; λ_{ex} = 366 nm) was used as the reference material.[2] (Ref: *Photochem*. **1974**, *3*, 315-320) Photoluminescence spectra were collected at 298 K in the emission range 400–740 nm and were integrated using the OriginLab, OriginPro 2022 software.

Photoluminescence Quenching Experiments. Photoluminescence spectra were obtained at 298 K using a Photon Technology International, Quanta Master 400 scanning spectrofluorometer. Stock solutions of 50 μM [Au(BZI)(TMCz)] and 500 mM and 5 M **1a** were prepared in DMSO. 3.0 mL of [Au(BZI)(TMCz)] solution was added into a quartz cell (Hellma, beam path length = 1.0 cm). Photoluminescence spectra of the [Au(BZI)(TMCz)] solution, which had been previously saturated with Ar, were taken (λ_{ex} = 380 nm) with the continuous addition of 3 μL of 500 μM and 5 mM **1a**. The final concentration of 1a was 100 mM.

Electrochemical Characterization. Cyclic and differential pulse voltammetry experiments were conducted using a CH Instruments, CHI630 B potentiostat with a three-electrode cell assembly. A Pt wire and a glassy carbon were used as the counter and working electrodes, respectively. An $Ag/AgNO_3$ couple was used as the pseudo-reference electrode. Measurements were carried out in Ar-saturated DMSO (3.0 mL) with 0.10 M $TBAPF_6$ as the supporting electrolyte at scan rates of 100 mV s^{-1} (cyclic voltammetry) and 4.0 mV s^{-1} (differential pulse voltammetry). A ferrocenium/ferrocene couple was employed as the external reference. The excited-state oxidation (E^*_{ox}) potentials were determined using the following relationship

$$E^*_{ox} = E_{ox} - \Delta E_g$$

In this equation, ΔE_g was determined from the onset wavelength of photoluminescence spectrum: 2.72 eV.

Determination of Photochemical Quantum Yields (PCQYs). The quantum yield for C–C cross coupling was determined by conducting standard ferrioxalate actinometry following the method reported before.[3] A 6 mM $K_3[Fe(C_2O_4)_3]$ solution as chemical actinometer prepared and 1 mL of solution was transferred to the same glassware used in the photoreaction (glass tube having diameter of 1.5 cm), and the solution was photoirradiated with a beam of photoreaction at 405 nm for 20 s. The same volume of 1 wt% 1,10-phenanthroline in sodium acetate buffer solution was added and stored in the dark for 1 h. The absorbance changes at 510 nm was measured by UV–Vis spectrophotometer (Agilent, Cary 300); inserting the value to the following equation returned light intensities 8.31×10^9 einstein s^{-1} at 405 nm:

light intensity (I_0, einstein s^{-1}) = (ΔAbs(510 nm) × V) / (Φ × 11050 M^{-1} cm^{-1} × Δt)

where, ΔAbs(510 nm), V, Φ, and Δt are the absorbance change at 510 nm, volume (L), quantum yield (1.15) of the ferrioxalate actinometer at 405 nm, and photoirradiation time (s), respectively. Finally, the reaction yield for C–C cross coupling with the reaction condition utilizing 0.1 mol% [Au(BZI)(TMCz)] as photoredoxcatalyst was quantified with GC-MS, and inserted into following equation to afford PCQY:

$$\mathrm{PCQY} = \frac{[\mathrm{product}] \times V}{I_0 \times \Delta t}$$

where, [product] is the molar concentration of the products calculated from GC-MS, Δt (s) is the photoirradiated time, V is the volume of the solution (L), and I_0 is the light intensity obtained by actinometry described above.

Spectroelectrochemical Measurements. UV–vis–NIR absorption spectra of the radical species were obtained on an Agilent, Cary 5000 spectrophotometer with applying the anodic potentials (–0.45 V vs $Ag/AgNO_3$) for [Au(BZI)(TMCz)], using the amperometric I–t curve method. A blank spectrum was taken for a 0.10 M NBu_4PF_6 solution (DMSO) in a spectroelectrochemical cell (path length = 0.5 mm) equipped with a Pt mesh working electrode, a Pt wire counter electrode, and an $Ag/AgNO_3$ pseudo reference electrode. 500 μL of a 2.0 mM sample solution was delivered into the spectroelectrochemical cell for the measurement.

Quantum Chemical Calculations. Geometry optimization was performed using the Becke's three-parameter exchange-correlation functional (CAM-B3LYP) exchange correlation functional, the "double-ξ" quality LANL2DZ basis set for the Au atom, and the 6–311+G(d) basis set for all the other atoms using the Gaussian 09 program. A pseudo potential (LANL2DZ) was applied to replace the inner core electrons of the Au(I) atom, leaving the outer core electrons and the valence electrons. Time-dependent density functional theory (TD−DFT) calculations were carried out for the optimized geometries using the same functional and basis sets.

Supplementary Table 1. Chemical structures, photoexcitation wavelengths (λ_{ex}s), excited-state lifetime (τ_{obs}), and excited-state oxidation potentials (E^*_{ox}s) of reported photoredoxcatalysts for organic transformations

	structure	condition	λ_{ex} (nm)	τ_{obs} (ns)	E^*_{ox} (V vs SCE)	Ref.
1	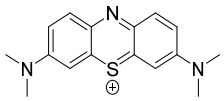	CH_3CN	650	1	–0.73	4
2	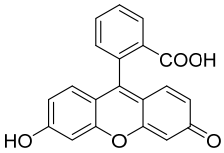	CH_3OH	437	4.2	–1.55	4
3	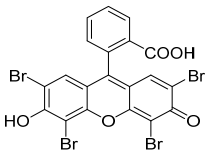	CH_3OH	520	2.1	–1.58	4
4	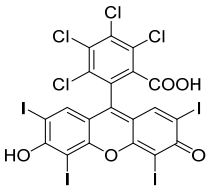	CH_3OH	549	0.50	–1.33	4
5	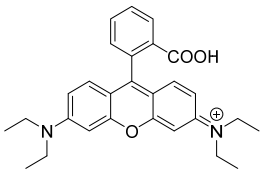	CH_3OH	550	2.45	–1.31	4
6	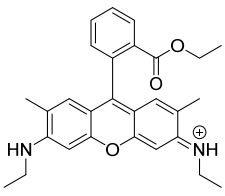	CH_3CN	530	4.13	–1.09	5

7	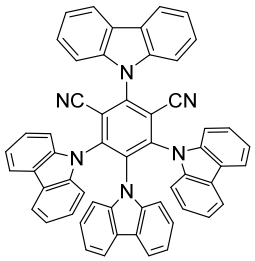 (CH3CN)	CH3CN	400	12.7	–1.18	6
8	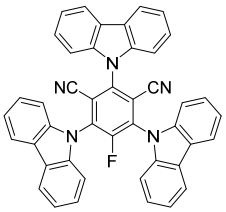	CH3CN	400	4.2	–1.38	6
9	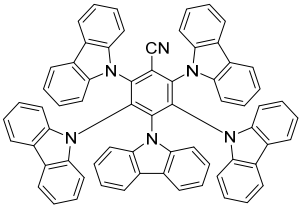	CH3CN	400	16.3	–1.42	6
10	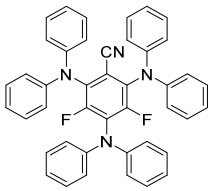	CH2Cl2	400	4.2	–1.60	6
11	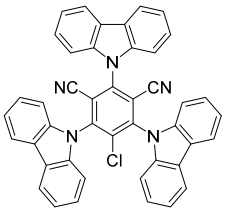	CH3CN	400	6.9	–0.93	6
12	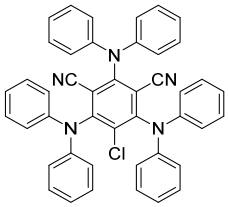	CH3CN	400	11.5	–1.34	6

13	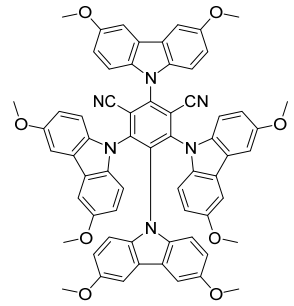	(CH_3CN:CH_2Cl_2 = 5:1, v/v)	450	N.R.	–1.50	6
14	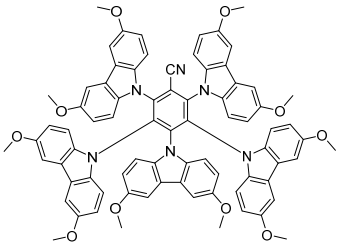	CH_2Cl_2	400	N.R.	–1.79	6
15	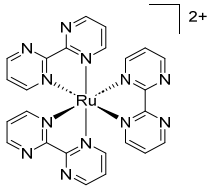	CH_3CN	454	131	–0.21	7
16	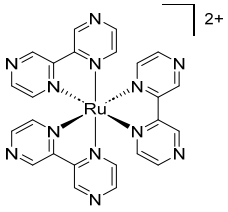	CH_3CN	443	740	–0.26	8
17	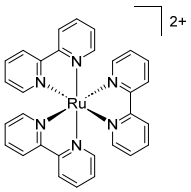	CH_3CN	452	1100	–0.81	9
18	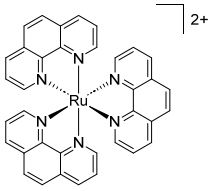	CH_3CN	422	500	–0.87	10

19	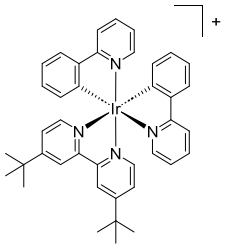	CH_3CN	455	557	–0.96	11
20	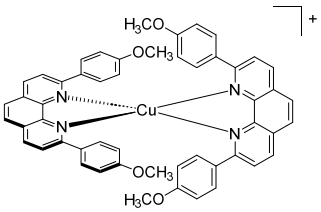	CH_3CN	470	270	–1.43	12
21	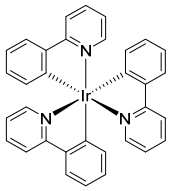	CH_3CN	455	1900	–1.73	13
22	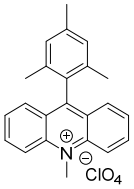	CH_3CN	455	6.4	–0.57	14, 15
23	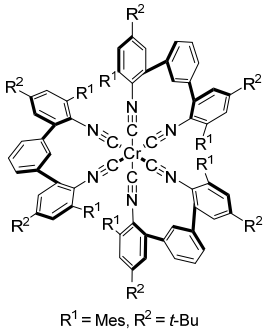 R^1 = Mes, R^2 = *t*-Bu	cyclohexane	623	31	–2.1	16

24	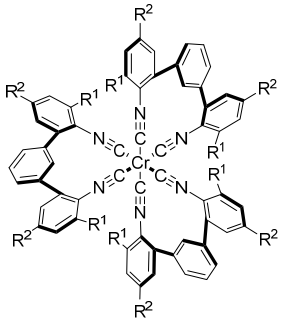 R^1 = *t*-Bu, R^2 = pyrenyl	cyclohexane	623	47	–2.0	16
25	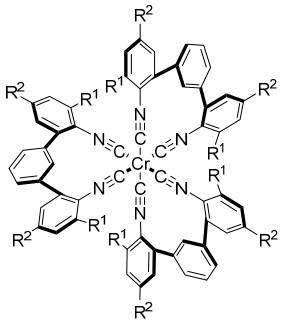 R^1, R^2 = *t*-Bu	THF	623	2.2	–1.9	16
26	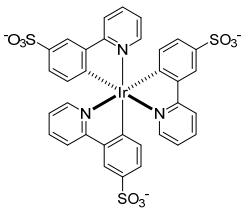	water	447	700	–1.89	17
27	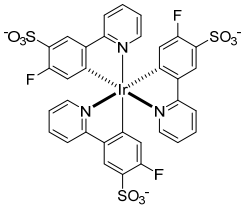	water containing 50 mM NaOH	447	2165	–1.85	18
28	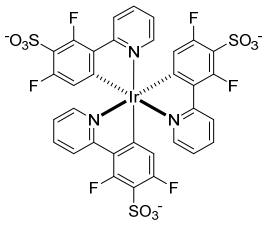	water containing 50 mM NaOH	447	2110	–1.76	18

29	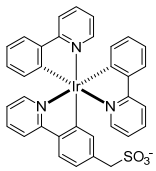	water containing 50 mM NaOH	447	1560	–1.94	18
30	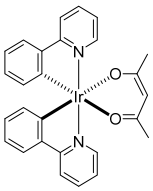	CH_2Cl_2	N.R.	1600	–1.35[a]	19
31	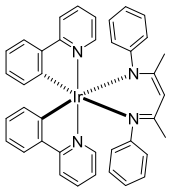	THF	420	N.R.	–1.85[a]	20
32	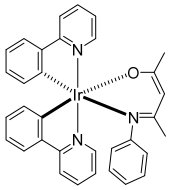	THF	420	N.R.	–1.65[a]	20
33	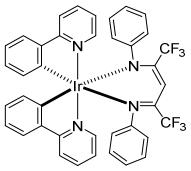	THF	420	N.R.	–1.55[a]	20
34	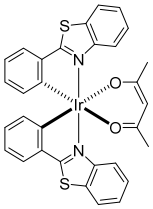	CH_2Cl_2	N.R.	1800	–1.05[a]	20
35	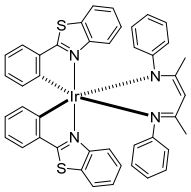	THF	420	N.R.	–1.55[a]	20

36	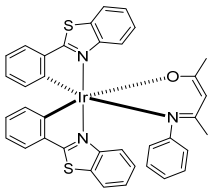	THF	420	N.R.	–1.35[a]	20
37	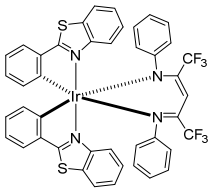	THF	420	N.R.	–1.25[a]	20
38	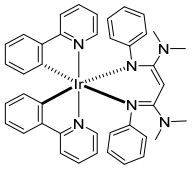	CH_3CN	420	750	–1.72[b]	21, 22
39	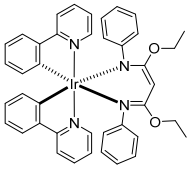	CH_3CN	420	2000	–1.62[b]	21
40	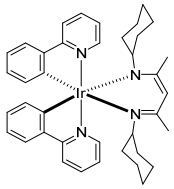	CH_3CN	520	350	–2.02[b]	22
41	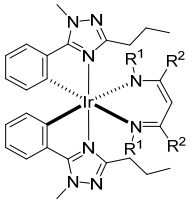 R^1 = Ph, R^2 = NMe_2	CH_3CN	465	130	–1.97[b,e]	23

42	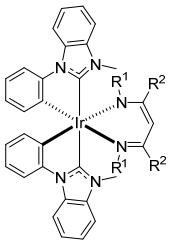	CH_3CN	465	850	–1.97[b,e]	23
43	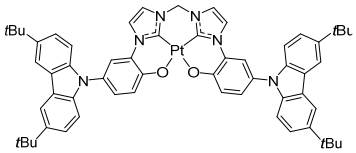	DMF		6700	–2.16[c]	24
44	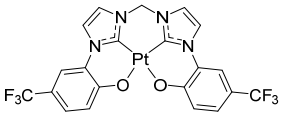	DMF		160	–2.16[c]	24
45	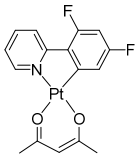	CH_3CN	450	382	–2.11	25
46	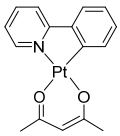	CH_3CN	450	2210	–2.07	25
47	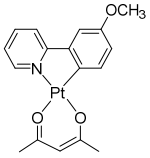	CH_3CN	450	11600	–1.93	25
48	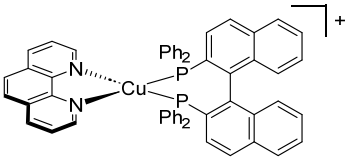	CH_3CN	450	3.10	–1.60[b]	26
49	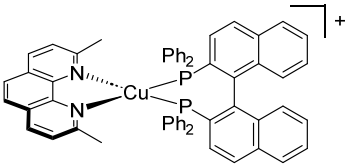	CH_3CN	450	2188	–1.64[b]	26

50	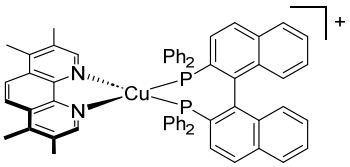	CH_3CN	450	4.00	–1.52[b]	26
51	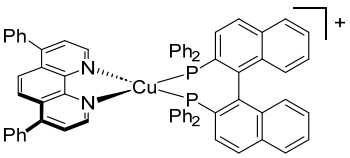	CH_3CN	450	2.64	–1.55[b]	26
52	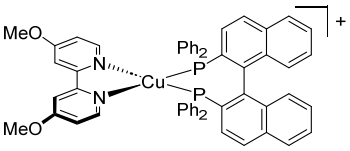	CH_3CN	450	2.19	–1.45[b]	26
53	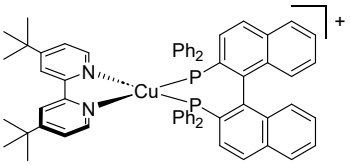	CH_3CN	450	2.78	–1.47[b]	26
54	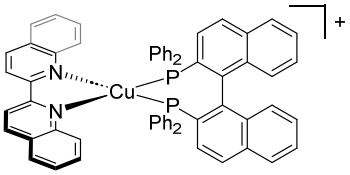	CH_3CN	450	4.00	–1.87[b]	26
55	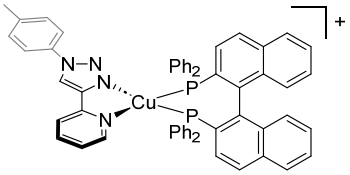	CH_3CN	450	2.40	–1.67[b]	26
56	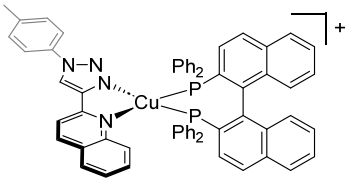	CH_3CN	450	3.11	–1.68[b]	26
57	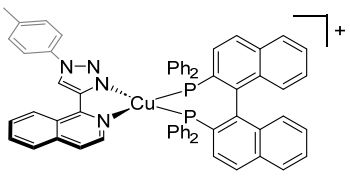	CH_3CN	450	3.58	–1.72[b]	26

58	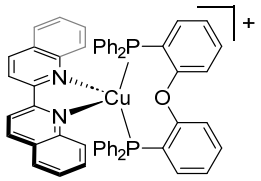	CH_3CN	450	274.7	–1.27[b]	26
59	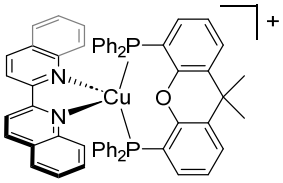	CH_3CN	450	393.7	–0.76[b]	26
60	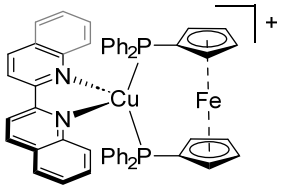	CH_3CN	450	2.70	–1.38[b]	26
61	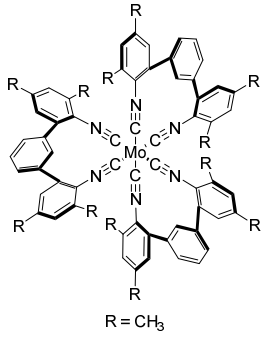	THF	455	74	–2.2	27, 28
62	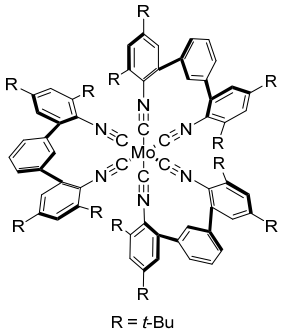	THF	470	1103	–2.3	28
63	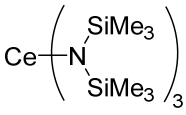	CH_2Cl_2	420	24	–1.71[d]	29

64	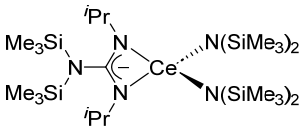	CH_2Cl_2	420	65	–1.83[d]	29
65	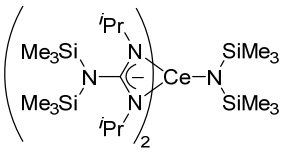	CH_2Cl_2	420	117	–2.12[d]	29
66	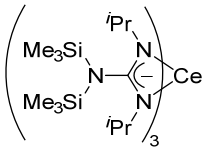	CH_2Cl_2	420	83	–2.45[d]	29
67	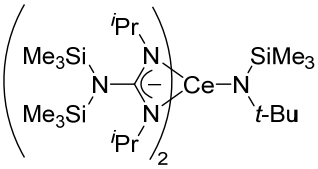	CH_2Cl_2	420	221	–2.13[d]	30
68	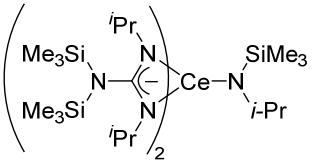	CH_2Cl_2	420	158	–2.13[d]	30
69	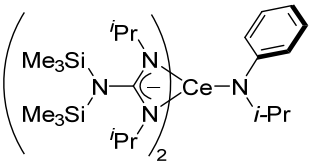	CH_2Cl_2	420	41	–2.43[d]	30
70	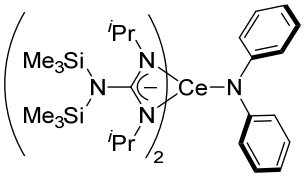	CH_2Cl_2	420	43	–2.43[d]	30
71	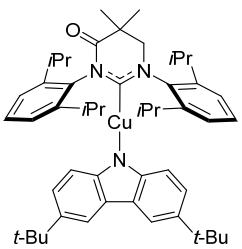	THF	355	350	–1.88[a]	31

72	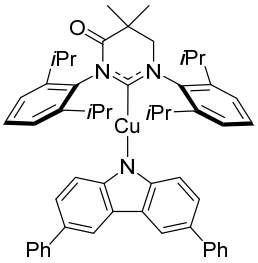	THF	355	460	–1.90[a]	31
73	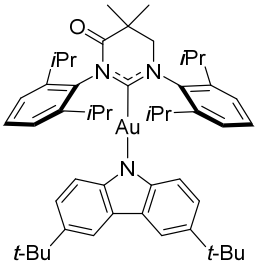	THF	355	250	–1.83[a]	31
74	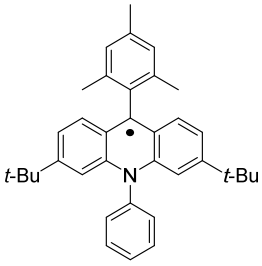	CH_3CN	390	<0.1	–3.36	32
75	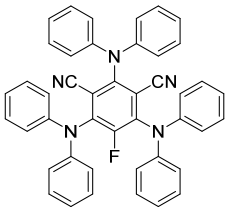	CH_3CN	455	4.2	–1.38	6, 33, 34
76	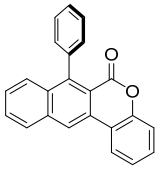	CH_3CN	421	1.44	–1.27	35
77	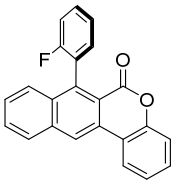	CH_3CN	421	2.07	–1.34	35

78	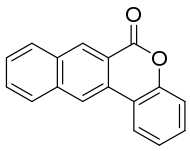	CH_3CN	411	3.86	–1.42	35
79	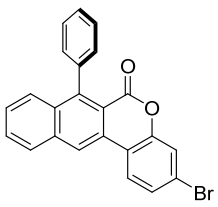	CH_3CN	421	1.49	–1.38	35
80	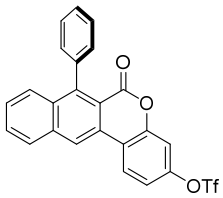	CH_3CN	413	0.81	–1.34	35
81	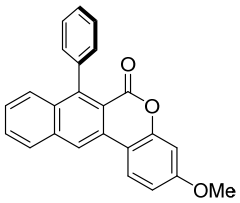	CH_3CN	462	7.78	–1.50	35
82	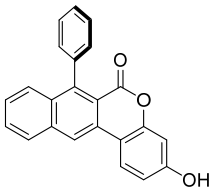	CH_3CN	461	8.50	–1.45	35
83	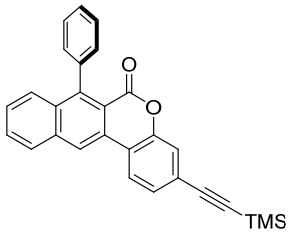	CH_3CN	426	2.53	–1.40	35

84	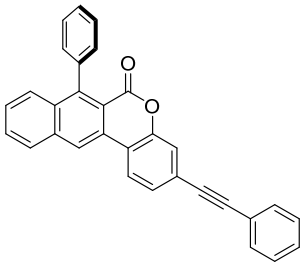	CH_3CN	434	3.34	–1.48	35
85	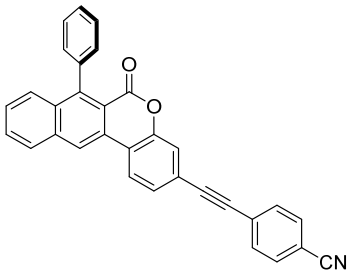	CH_3CN	427	3.05	–1.45	35
86	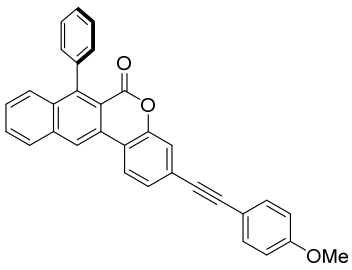	CH_3CN	449	4.21	–1.64	35
87	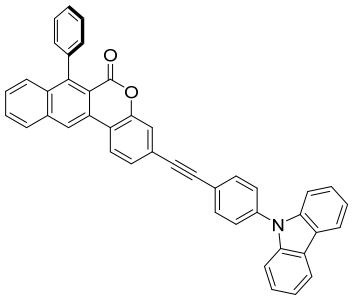	CH_3CN	459	2.49	–1.77	35
88	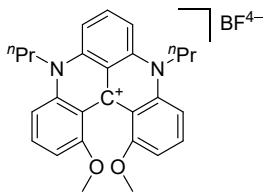	CH_3CN	616	5.50	–0.61	36

89	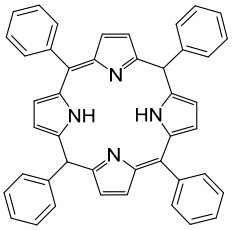	CH_3CN	417	N.R.	–0.59	37
90	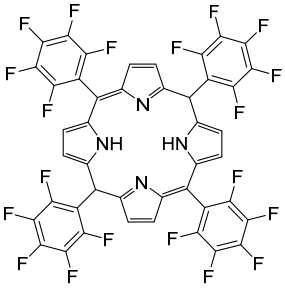	CH_3CN	412	N.R.	–0.11	37
91	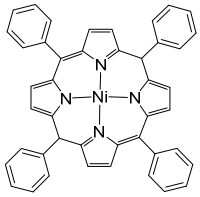	DMF	390	12900	–1.57	38
92	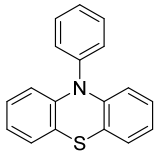	DMF	320	4.5	–2.03	39
93	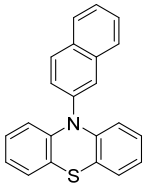	DMF	315	7.6	–1.71	39
94	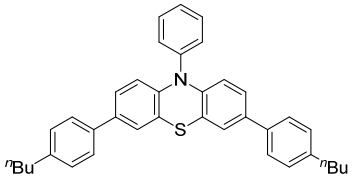	DMF	350	5.5	–1.93	39

95	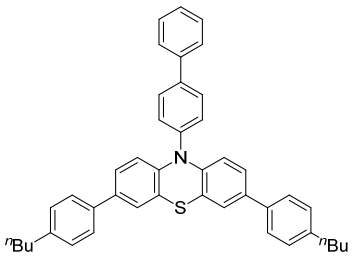	DMF	345	4.7	–1.94	39
96	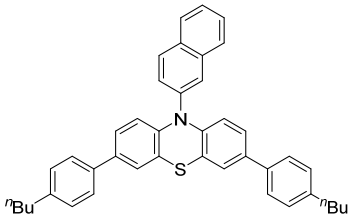	DMF	350	5.1	–1.92	39
97	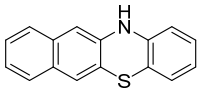	CH_3CN	371	N.R.	–2.24	40
98	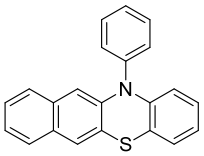	CH_3CN	376	N.R.	–2.08	40
99	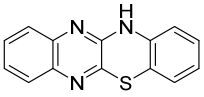	CH_3CN	420	N.R.	–1.60	40
100	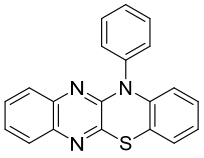	CH_3CN	412	N.R.	–1.39	40
101	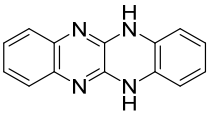	CH_3CN	414	N.R.	–2.31	40
102	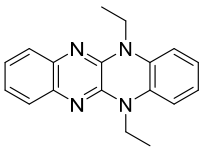	CH_3CN	412	N.R.	–2.01	40

103	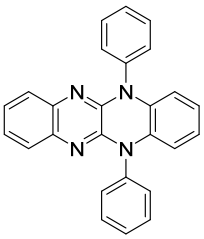	CH_3CN	408	N.R.	–1.89	40
104	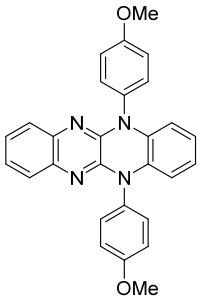	CH_3CN	410	N.R.	–1.91	40
105	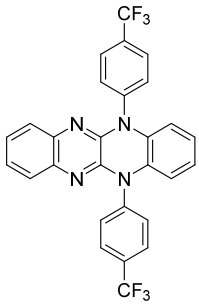	CH_3CN	408	N.R.	–1.79	40
106	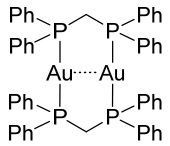	CH_3CN	324	510	–1.63	41, 42
107	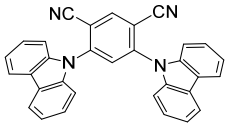	CH_3CN	362	N.R.	–1.41	43
108	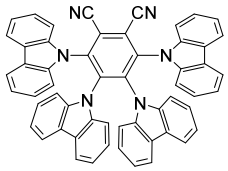	CH_3CN	435	N.R.	–1.06	43,44

109	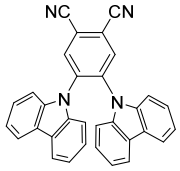	CH_3CN	365	N.R.	–1.30	43,44
110	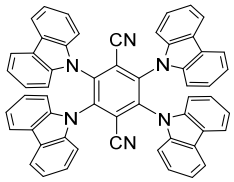	CH_3CN	463	N.R.	–0.99	43,44
111	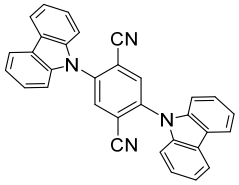	CH_3CN	430	N.R.	–1.24	43
112	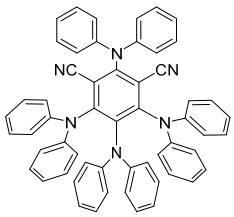	CH_3CN	425	N.R.	–1.28	43
113	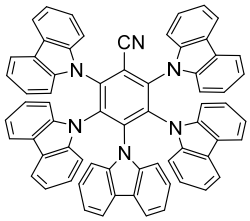	CH_3CN	400	N.R.	–1.42	45
114	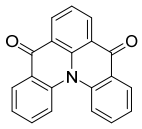	CH_3CN	440	8.2	–1.16	46
115	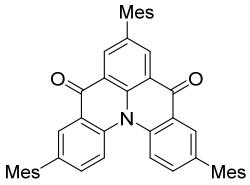	CH_3CN	440	N.R.	–1.05	46
116	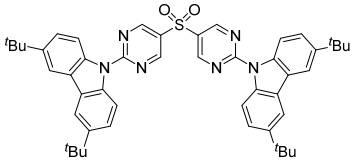	CH_2Cl_2	390	3392	–1.44	47

117	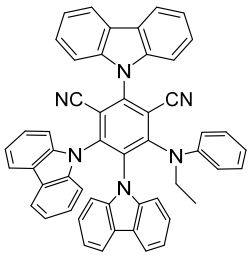	CH_2Cl_2	456	N.R.	–1.49	48
118	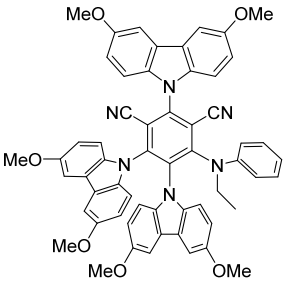	CH_2Cl_2	456	N.R.	–1.49	48
119	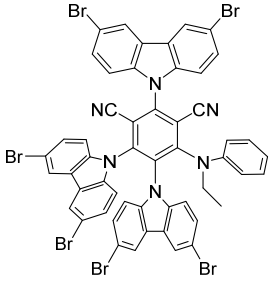	CH_2Cl_2	456	N.R.	–1.62	48
120	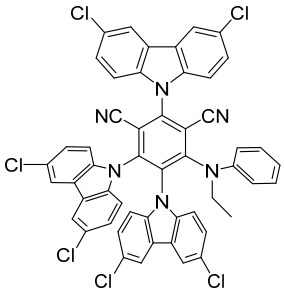	CH_2Cl_2	456	N.R.	–1.62	48
121	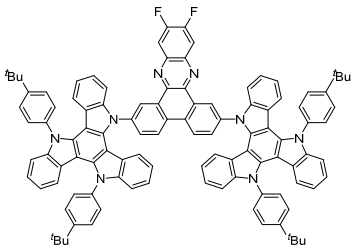	CH_2Cl_2	394	40	–1.44	49

122	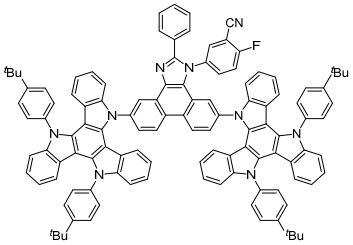	CH_2Cl_2	394	14	–1.48	49

[a–d]Potential originally reported as V vs Fc^+/Fc is converted to V vs SCE by adding 0.547 (THF),[a] 0.385 (CH_3CN),[b] 0.470 (DMF),[c] and 0.475 (CH_2Cl_2)[d] according to the previous report.[50] [e]Overestimated E^*_{ox} value is corrected using the bandgap energy energy obtained from onset wavelength of the photoluminescence spectrum.

Supplementary Table 2. Oxidation potentials of chemical reducing agents

	structure	condition	E_{ox} (V vs SCE)	Ref.
1	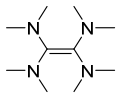	DMF	–0.64[a]	51
2	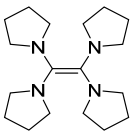	DMF	–0.85[a]	51
3	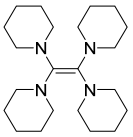	DMF	–0.59[a]	51
4	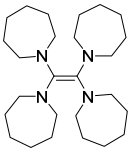	DMF	–0.62[a]	51
5	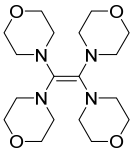	DMF	–0.38[a]	51
6	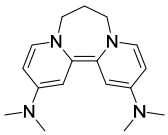	DMF	–1.22[a]	52
7	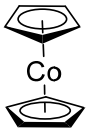	CH_2Cl_2	–0.86[b]	53
8	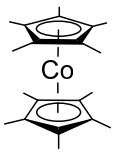	CH_3CN	–1.53	50
9	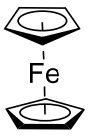	CH_3CN	0.38	50

10	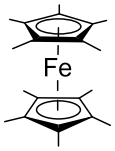	CH_3CN	–0.13	50
11	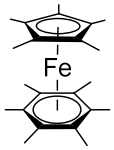	CH_3CN	–1.87	50
12	N_2H_4	DMSO	0.02[c]	53
13	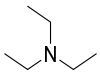	CH_3CN	0.9[d]	53
14	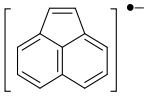	THF	–1.71[e]	53
15	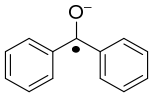	THF	–1.72[e]	53
16	Li	NH_3	–2.49[f]	53
17	Li(Hg)	H_2O	–2.45[f]	53
18	K	NH_3	–2.23[f]	53
19	Na(Hg)	Nonaqueous	–2.21[f]	53
20	Na	NH_3	–2.10[f]	53
21	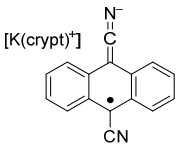	CH_3CN	–1.0	54
22	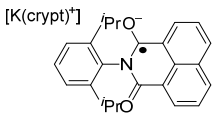	CH_3CN	–1.3	54

[a–f]Potential values referenced to the Fc^+/Fc couple were converted to SCE by adding 0.470 (DMF),[a] 0.475 (CH_2Cl_2),[b] 0.435 (DMSO),[c] 0.385 (CH_3CN),[d] 0.547 (THF),[e] and –0.160 (H_2O),[f] based on the previous report.[50,53]

Supplementary Table 3. Photophysical and electrochemical parameters of [Au(BZI)(TMCz)]

solvent	λ_{abs} (nm)[a]	λ_{em} (nm)[b]	Φ_{PL} (%)[c]	τ_{obs} (ns)[d]	k_r (10^5 s^{-1})[e]	k_{nr} (10^7 s^{-1})[f]	E_{ox} (V vs SCE)[g]	E_{red} (V vs SCE)[h]	E_{ox}* (V vs SCE)[i]	E_{red} (V vs SCE)[j]
toluene	407 ($\varepsilon = 0.94 \times 10^4$ M^{-1} cm^{-1})	515	11	207	5.3	0.4				
DMSO	380 ($\varepsilon = 1.5 \times 10^4$ M^{-1} cm^{-1}	540	1.8	45	4.0	2.2	0.56	–2.26	–2.16	0.46

[a]Absorption peak wavelength. [b]Emission peak wavelength. [c]Photoluminescence quantum yield determined relatively, using the equation $\Phi_{PL} = \Phi_{PL,ref} \times (I/I_{ref}) \times (A_{ref}/A) \times (n/n_{ref})^2$, where A, I, and n are the absorbance at the excitation wavelength, the integrated photoluminescence intensity, and the refractive index of the solvent, respectively. 9,10-Diphenylanthracene (Φ_{PL} = 1.00, toluene; λ_{ex} = 366 nm) was used as the reference material. [d]Photoluminescence lifetime. [g]Radiative rate constant, $k_r = \Phi_{PL} / \tau_{obs}$. [h]Non-radiative rate constant, $k_{nr} = (1 - \Phi_{PL}) / \tau_{obs}$. [i]Oxidation potential determined by cyclic and differential pulse voltammetry for Ar-saturated DMSO containing 2.0 mM [Au(BZI)(TMCz)] and 0.10 M tetrabutylammonium hexafluorophosphate; A glassy carbon and a Pt wire for the working and counter electrodes, respectively; an $Ag/AgNO_3$ pseudo reference electrode; scan rates = 0.10 V s^{-1} and 0.004 V s^{-1} for cyclic and differential pulse voltammetry, respectively.

Supplementary Table 4. Optimization and control experiments

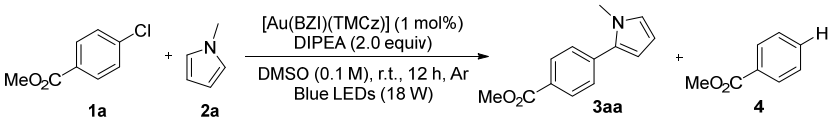

entry	variations	conversion (%)	**3aa** / **4** (%)[b]
1	none	100	82 / 11
2	[Au(BZl)(Cz)] instead of [Au(BZl)(TMCz)]	100	67 / 8
3	[Au(^{Dipp}I)(Cz)] instead of [Au(BZl)(TMCz)]	100	62 / 22
4	[Au(^{Dipp}BZl)(Cz)] instead of [Au(BZl)(TMCz)]	40	34 / trace
5	[Au(^{Dipp}BZl)(TMCz)] instead of [Au(BZl)(TMCz)]	40	33 / trace
6	DMA instead of DMSO	N.R	0 / 0
7	DCM instead of DMSO	N.R	0 / 0
8	THF instead of DMSO	100	41 / 49
9	TFE instead of DMSO	100	0 / 0
10	MeCN instead of DMSO	100	55 / 38
11	no DIPEA	trace	0 / 0
12	NaOAc instead of DIPEA	trace	0 / 0
13	$NaHCO_3$ instead of DIPEA	10	6 / trace
14	KOAc instead of DIPEA	trace	0 / 0
15	K_2CO_3 instead of DIPEA	trace	0 / 0
16	K_3PO_4 instead of DIPEA	21	15 / 3
17	TEA instead of DIPEA	86	63 / 16
18	TMEDA instead of DIPEA	100	74 / 19
19	DBU instead of DIPEA	15	11 / trace
20	DMSO (0.25 M)	100	86 / 8
21	DMSO (0.5 M)	100	91 / trace
22	DMSO (1.0 M)	60	45 / 14
23	neat	N.R	0 / 0
	variations from optimal conditions (entry 21)		
24	[Au(BZl)(TMCz)] (0.5 mol%)	100	92 / trace
25[c]	[Au(BZl)(TMCz)] (0.25 mol%)	100	91 / trace
26[c]	[Au(BZl)(TMCz)] (0.1 mol%)	23	19 / 0
27[c]	no [Au(BZl)(TMCz)]	N.R	0 / 0
28[c]	no hv	N.R	0 / 0

[a]Reaction scale : **1a** (0.05 mmol) and **2a** (0.5 mmol). [b]Yields were determined by ^{1}H NMR spectroscopy using bromoform as the internal standard. [c]24 h reaction time

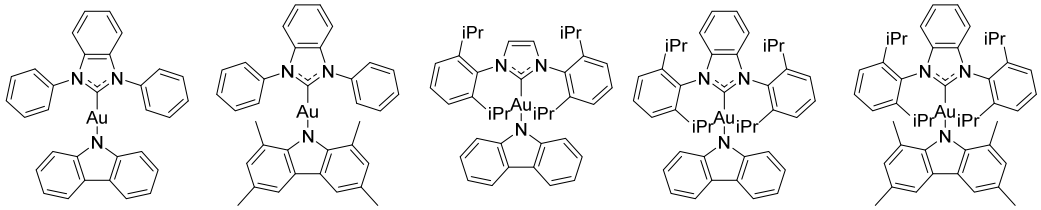

[Au(BZl)(Cz)] [Au(BZl)(TMCz)] [Au(^{Dipp}I)(Cz)] [Au(^{Dipp}BZl)(Cz)] [Au(^{Dipp}BZl)(TMCz)]

Supplementary Table 5. Photoredoxcatalytic C–B bond formation reactions

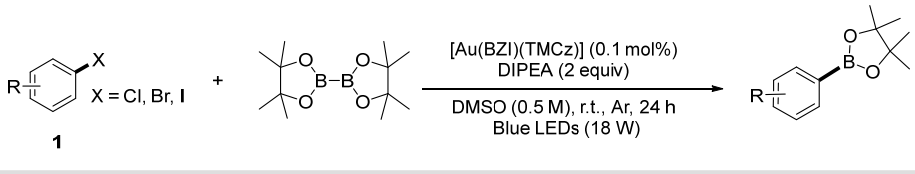

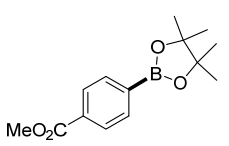

86% (X=Cl)

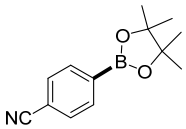

79% (X=Cl)

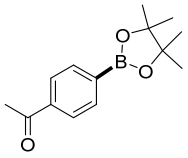

91% (X=Br)

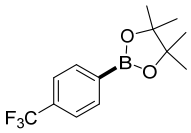

64% (X=I)

An oven-dried reaction vial equipped with a magnetic stir bar was charged with aryl halide **1** (0.30 mmol, 1.0 equiv), [Au(BZI)(TMCz)] (0.2 mg, 0.1 mol%), 4,4,4',4',5,5,5',5'-octamethyl-2,2'-bi(1,3,2-dioxaborolane) (0.9 mmol, 3 equiv), DIPEA (0.6 mmol, 2 equiv), and anhydrous DMSO (0.20 M, 1.5 mL). The vial was sealed with a silicon septum screw cap and purged with argon via a balloon for 10 minutes. The setup was then exposed to a 405 nm lamp in a photoreactor with continuous stirring. The reaction progress was monitored using thin-layer chromatography (TLC) or gas chromatography (GC). Upon completion, the reaction was quenched by adding water. The reaction mixture was extracted three times using dichloromethane. The combined organic phases were dried over $MgSO_4$, concentrated under reduced pressure using a rotary evaporator, and purified by silica gel flash column chromatography using a hexane-ethyl acetate (20/1) as the eluent to give the corresponding product.

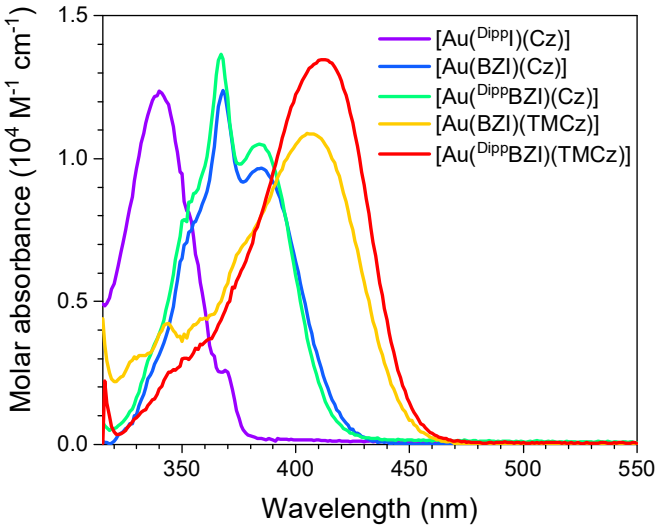

Supplementary Fig. 1 UV–Vis absorption spectra. a–e, UV–Vis absorption spectra (toluene) of 10 μM Au(I) complexes tested in this study.

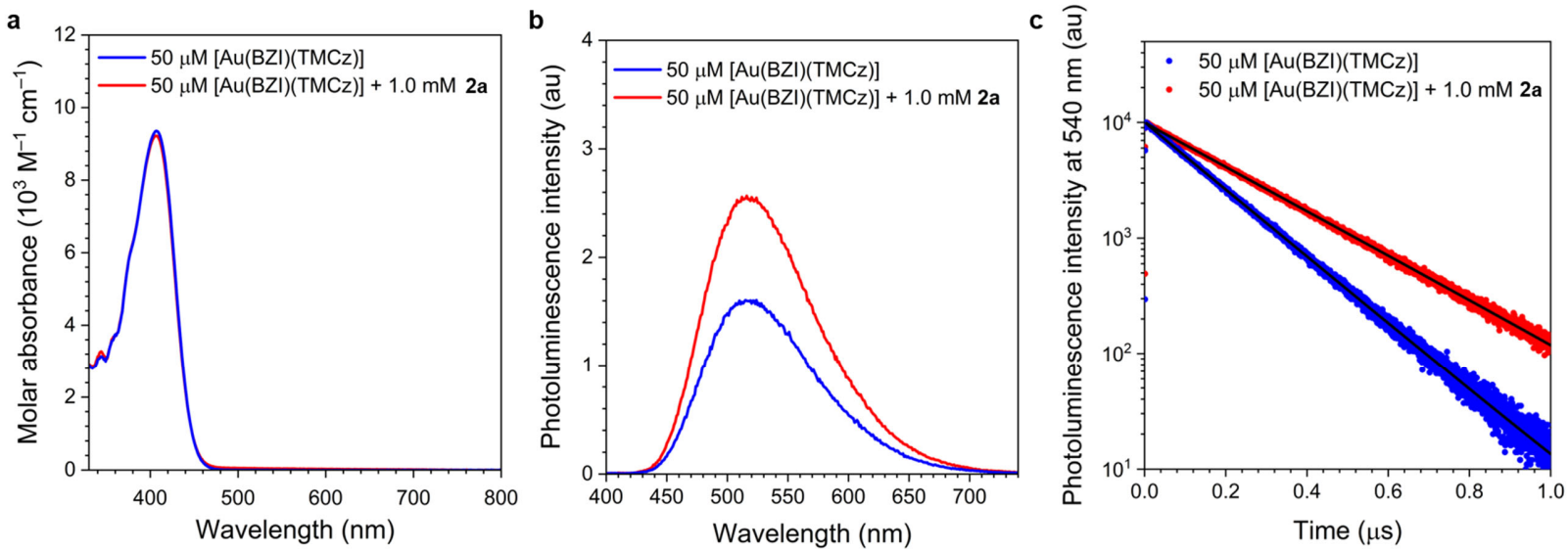

Supplementary Fig. 2 Effect of added substrate. a–c, UV–Vis absorption (**a**) and photoluminescence (**b**; λ_{ex} = 380 nm) spectra and photoluminescence decay traces (**c**; λ_{obs} = 540 nm) of 50 μM [Au(BZI)(TMCz)] in the absence (blue curves) and presence (red curves) of 1.0 mM **2a**. The black lines in **c** are nonlinear least-squares fit of the decay traces to a mono-exponential decay model. The corresponding τ_{obs} are 227 ns and 150 ns without and with **2a**, respectively.

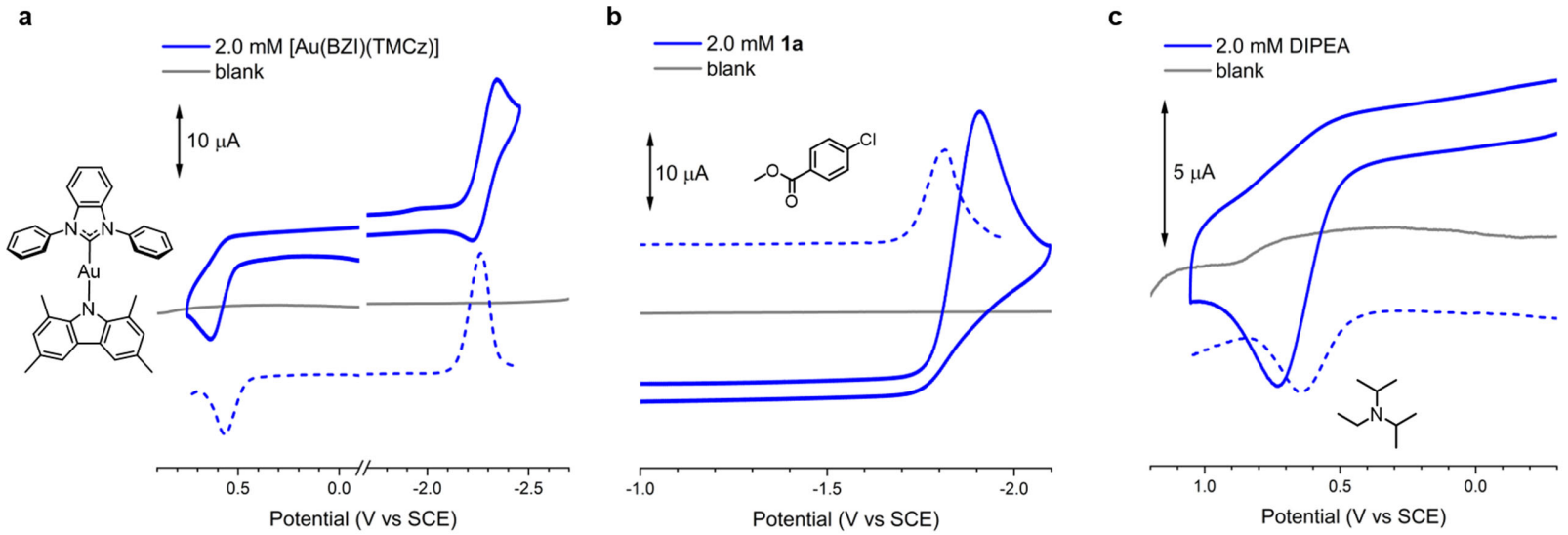

Supplementary Fig. 3 Electrochemical potentials. a–c, Cyclic (CV, blue solid curves) and differential pulse voltammograms (DPV, blue dashed lines) of Ar-saturated DMSO containing 0.10 M Bu_4NPF_6 and 2.0 mM sample: **a**, [Au(BZI)(TMCz)]; **b**, 1a; **c**, DIPEA. Grey lines are signals recorded for an Ar-saturated DMSO containing 0.10 M Bu_4NPF_6 blank. Conditions: a glassy carbon disc and a Pt wire as the working and counter electrodes, respectively. An $Ag/AnNO_3$ pseudo reference electrode. Scan rate = 0.10 V s^{-1} for CV and 4 mV s^{-1} for DPV. The electrochemical potentials were corrected using a Fc^+/Fc redox couple as an external standard.

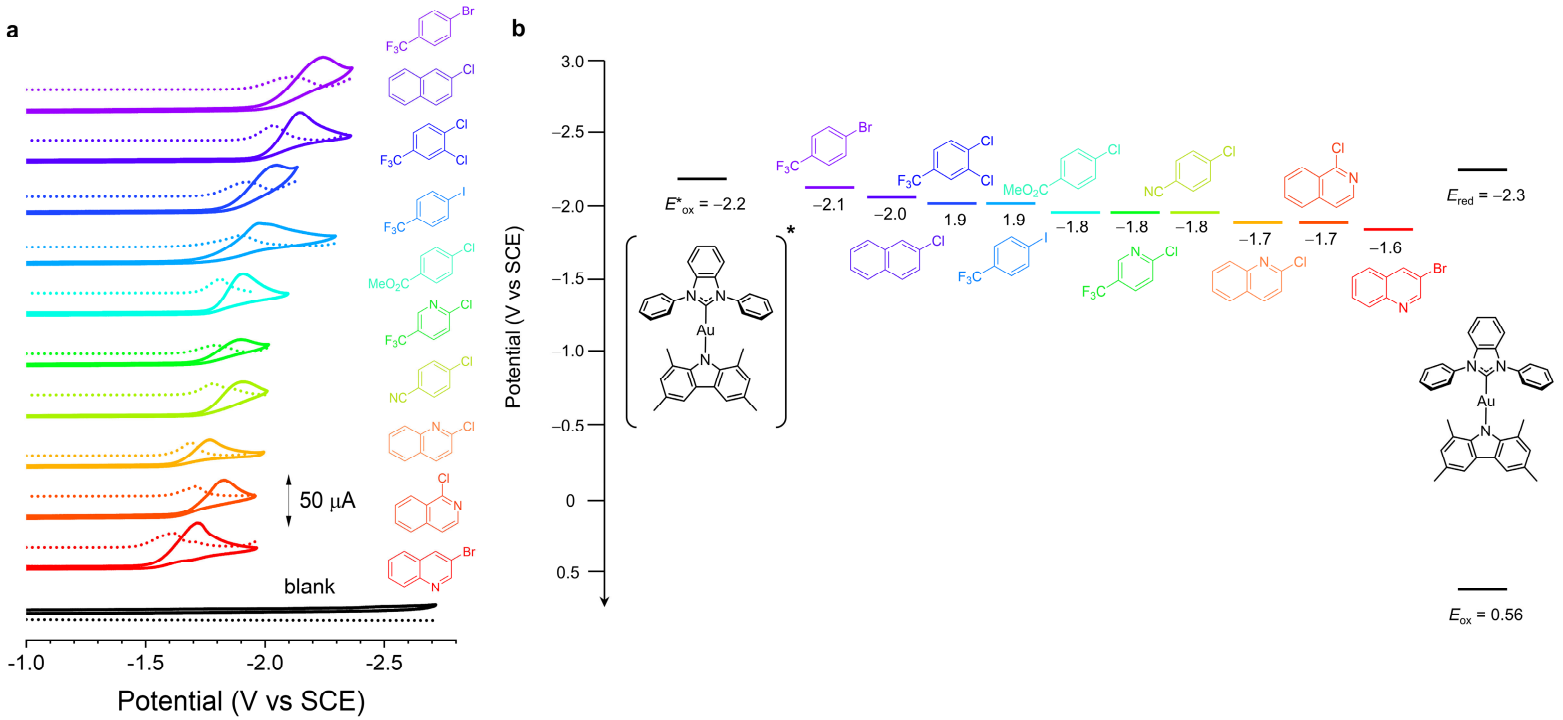

Supplementary Fig. 4 Electrochemical potentials. a, Cyclic (CV, blue solid curves) and differential pulse voltammograms (DPV, blue dashed lines) of Ar-saturated DMSO containing 0.10 M Bu_4NPF_6 and 2.0 mM aryl halide substrate. Conditions: a glassy carbon disc and a Pt wire as the working and counter electrodes, respectively. An $Ag/AgNO_3$ pseudo reference electrode. Scan rate = 0.10 V s^{-1} for CV and 4 mV s^{-1} for DPV. The electrochemical potentials were corrected using a Fc^+/Fc redox couple as an external standard. **b**, Comparison of E^*_{ox} of [Au(BZI)(TMCz)]*, E_{red} of substrates, and E_{red} and E_{ox} of [Au(BZI)(TMCz)].

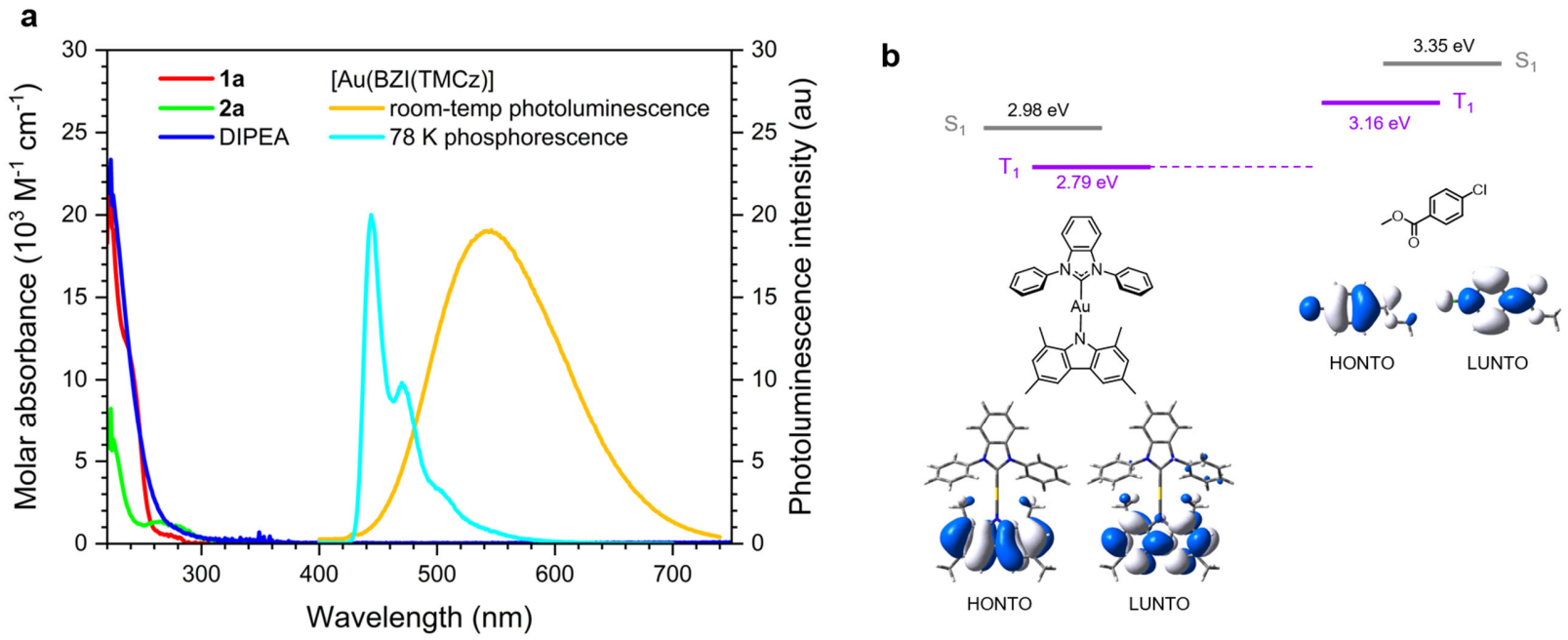

Supplementary Fig. 5 Examination of energy transfer. a, Overlays of the UV–vis absorption spectra of 10 μM 1a (red), 10 μM 2a (green), and 10 μM DIPEA (blue), and the steady-state room-temperature photoluminescence (orange; λ_{ex} = 380 nm) and 78 K phosphorescence (cyan; λ_{ex} = 380 nm) spectra of 50 μM [Au(BZI)(TMCz)]. **b**, Energy level alignments of the lowest singlet (S_1; grey) and the triplet (T_1; purple) states of [Au(BZI)(TMCz)] and 1a calculated the TD–CAM–B3LYP functional and the 6–311G(d) basis set.

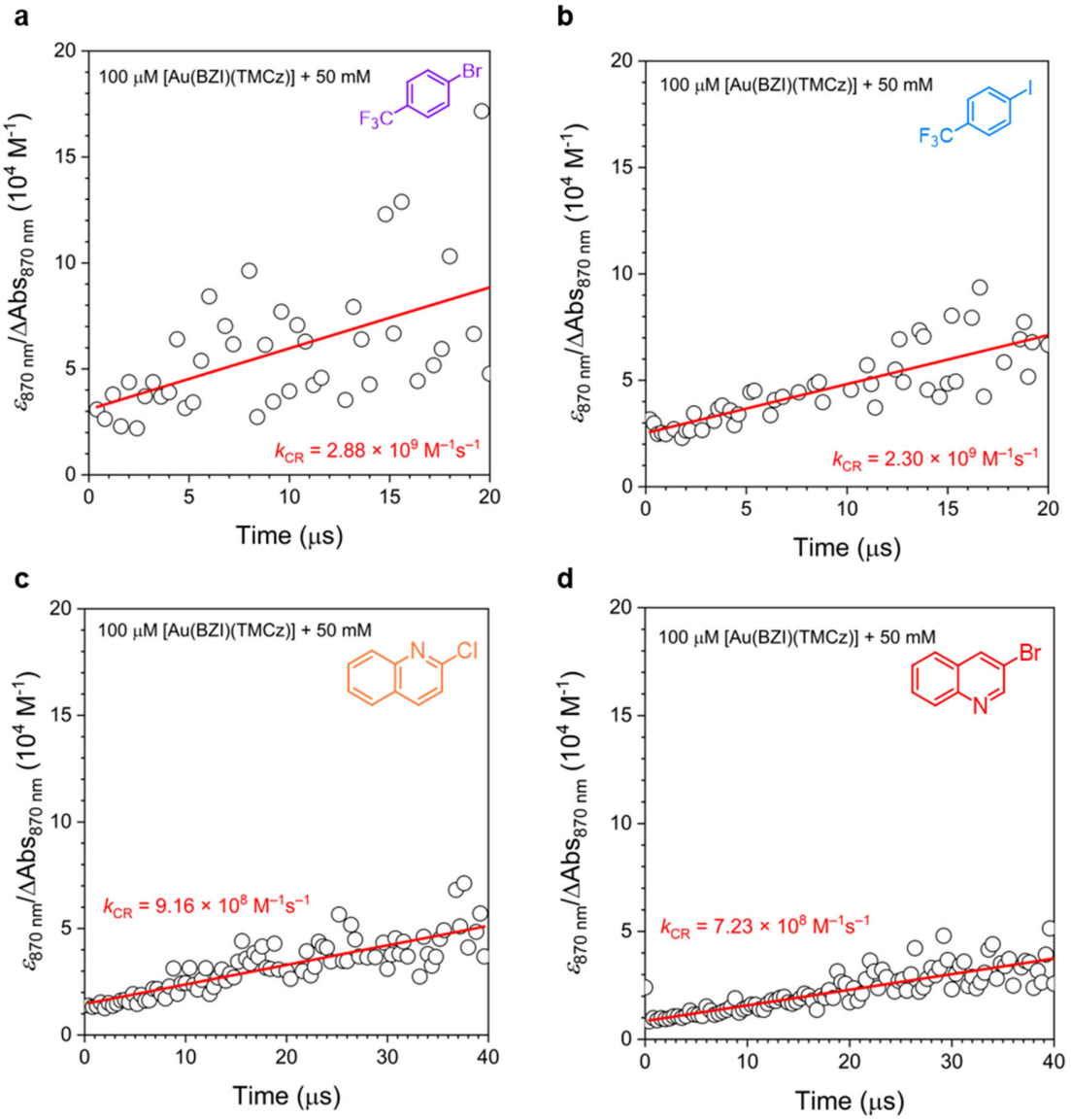

Supplementary Fig. 6 Charge recombination. a–d, Second-order kinetics analysis for charge recombination between $[Au(BZI)(TMCz)]^{\bullet+}$ and the substrate radical anion. (**a**, 4-trifluorophennyl bromide; **b**, 4-trifluorophennyl iodide; **c**, 2-chlroquinoline; **d**, 3-bromoquiniline) The 870 nm photoinduced absorption kinetic traces were recorded for 100 μM [Au(BZI)(TMCz)] and 50 mM substrate, recorded after 355 nm pulsed laser photoexcitation (Ar-saturated DMSO).

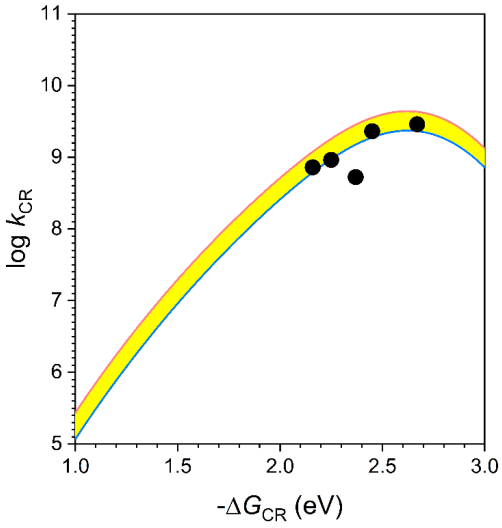

Supplementary Fig. 7 Fits of k_{CR} values to Jortner electron-transfer theory. Plot of log k_{CR} as a function of $-\Delta G_{CR}$ with five different aryl halide substrates. The red and blue lines correspond to theoretical Jortner plots with λ = 4.6 and 4.8 eV, respectively.

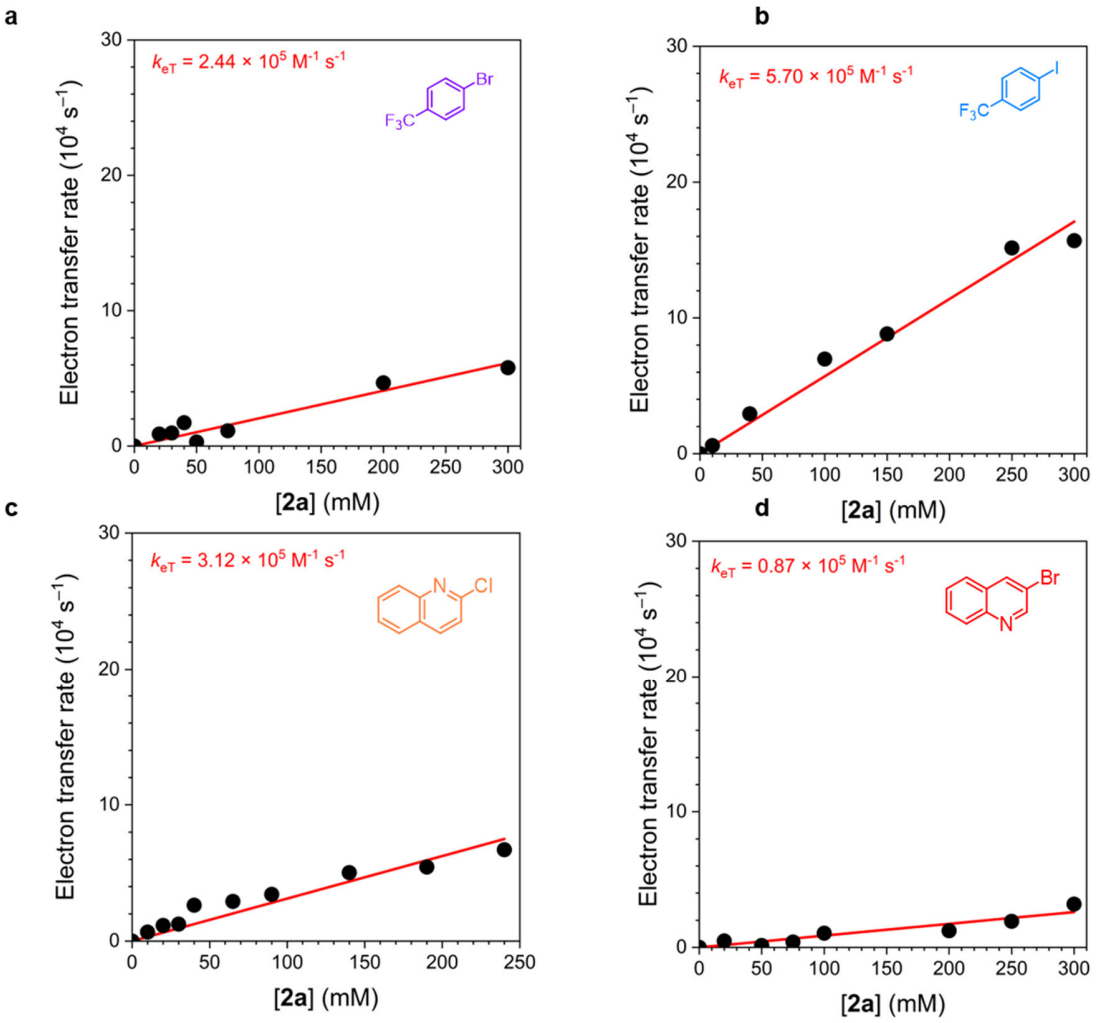

Supplementary Fig. 8 Catalyst recovery. a–d, Pseudo-first-order kinetics analysis for the recovery of [Au(BZI)(TMCz)] through electron transfer from the radical adduct of **2a** and the aryl halide to [Au(BZI)(TMCz)]$^{\bullet+}$: **a**, 50 mM trifluorophenyl bromide and 0–300 mM **2a**; **b**, 50 mM trifluorophenyl iodide and 0–300 mM **2a**; **c**, 50 mM 2-chloroquinoline and 0–250 mM **2a**; **d**, 50 mM 3-boromoquinoline and 0–300 mM **2a**.

Supplementary Data. Analytical data for the synthesized compounds

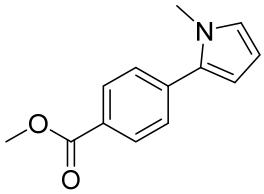

Methyl 4-(1-methyl-1H-pyrrol-2-yl)benzoate, **3aa**: pale yellow solid; **^{1}H NMR (600 MHz, $CDCl_3$)** δ 8.06 (d, *J* = 8.4 Hz, 2H), 7.48 (d, *J* = 8.4 Hz, 2H), 6.76 (dd, *J* = 1.8, 2.8 Hz, 1H), 6.34 (dd, *J* = 1.8, 3.7 Hz, 1H), 6.22 (dd, *J* = 2.8, 3.7 Hz, 1H), 3.93 (s, 3H), 3.71 (s, 3H); **^{13}C NMR (151 MHz, $CDCl_3$)** δ 167.17, 137.96, 133.72, 129.95, 128.15, 128.08, 125.32, 110.25, 108.49, 52.29, 35.59; **IR (neat):** ν_{max} = 3111, 2953, 1712, 1607, 1275, 1114 cm^{-1}; ***R**$_f$* 0.40 (hex/EtOAc 5/1).

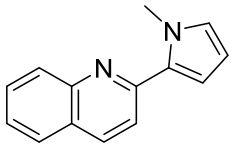

2-(1-Methyl-1H-pyrrol-2-yl)quinoline, **3ba**: yellow solid; **^{1}H NMR (600 MHz, $CDCl_3$)** δ 8.07 (d, *J* = 8.8 Hz, 1H), 8.06-8.02 (brs, 1H), 7.75 (d, *J* = 8.0 Hz, 1H), 7.70 (d, *J* = 8.6 Hz, 1H), 7.67 (dd, *J* = 7.6, 8.8 Hz, 1H), 7.46 (dd, *J* = 7.6, 8.6 Hz, 1H), 6.82-6.78 (m, 2H), 6.23 (dd, *J* = 2.6, 3.8 Hz, 1H), 4.21 (s, 3H); **^{13}C NMR (151 MHz, $CDCl_3$)** δ 152.46, 147.87, 136.02, 132.40, 129.53, 129.26, 127.82, 127.63, 126.25, 125.66, 120.30, 112.51, 108.02, 37.88; **IR (neat):** ν_{max} = 3055, 2924, 2854, 1465, 1322 cm^{-1}; ***R**$_f$* 0.38 (hex/EtOAc 10/1).

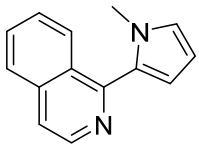

1-(1-methyl-1H-pyrrol-2-yl)isoquinoline, **3ca**: yellow solid; **^{1}H NMR (600 MHz, $CDCl_3$)** δ 9.04 (dd, *J* = 1.8, 4.2 Hz, 1H), 8.26 (dd, *J* = 1.8, 8.5 Hz, 1H), 7.89 – 7.85 (d, *J* = 8.5 Hz, 1H), 7.76 (dd, *J* = 1.8, 7.2 Hz, 1H), 7.61 (dd, *J* = 7.2, 8.5 Hz, 1H), 7.46 (dd, *J* = 4.2, 8.2 Hz, 1H), 6.85 (dd, *J* = 1.8, 2.7 Hz, 1H), 6.33 (dd, *J* = 1.8, 3.7 Hz, 1H), 6.31 (dd, *J* = 2.7, 3.7 Hz, 1H), 3.48 (s, 3H); **^{13}C NMR (151 MHz, $CDCl_3$)** δ 150.58, 147.13, 136.48, 133.21, 132.33, 132.23, 128.74, 128.14, 126.42, 123.45, 121.17, 110.34, 107.98, 35.53; **IR (neat):** ν_{max} = 3107, 2958, 1275, 1170, 1125 cm^{-1}; ***R**$_f$* 0.30 (hex/EtOAc 10/1).

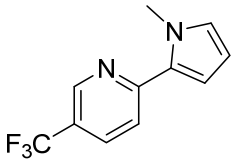

2-(1-methyl-1H-pyrrol-2-yl)-5-(trifluoromethyl)pyridine, **3da**: pale yellow solid; **^{1}H NMR (600 MHz, $CDCl_3$)** δ 8.79 (s, 1H), 7.83 (d, *J* = 8.4 Hz, 1H), 7.63 (d, *J* = 8.5 Hz, 1H), 6.80 (dd, *J* = 1.9, 2.7 Hz, 1H), 6.73 (dd, *J* = 1.9, 3.9 Hz, 1H), 6.21 (dd, *J* = 2.7, 3.9 Hz, 1H), 4.05 (s, 3H); **^{13}C NMR (151 MHz, $CDCl_3$)** δ 155.66, 145.68 (q, *J* = 4.3 Hz), 133.45 (q, *J* = 3.5 Hz), 130.93, 128.47, 124.12 (q, *J* = 272.0 Hz), 122.59 (q, *J* = 33.0 Hz), 120.45, 113.08, 108.46 (d, *J* = 2.3 Hz), 37.80; **^{19}F NMR (564 MHz, $CDCl_3$)** δ -62.20; **IR (neat):** ν_{max} = 3109, 2927, 2854, 1605, 1321, 1119, 1080 cm^{-1}; ***R**$_f$* 0.32 (hex/EtOAc 7/1).

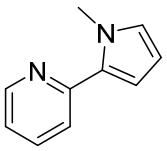

2-(1-methyl-1H-pyrrol-2-yl)pyridine, **3ea**: pale green oil; **^{1}H NMR (600 MHz, $CDCl_3$)** δ 8.57 (d, *J* = 5.4 Hz, 1H), 7.64 (dd, *J* = 7.5, 7.8 Hz, 1H), 7.54 (d, *J* = 7.8 Hz, 1H), 7.07 (dd, *J* = 5.4, 7.5 Hz, 1H), 6.74 (dd, *J* = 1.8. 2.6 Hz, 1H), 6.59 (dd, *J* = 1.8, 3.7 Hz, 1H), 6.19 (dd, *J* = 2.6, 3.7 Hz, 1H), 4.01 (s, 3H); **^{13}C NMR (151 MHz, $CDCl_3$)** δ 152.84, 148.67, 136.47, 132.43, 126.61, 121.67, 120.41, 110.99, 107.87, 37.06; **IR (neat):** ν_{max} = 3102, 2950, 2808, 1586, 1453 cm^{-1}; ***R*$_f$** 0.45 (hex/EtOAc 10/1).

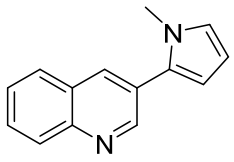

3-(1-methyl-1H-pyrrol-2-yl)quinoline, **3fa**: yellow solid; **^{1}H NMR (600 MHz, $CDCl_3$)** δ 9.02 (d, *J* = 2.2 Hz, 1H), 8.14 – 8.10 (m, 2H), 7.83 (dd, *J* = 1.4, 8.0 Hz, 1H), 7.71 (ddd, *J* = 1.4, 6.9, 8.4 Hz, 1H), 7.57 (ddd, *J* = 1.1, 6.9, 8.0 Hz, 1H), 6.82 (dd, *J* = 1.9, 2.7 Hz, 1H), 6.42 (dd, *J* = 1.9, 3.7 Hz, 1H), 6.28 (dd, *J* = 2.7, 3.7 Hz, 1H), 3.75 (s, 3H); **^{13}C NMR (151 MHz, $CDCl_3$)** δ 151.09, 146.80, 134.03, 131.17, 129.49, 129.39, 127.99, 127.98, 127.28, 126.72, 125.18, 110.48, 108.65, 35.45; **IR (neat):** ν_{max} = 3051, 2987, 2932, 1608, 1464, 1238 cm^{-1}; ***R*$_f$** 0.30 (hex/EtOAc 10/1).

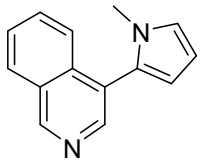

4-(1-methyl-1H-pyrrol-2-yl)isoquinoline, **3ga**: pale yellow solid; **^{1}H NMR (600 MHz, $CDCl_3$)** δ 8.57 (d, *J* = 5.6 Hz, 1H), 8.40 (dq, *J* = 1.0, 8.5 Hz, 1H), 7.84 (d, *J* = 8.2 Hz, 1H), 7.68 (ddd, *J* = 1.2, 6.8, 8.1 Hz, 1H), 7.59 – 7.53 (m, 2H), 6.86 (dd, *J* = 1.7, 2.7 Hz, 1H), 6.54 (dd, *J* = 1.8, 3.7 Hz, 1H), 6.29 (dd, *J* = 2.6, 3.7 Hz, 1H), 3.80 (s, 3H); **^{13}C NMR (151 MHz, $CDCl_3$)** δ 153.23, 141.90, 137.18, 130.24, 128.25, 127.97, 127.40, 127.01, 125.53, 119.21, 114.02, 107.78, 35.65; **IR (neat):** ν_{max} = 3047, 2926, 1591, 1273, 1066 cm^{-1}; ***R*$_f$** 0.40 (hex/EtOAc 10/1).

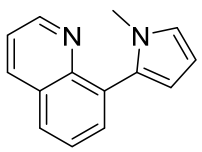

8-(1-methyl-1H-pyrrol-2-yl)quinoline, **3ha**: white solid; **^{1}H NMR (600 MHz, $CDCl_3$)** δ 9.04 (dd, *J* = 1.8, 4.2 Hz, 1H), 8.26 (dd, *J* = 1.8, 8.5 Hz, 1H), 7.87 (d, *J* = 8.5 Hz, 1H), 7.76 (dd, *J* = 1.8, 7.2 Hz, 1H), 7.61 (dd, *J* = 7.2, 8.5 Hz, 1H), 7.46 (dd, *J* = 4.2, 8.2 Hz, 1H), 6.85 (dd, *J* = 1.8, 2.7 Hz, 1H), 6.33 (dd, *J* = 1.8, 3.7 Hz, 1H), 6.31 (dd, *J* = 2.7, 3.7 Hz, 1H), 3.48 (s, 3H); **^{13}C NMR (151 MHz, $CDCl_3$)** δ 150.58, 147.13, 136.48, 133.21, 132.33, 132.23, 128.74, 128.14, 126.42, 123.45, 121.17, 110.34, 107.98, 35.53; **IR (neat):** ν_{max} = 3103, 3056, 2926, 2854, 1601, 1427, 1068 cm^{-1}; ***R*$_f$** 0.35 (hex/EtOAc 10/1).

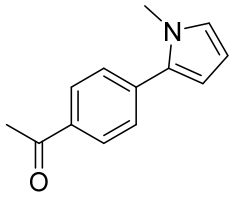

1-(4-(1-methyl-1H-pyrrol-2-yl)phenyl)ethan-1-one, **3ia**: white solid; **^{1}H NMR (600 MHz, $CDCl_3$)** δ 7.99 (d, *J* = 8.4 Hz, 2H), 7.50 (d, *J* = 8.4 Hz, 2H), 6.77 (dd, *J* = 1.7, 2.9 Hz, 1H), 6.35 (dd, *J* = 1.7, 3.8 Hz, 1H), 6.23 (dd, *J* = 2.9, 3.8 Hz, 1H), 3.72 (s, 3H), 2.62 (s, 3H); **^{13}C NMR (151 MHz, $CDCl_3$)** δ 197.71, 138.08, 135.09, 133.56, 128.75, 128.10, 125.49, 110.39, 108.53, 35.59, 26.72; **IR (neat):** ν_{max} = 3104, 2954, 2851, 1676, 1601, 1269 cm^{-1}; ***R*$_f$** 0.35 (hex/EtOAc 7/1).

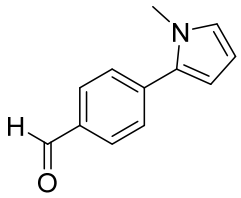

4-(1-methyl-1H-pyrrol-2-yl)benzaldehyde, **3ja**: pale yellow oil; **^{1}H NMR (600 MHz, $CDCl_3$)** δ 10.02 (s, 1H), 7.90 (d, *J* = 8.4 Hz, 2H), 7.57 (d, *J* = 8.4 Hz, 2H), 6.79 (dd, *J* = 1.8, 2.7 Hz, 1H), 6.39 (dd, *J* = 1.8, 3.7 Hz, 1H), 6.24 (dd, *J* = 2.7, 3.7 Hz, 1H), 3.74 (s, 3H); **^{13}C NMR (151 MHz, $CDCl_3$)** δ 191.89, 139.44, 134.43, 133.43, 130.15, 128.40, 125.97, 110.94, 108.73, 77.02, 35.73; **IR (neat):** ν_{max} = 3104, 2952, 2827, 2734, 1693, 1600, 1168 cm^{-1}; ***R*$_f$** 0.40 (hex/EtOAc 7/1).

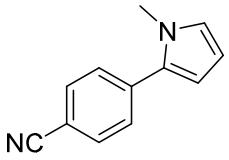

4-(1-methyl-1H-pyrrol-2-yl)benzonitrile, **3ka**: white solid; **^{1}H NMR (600 MHz, $CDCl_3$)** δ 7.67 (d, *J* = 8.0 Hz, 2H), 7.50 (d, *J* = 8.0 Hz, 2H), 6.78 (dd, *J* = 1.8, 2.7 Hz, 1H), 6.37 – 6.33 (dd, *J* = 1.8, 3.9 1H), 6.23 (dd, *J* = 2.7, 3.9 Hz, 1H), 3.72 (s, 3H); **^{13}C NMR (151 MHz, $CDCl_3$)** δ 132.83, 132.46, 128.48, 126.04, 110.95, 109.90, 108.79, 35.66; **IR (neat):** ν_{max} = 3105, 2922, 2851, 2224, 1605, 1498 cm^{-1}; ***R*$_f$** 0.30 (hex/EtOAc 10/1).

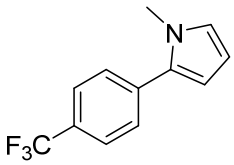

1-methyl-2-(4-(trifluoromethyl)phenyl)-1H-pyrrole, 3la: colorless oil; **^{1}H NMR (600 MHz, $CDCl_3$)** δ 7.65 (d, *J* = 8.0 Hz, 2H), 7.52 (d, *J* = 8.0 Hz, 2H), 6.77 (dd, *J* = 1.8, 2.7 Hz, 1H), 6.31 (dd, *J* = 1.8, 3.6 Hz, 1H), 6.23 (dd, *J* = 2.7, 3.6 Hz, 1H), 3.70 (s, 3H); **^{13}C NMR (151 MHz, $CDCl_3$)** δ 137.03, 133.32, 128.61, 125.58 (q, *J* = 3.8 Hz), 125.13, 124.48 (q, *J* = 272.0 Hz), 110.14, 108.46, 35.45; **^{19}F NMR (564 MHz, $CDCl_3$)** δ -62.82; **IR (neat):** ν_{max} = 3105, 2929, 1616, 1325, 1122, 1070 cm^{-1}; ***R*$_f$** 0.40 (hex/EtOAc 10/1).

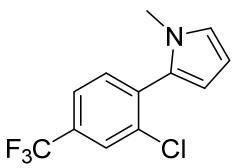

2-(2-chloro-4-(trifluoromethyl)phenyl)-1-methyl-1H-pyrrole, **3ma**: pale yellow solid; **^{1}H NMR (600 MHz, $CDCl_3$)** δ 7.74 (s, 1H), 7.56 (d, *J* = 8.0 Hz, 1H), 7.48 (d, *J* = 8.0 Hz, 1H), 6.78 (dd, *J* = 1.8, 3.0 Hz, 1H), 6.25 (dd, *J* = 3.0, 3.7 Hz, 1H), 6.22 (dd, *J* = 1.8, 3.7 Hz, 1H), 3.51 (s, 3H); **^{13}C NMR**

(151 MHz, $CDCl_3$) δ 136.51, 135.65, 133.30, 131.48 (q, *J* = 33.3 Hz), 129.99, 126.94 (q, *J* = 14.9 Hz), 126.25, 123.75, 123.60 (q, *J* = 14.9 Hz), 123.51 (q, *J* = 273.1 Hz), 110.62, 108.13, 34.75; **^{19}F NMR (564 MHz, $CDCl_3$)** δ -62.78; **IR (neat):** ν_{max} = 2925, 2854, 1324, 1124 cm^{-1}; R_f 0.25 (hex/EtOAc 7/1).

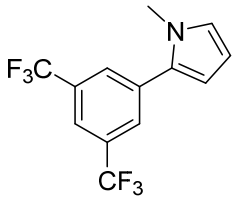

2-(3,5-bis(trifluoromethyl)phenyl)-1-methyl-1H-pyrrole, **3na**: white solid; **3ma**: pale yellow solid; **^{1}H NMR (600 MHz, $CDCl_3$)** δ 7.84 (s, 2H), 7.79 (s, 1H), 6.80 (dd, *J* = 1.8, 2.7 Hz, 1H), 6.37 (dd, *J* = 1.8, 3.7 Hz, 1H), 6.25 (dd, *J* = 2.7, 3.7 Hz, 1H), 3.71 (s, 3H); **^{13}C NMR (151 MHz, $CDCl_3$)** δ 135.52, 132.05 (q, *J* = 33.3 Hz), 131.65, 128.18, 125.88, 123.47 (q, *J* = 272.8 Hz), 120.20 (sep, *J* = 4.1 Hz), 111.00, 108.84, 35.38; **^{19}F NMR (564 MHz, $CDCl_3$)** δ -63.02; **IR (neat):** ν_{max} = 3106, 2927, 1362, 1277, 1129 cm^{-1}; R_f 0.40 (hex/EtOAc 5/1).

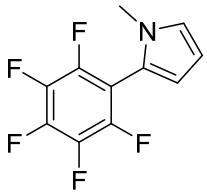

1-methyl-2-(perfluorophenyl)-1H-pyrrole, **3oa**: white solid; **^{1}H NMR (600 MHz, $CDCl_3$)** δ 6.86 (dd, *J* = 1.8, 2.7 Hz, 1H), 6.32 (dd, *J* = 1.8, 3.8Hz, 1H), 6.29 *J* = 2.7, 3.8 Hz, 1H), 3.55 (s, 3H); **^{13}C NMR (151 MHz, $CDCl_3$)** δ 144.84 (dm, *J* = 246.8 Hz), 140.97 (dm, *J* = 254.6 Hz), 138.03 (dm, *J* = 251.4 Hz), 125.22, 116.89, 113.08, 108.84, 108.63 (td, *J* = 4.3, 18.2 Hz), 34.69; **^{19}F NMR (564 MHz, $CDCl_3$)** -139.51 (dd, *J* = 8.2, 23.8 Hz, 2F), -154.68 (t, *J* = 20.9 Hz, 1F), -162.16 (ddd, *J* = 8.2, 20.9, 23.8 Hz, 2F); **IR (neat):** ν_{max} = 2986, 2931, 2806, 1483, 1297 cm^{-1}; R_f 0.45 (hex/EtOAc 10/1).

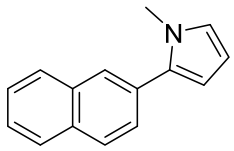

1-methyl-2-(naphthalen-2-yl)-1H-pyrrole, **3pa**: pale yellow solid; **^{1}H NMR (600 MHz, $CDCl_3$)** δ 7.89 – 7.82 (m, 4H), 7.56 (dd, *J* = 1.8, 8.4 Hz, 1H), 7.53 – 7.45 (m, 2H), 6.77 (dd, *J* = 1.7, 2.7 Hz, 1H), 6.35 (dd, *J* = 1.7, 3.8 Hz, 1H), 6.26 (dd, *J* = 2.7, 3.8 Hz, 1H), 3.75 (s, 3H); **^{13}C NMR (151 MHz, $CDCl_3$)** δ 134.78, 133.59, 132.38, 130.98, 128.15, 128.11, 127.88, 127.33, 127.14, 126.51, 126.04, 124.17, 109.36, 108.18; **IR (neat):** ν_{max} = 3118, 2954, 2854, 1511, 1471, 979 cm^{-1}; R_f 0.45 (hex/EtOAc 10/1).

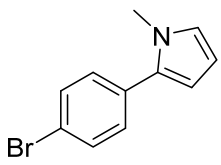

2-(4-bromophenyl)-1-methyl-1H-pyrrole, 3qa: colorless oil; 1-methyl-2-(naphthalen-2-yl)-1H-pyrrole, **3pa**: pale yellow solid; **^{1}H NMR (600 MHz, $CDCl_3$)** δ 7.52 (d, *J* = 8.4 Hz, 2H), 7.27 (d, *J* = 8.4 Hz, 2H), 6.73 (dd, *J* = 1.5, 2.7 Hz, 1H), 6.24 (dd, *J* = 1.5, 3.7 Hz, 1H), 6.21 (dd, *J* = 2.7, 3.7 Hz,

1H), 3.66 (s, 3H); **^{13}C NMR (151 MHz, $CDCl_3$)** δ 133.55, 132.45, 131.72, 130.27, 124.34, 120.99, 109.23, 108.20, 35.26; **IR (neat):** ν_{max} = 3101, 2948, 2921, 1489, 1309, 1074 cm^{-1}; R_f 0.30 (hex/EtOAc 15/1).

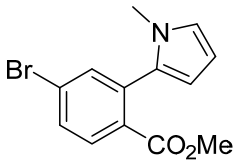

methyl 4-bromo-2-(1-methyl-1H-pyrrol-2-yl)benzoate, **3ra**: pale yellow solid; **^{1}H NMR (600 MHz, $CDCl_3$)** δ 8.04 (d, *J* = 2.0 Hz, 1H), 7.65 (dd, *J* = 2.0, 8.2 Hz, 1H), 7.26 (d, *J* = 8.2 Hz, 1H), 6.71 (dd, *J* = 1.9, 2.9 Hz, 1H), 6.19 (dd, *J* = 2.9, 3.7 Hz, 1H), 6.06 (dd, J = 1.9, 3.7 Hz 1H), 3.74 (s, 3H), 3.39 (s, 3H); **^{13}C NMR (151 MHz, $CDCl_3$)** δ 166.83, 134.55, 134.05, 133.55, 133.01, 132.95, 131.55, 122.92, 121.89, 109.04, 107.89, 52.69, 34.39; **IR (neat):** ν_{max} = 3100, 2996, 2948, 2848, 1730, 1281, 1246, 1089 cm^{-1}; R_f 0.40 (hex/EtOAc 5/1).

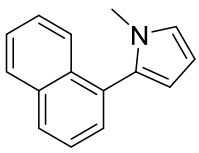

1-methyl-2-(naphthalen-1-yl)-1H-pyrrole, **3sa**: pale yellow solid; **^{1}H NMR (600 MHz, $CDCl_3$)** δ 7.90 (d, *J* = 8.8 Hz, 1H), 7.88 (d, *J* = 8.2 Hz, 1H), 7.72 (d, *J* = 8.8 Hz, 1H), 7.53 – 7.43 (m, 4H), 6.82 (dd, 1.9, 2.9 Hz, 1H), 6.31 (dd, *J* = 1.9, 3.7 Hz, 1H), 6.27 (dd, *J* = 2.9, 3.7 Hz, 1H), 3.40 (s, 3H); **^{13}C NMR (151 MHz, $CDCl_3$)** δ 133.85, 133.54, 132.41, 131.45, 128.95, 128.42, 128.39, 126.51, 126.48, 126.07, 125.42, 122.63, 110.21, 107.75, 34.72; **IR (neat):** ν_{max} = 3053, 2923, 2852, 1504, 1305, 520 cm^{-1}; R_f 0.40 (hex/EtOAc 15/1).

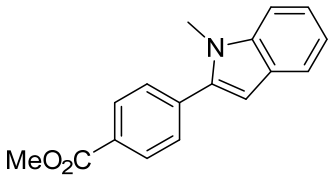

methyl 4-(1-methyl-1H-indol-2-yl)benzoate, **3ab**: yellow solid; **^{1}H NMR (600 MHz, $CDCl_3$)** δ 8.16 (d, *J* = 8.4 Hz, 2H), 7.68 (d, *J* = 7.8 Hz, 1H), 7.61 (d, *J* = 8.4 Hz, 2H), 7.40 (d, *J* = 8.0 Hz, 1H), 7.30 (dd, *J* = 7.8, 8.6 Hz, 1H), 7.19 (dd, *J* = 8.0, 8.6 Hz, 1H), 6.67 (s, 1H), 3.98 (s, 3H), 3.78 (s, 3H); **^{13}C NMR (151 MHz, $CDCl_3$)** δ 166.98, 140.50, 139.04, 137.46, 129.97, 129.41, 129.19, 128.04, 122.48, 120.95, 120.32, 109.93, 103.06, 52.41, 31.59; **IR (neat):** ν_{max} = 3052, 2948, 2842, 1717, 1271, 1101 cm^{-1}; R_f 0.32 (hex/EtOAc 5/1).

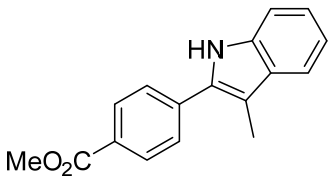

methyl 4-(3-methyl-1H-indol-2-yl)benzoate, **3ac**: pale green solid; **^{1}H NMR (600 MHz, $CDCl_3$)** δ 8.14 (d, *J* = 8.3 Hz, 2H), 8.09 (brs, 1H), 7.66 (d, *J* = 8.3 Hz, 2H), 7.62 (d, *J* = 7.8 Hz, 1H), 7.39 (d, *J* = 8.3 Hz, 1H), 7.24 (dd, *J* = 7.8, 8.3 Hz, 1H), 7.16 (dd, *J* = 7.3, 8.3 Hz, 1H), 3.95 (s, 3H), 2.50 (s, 3H); **^{13}C NMR (151 MHz, $CDCl_3$)** δ 167.06, 137.96, 136.42, 132.98,

130.34, 130.19, 128.75, 127.44, 123.29, 120.03, 119.50, 111.05, 110.80, 52.41, 10.11; **IR (neat):** ν_{max} = 3373, 3052, 2923, 2852, 1692, 1607, 1300 cm^{-1}; $\boldsymbol{R_f}$ 0.25 (hex/EtOAc 5/1).

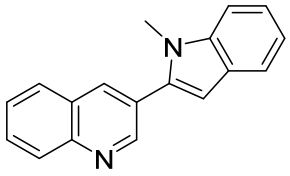

3-(1-methyl-1H-indol-2-yl)quinoline, **3fb**: orange solid; **^{1}H NMR (600 MHz, $CDCl_3$)** δ 9.12 (s, 1H), 8.27 (s, 1H), 8.20 (d, *J* = 8.6 Hz, 1H), 7.91 (d, *J* = 8.0 Hz, 1H), 7.78 (dd, *J* = 6.8, 8.6 Hz, 1H), 7.69 (d, *J* = 8.2 Hz, 1H), 7.63 (dd, *J* = 6.8, 8.0 Hz, 1H), 7.42 (d, *J* = 8.2 Hz, 1H), 7.31 (dd, *J* = 7.0, 8.6 Hz, 1H), 7.20 (dd, *J* = 7.0, 8.2 Hz, 1H), 6.75 (s, 1H), 3.84 (s, 3H); **^{13}C NMR (151 MHz, $CDCl_3$)** δ 150.99, 138.97, 137.98, 135.72, 130.18, 129.48, 128.19, 128.12, 127.59, 126.28, 125.29, 122.64, 121.00, 120.47, 109.97, 103.55, 101.75, 31.56; **IR (neat):** ν_{max} = 3063, 2934, 2861, 1581, 1476, 1330, 1284 cm^{-1}; $\boldsymbol{R_f}$ 0.30 (hex/EtOAc 10/1).

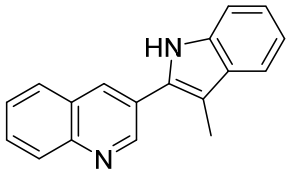

3-(3-methyl-1H-indol-2-yl)quinoline, **3fc**: yellow solid; **^{1}H NMR (600 MHz, $CDCl_3$)** δ 9.19 (s, 1H), 8.38 (s, 1H), 8.29 (s, 1H), 8.15 (d, *J* = 8.4 Hz, 1H), 7.88 (d, *J* = 8.0 Hz, 1H), 7.74 (dd, *J* = 7.6, 8.6 Hz, 1H), 7.65 (d, *J* = 8.0 Hz, 1H), 7.60 (dd, *J* = 8.0, 8.6 Hz, 1H), 7.44 (d, *J* = 8.0 Hz, 1H), 7.26 (dd, *J* = 7.6, 8.4 Hz, 1H), 7.19 (dd, *J* = 8.0, 8.6 Hz, 1H), 2.54 (s, 3H); **^{13}C NMR (151 MHz, $CDCl_3$)** δ 150.99, 138.97, 137.98, 135.72, 130.18, 129.48, 128.19, 128.12, 127.59, 126.28, 125.29, 122.64, 121.00, 120.47, 109.97, 103.55, 101.75, 31.56; **IR (neat):** ν_{max} = 3455, 2922, 2853, 1452, 1330 cm^{-1}; $\boldsymbol{R_f}$ 0.25 (hex/EtOAc 10/1).

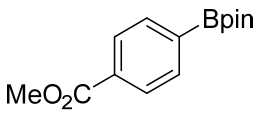

methyl 4-(4,4,5,5-tetramethyl-1,3,2-dioxaborolan-2-yl)benzoate, white solid; **^{1}H NMR (600 MHz, $CDCl_3$)** δ 8.02 (d, *J* = 8.1 Hz, 2H), 7.87 (d, *J* = 8.1 Hz, 2H), 3.92 (s, 3H), 1.35 (s, 12H); **^{13}C NMR (151 MHz, $CDCl_3$)** δ 167.32, 134.86, 132.51, 128.79, 84.37, 77.44, 52.33, 25.08; **IR (neat):** ν_{max} = 2984, 1932, 1720, 1357, 1268, 1108 cm^{-1}; $\boldsymbol{R_f}$ 0.25 (hex/EtOAc 10/1).

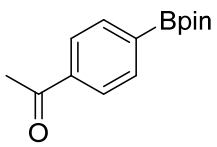

1-(4-(4,4,5,5-tetramethyl-1,3,2-dioxaborolan-2-yl)phenyl)ethan-1-one, white solid; **^{1}H NMR (600 MHz, $CDCl_3$)** δ 7.93 (d, *J* = 8.4 Hz, 2H), 7.89 (d, *J* = 8.2 Hz, 2H), 2.61 (s, 3H), 1.36 (s, 12H); **^{13}C NMR (151 MHz, $CDCl_3$)** δ 198.74, 139.22, 135.14, 127.51, 84.44, 26.97, 25.09; **IR (neat):** ν_{max} = 2979, 2931, 1687, 1357, 1278, 1123 cm^{-1}; $\boldsymbol{R_f}$ 0.40 (hex/EtOAc 10/1).

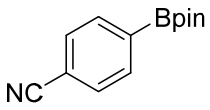

4-(4,4,5,5-tetramethyl-1,3,2-dioxaborolan-2-yl)benzonitrile, white solid; **^{1}H NMR (600 MHz, $CDCl_3$)** δ 7.88 (d, *J* = 7.8 Hz, 2H), 7.64 (d, *J* = 7.8 Hz, 2H), 1.35 (s, 12H); **^{13}C NMR (151 MHz, $CDCl_3$)** δ 135.31, 131.35, 119.09, 114.77, 84.71, 25.08; **IR (neat):** ν_{max} = 2982, 2933, 2228, 1395, 1356, 1141, 1086 cm^{-1}; ***R*$_f$** 0.30 (hex/EtOAc 7/1).

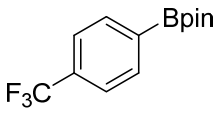

4,4,5,5-tetramethyl-2-(4-(trifluoromethyl)phenyl)-1,3,2-dioxaborolane, colorless oil; **^{1}H NMR (600 MHz, $CDCl_3$)** δ 7.92 (d, *J* = 7.8 Hz, 2H), 7.62 (d, *J* = 7.8 Hz, 2H), 1.36 (s, 12H); **^{13}C NMR (151 MHz, $CDCl_3$)** δ 135.23, 133.06 (q, *J* = 32.12 Hz), 124.53 (q, *J* = 3.76 Hz), 124.37 (q, *J* = 272.52 Hz), 84.49, 25.07; **^{19}F NMR (564 MHz, $CDCl_3$)** δ -63.06; **IR (neat):** ν_{max} = 2961, 2923, 2854, 1261, 1058 cm^{-1}; ***R*$_f$** 0.40 (hex/EtOAc 20/1).

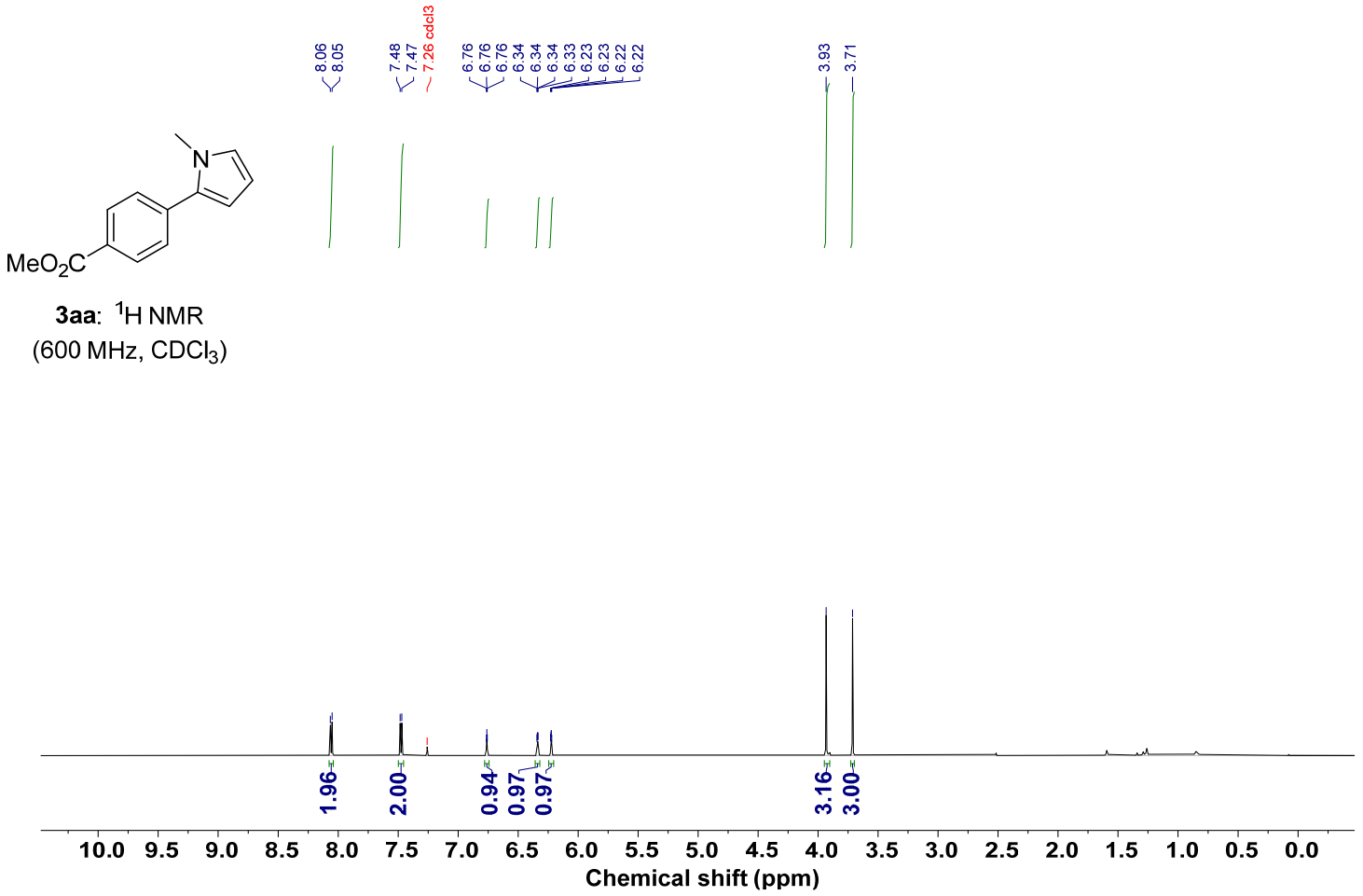

Supplementary Fig. 9 ^{1}H NMR (600 MHz, $CDCl_3$) spectrum of 3aa.

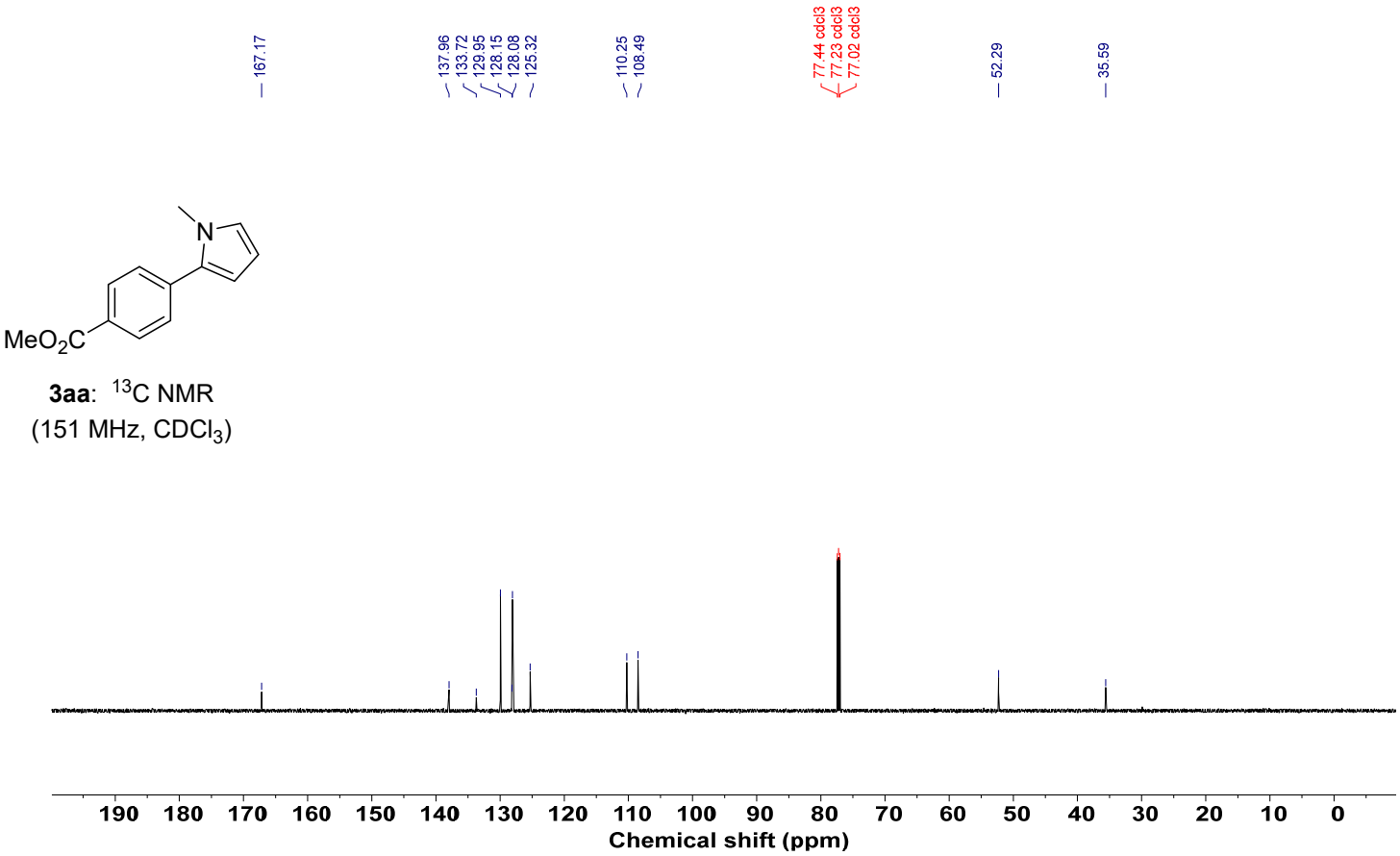

Supplementary Fig. 10 $^{13}C\{^{1}H\}$ NMR (151 MHz, $CDCl_3$) spectrum of 3aa.

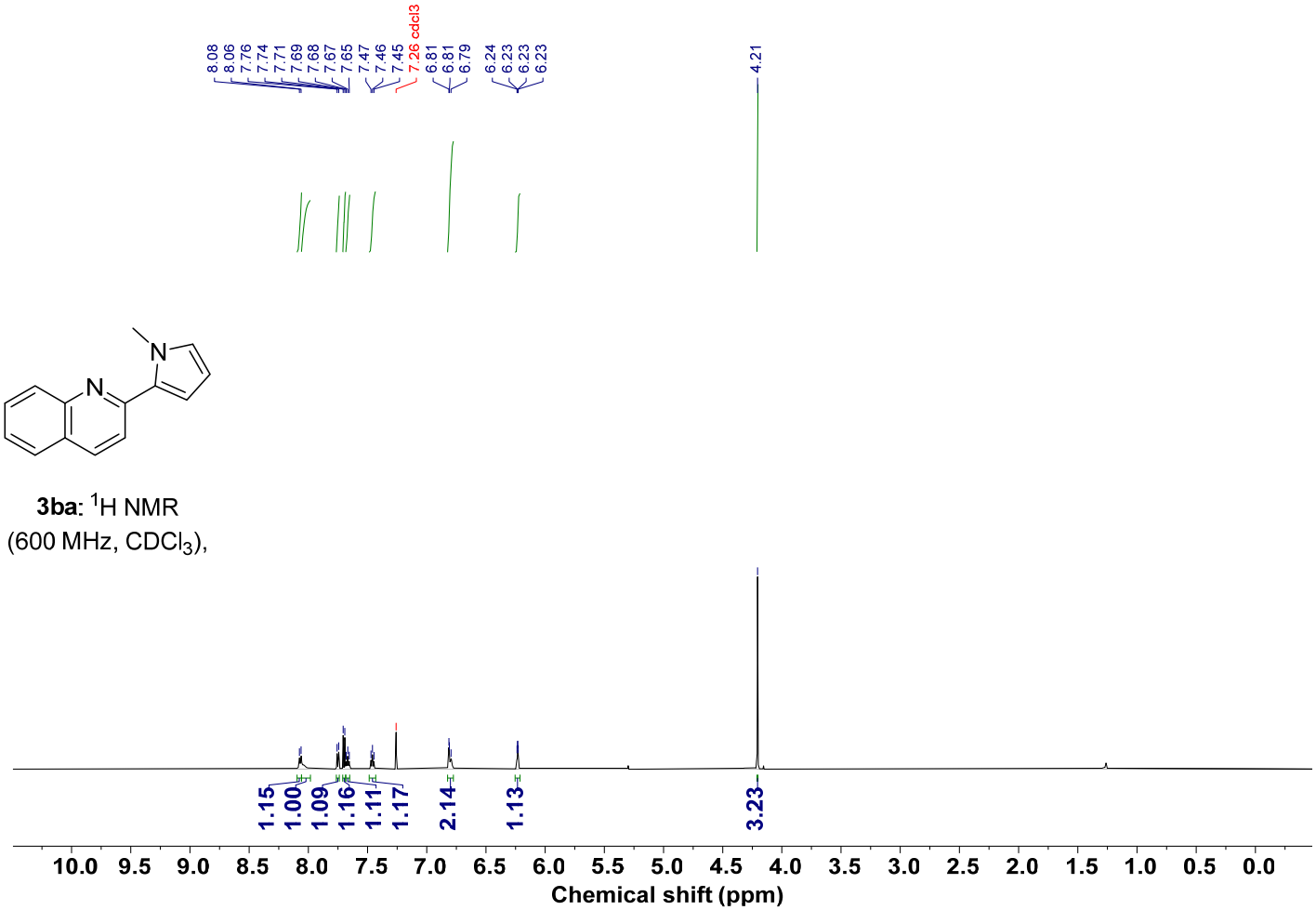

Supplementary Fig. 11 ^{1}H NMR (600 MHz, $CDCl_3$) spectrum of 3ba.

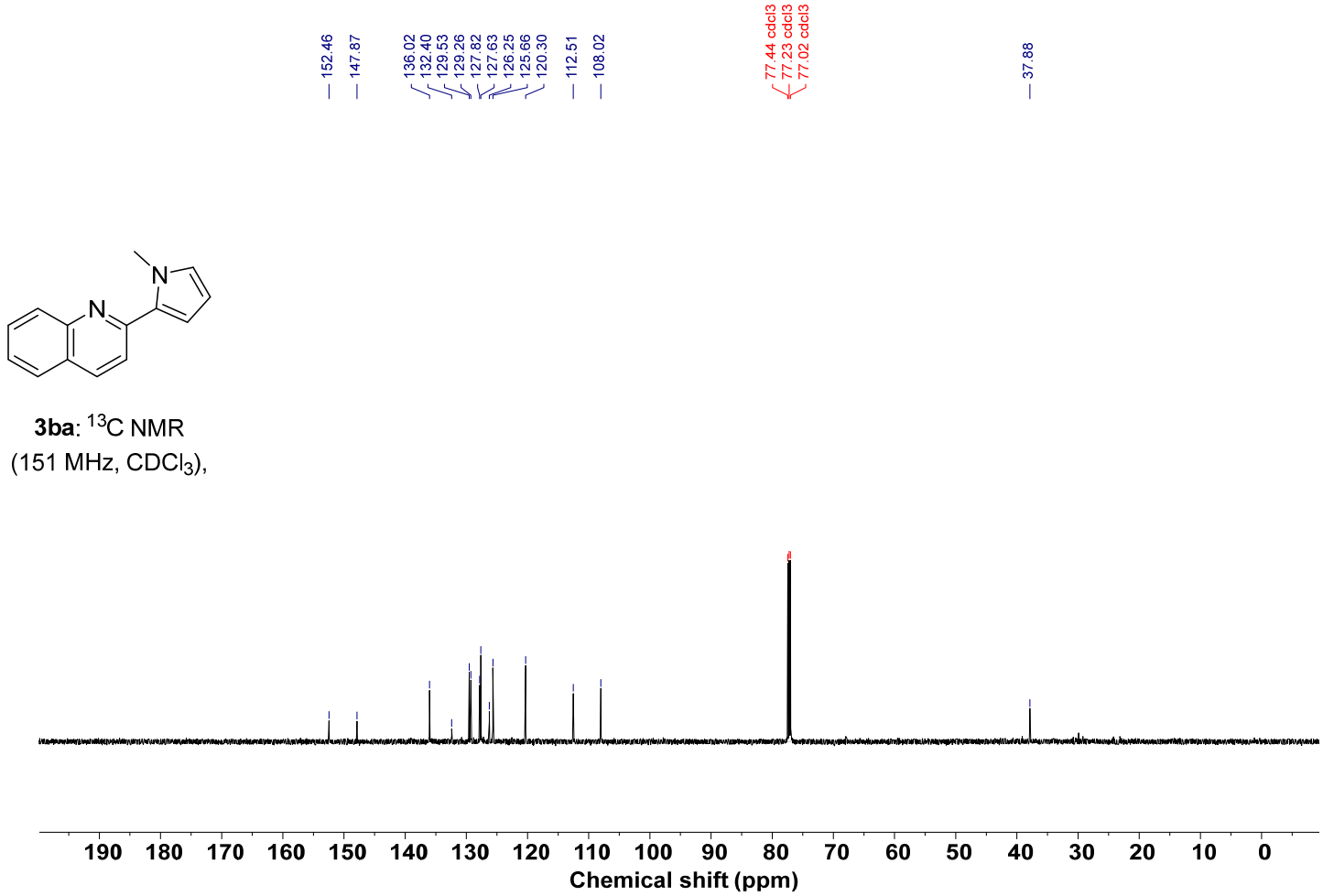

Supplementary Fig. 12 $^{13}C\{^{1}H\}$ NMR (151 MHz, $CDCl_3$) spectrum of 3ba.

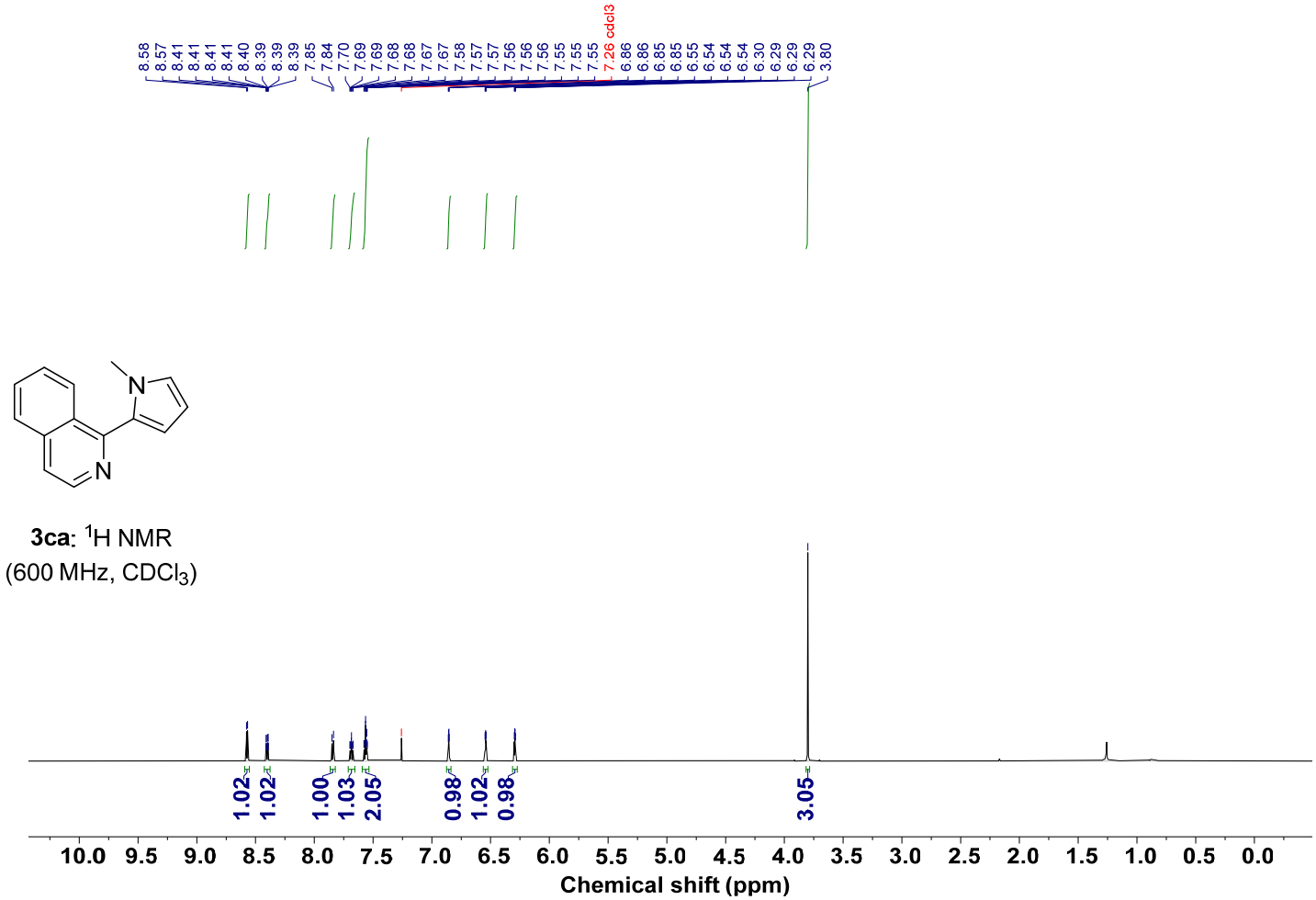

Supplementary Fig.13 ^{1}H NMR (600 MHz, $CDCl_3$) spectrum of 3ca.

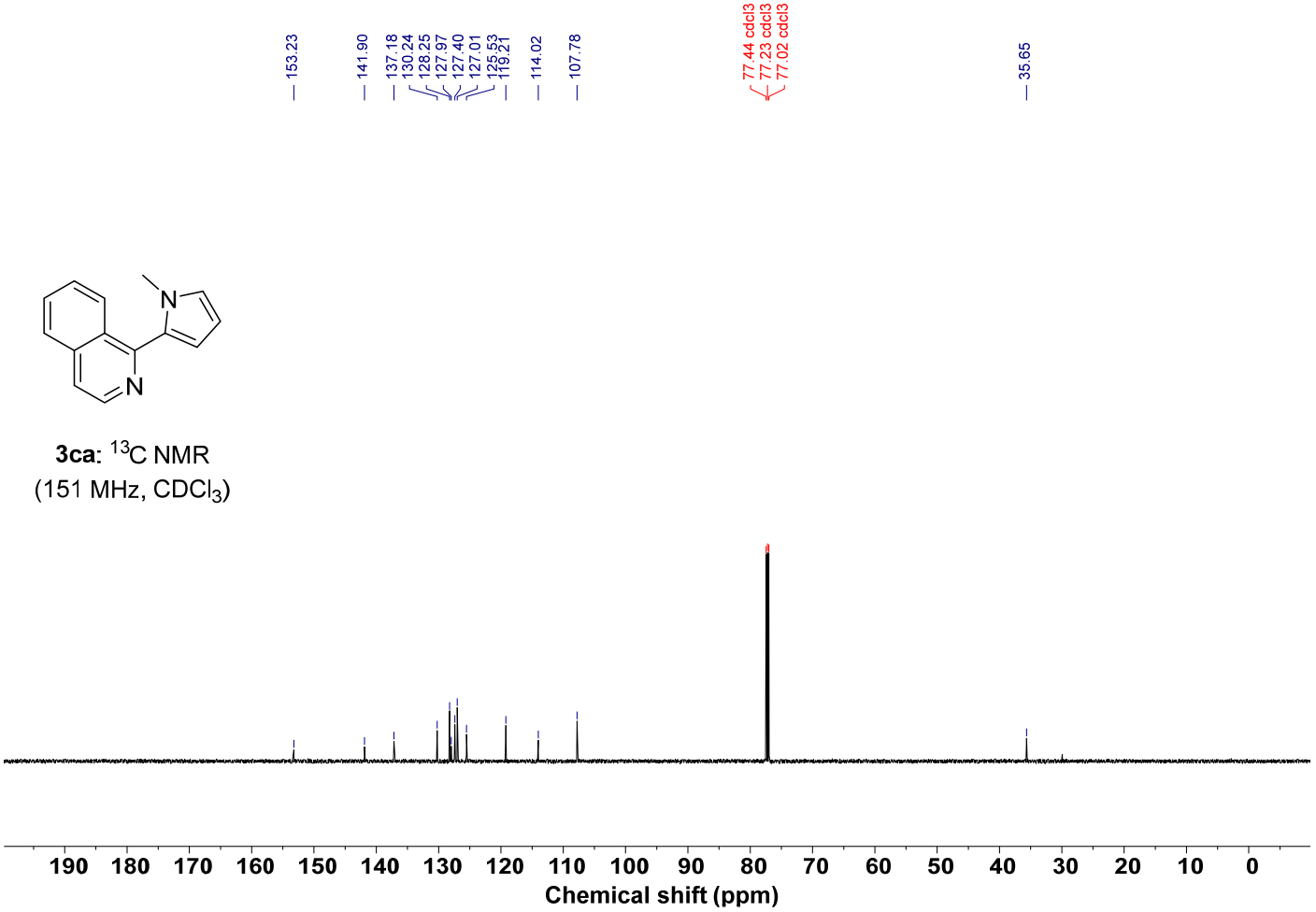

Supplementary Fig.14 $^{13}C\{^{1}H\}$ NMR (151 MHz, $CDCl_3$) spectrum of 3ca.

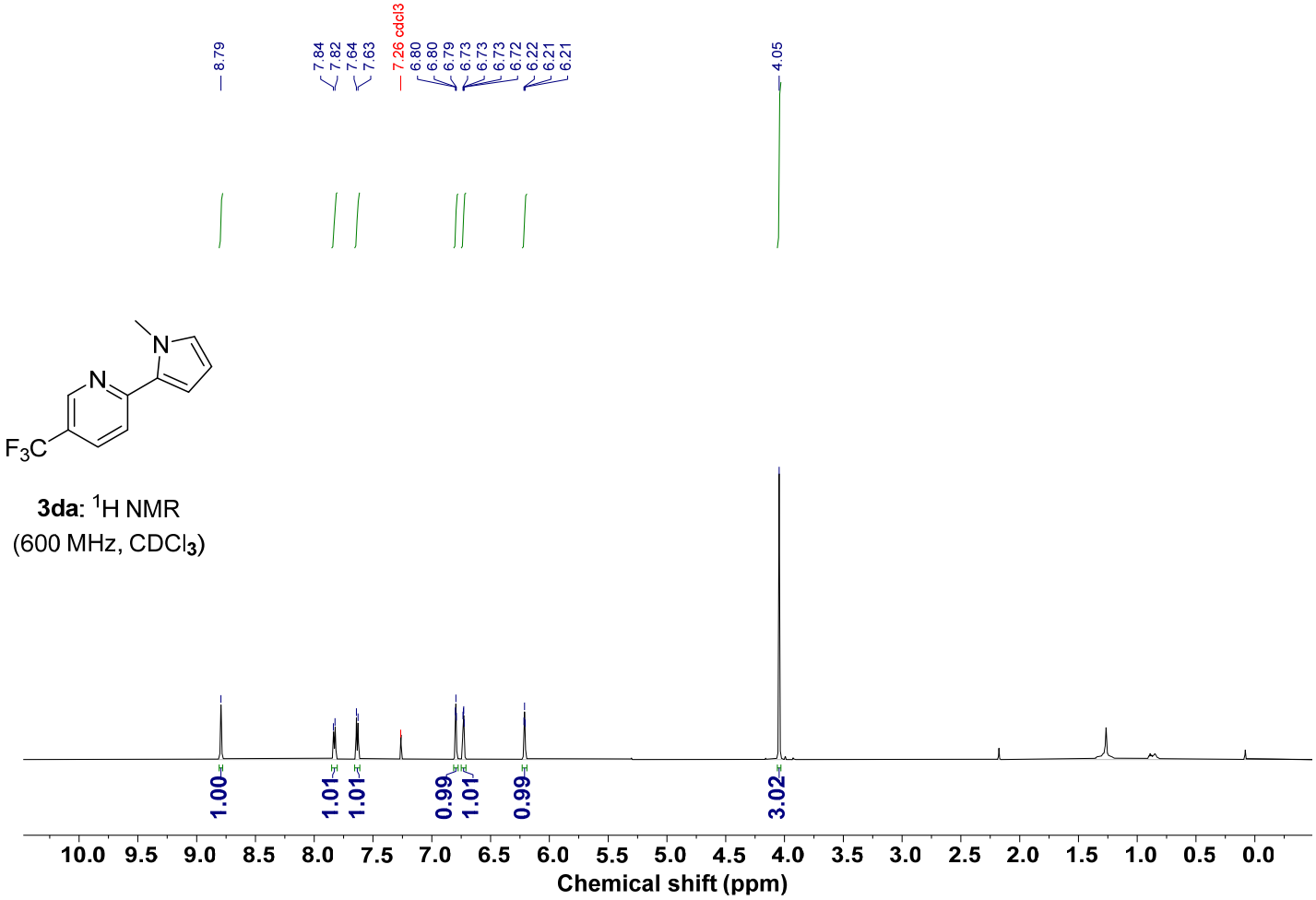

Supplementary Fig. 15 ^{1}H NMR (600 MHz, $CDCl_3$) spectrum of 3da.

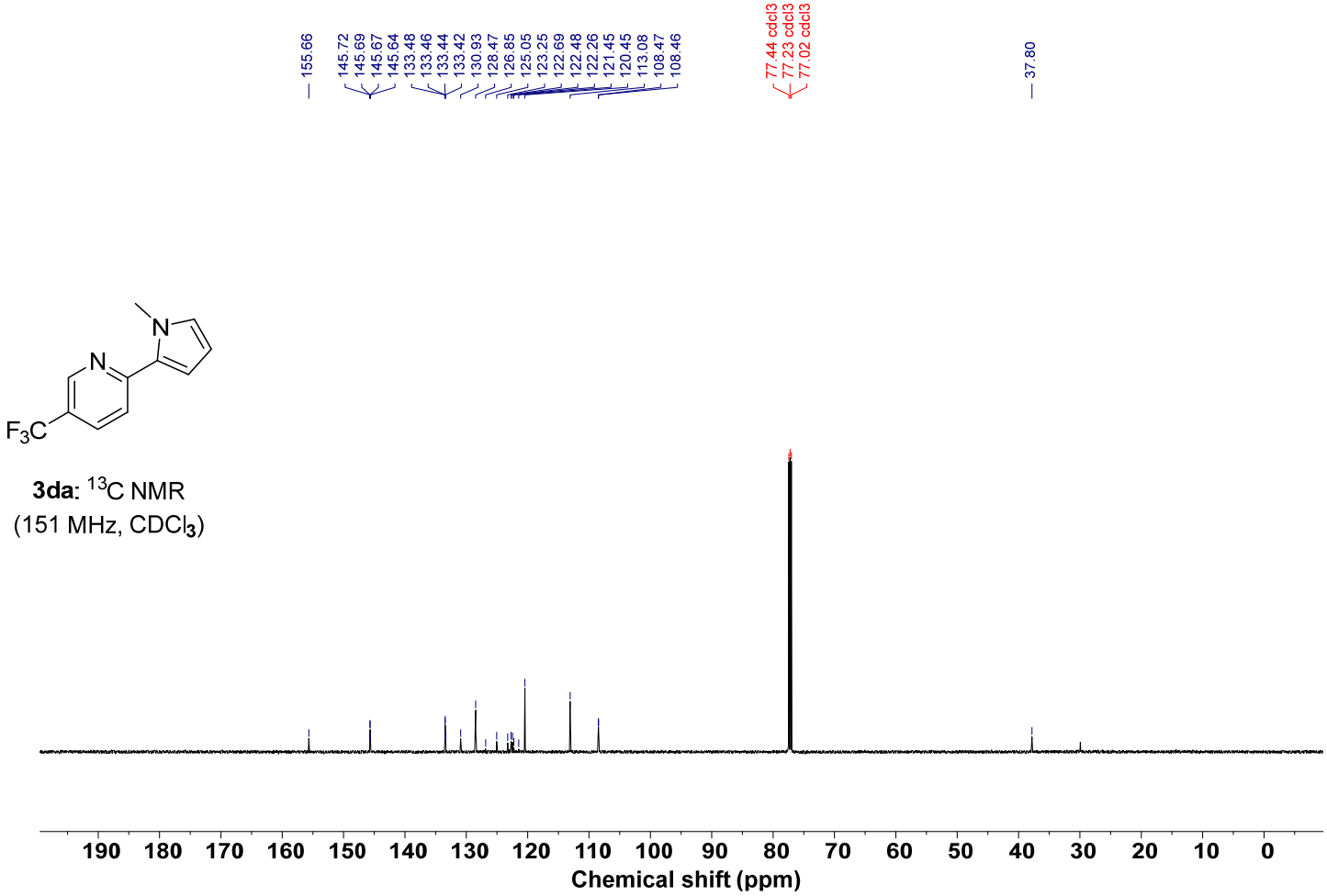

Supplementary Fig. 16 $^{13}C\{^{1}H\}$ NMR (151 MHz, $CDCl_3$) spectrum of 3da.

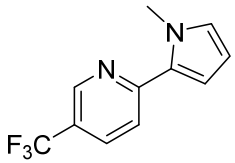

3da: ^{19}F NMR
(564 MHz, $CDCl_3$)

Supplementary Fig. 17 $^{19}F\{^1H\}$ NMR (564 MHz, $CDCl_3$) spectrum of 3da.

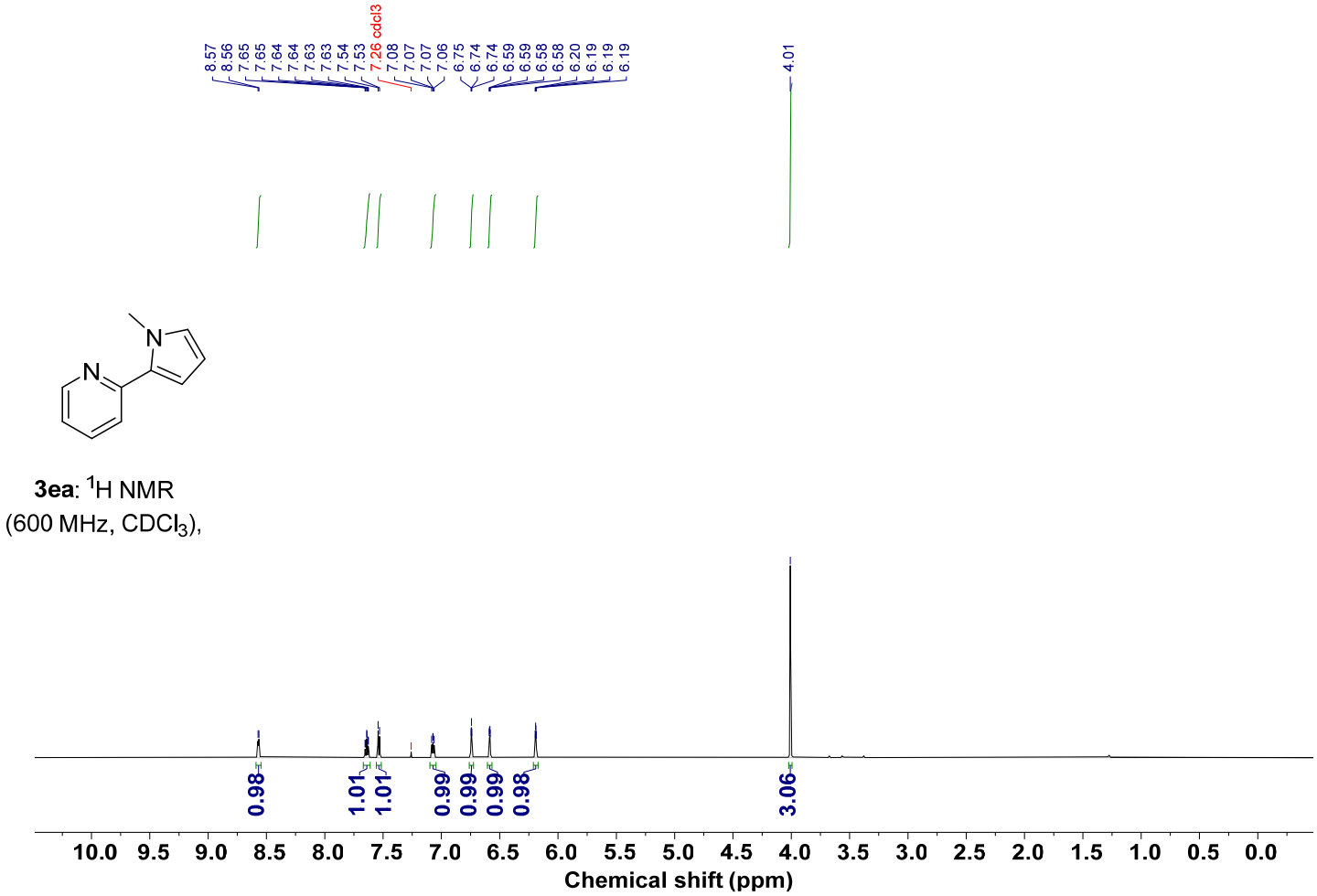

Supplementary Fig. 18 ^{1}H NMR (600 MHz, $CDCl_3$) spectrum of 3ea.

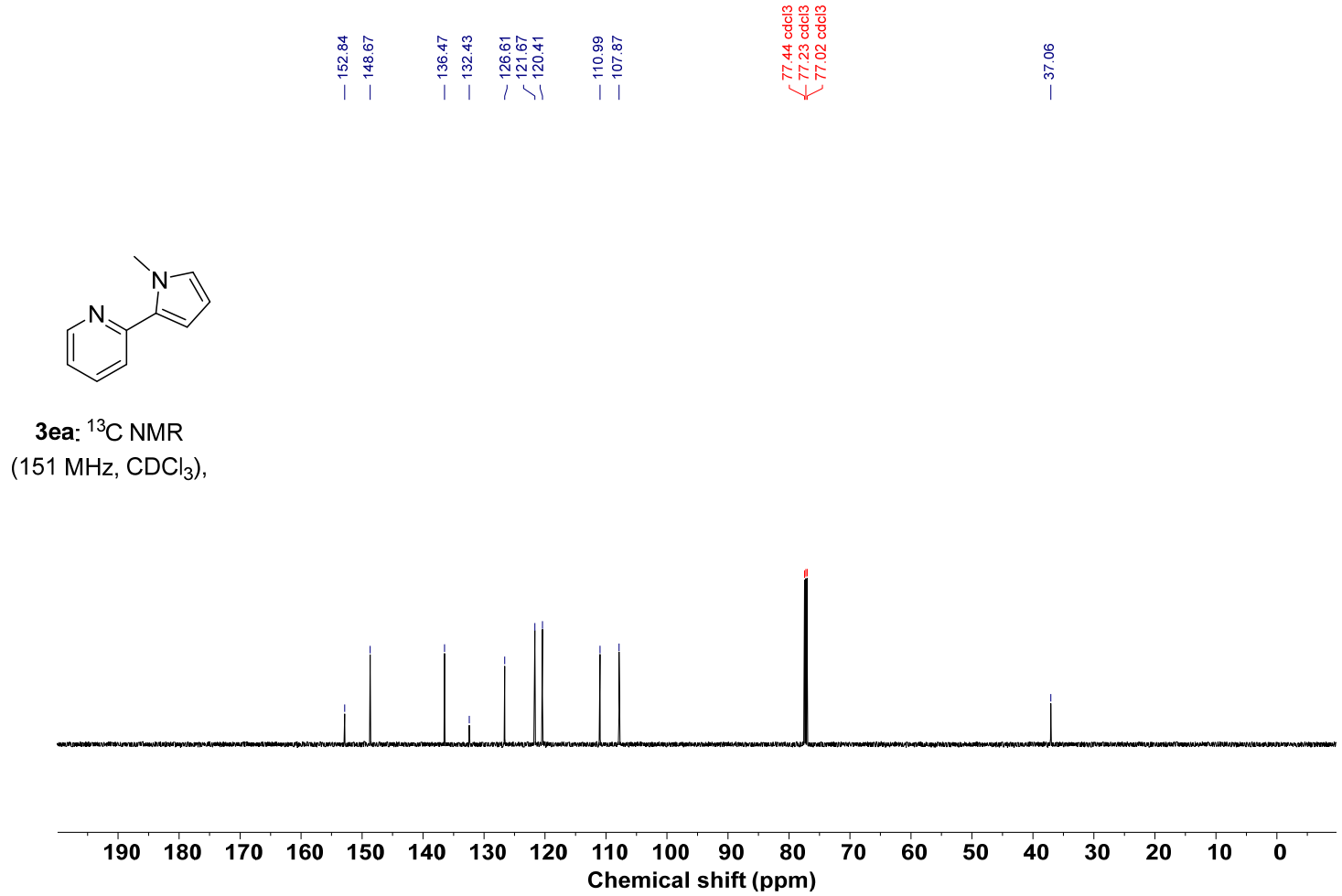

Supplementary Fig. 19 $^{13}C\{^{1}H\}$ NMR (151 MHz, $CDCl_3$) spectrum of 3ea.

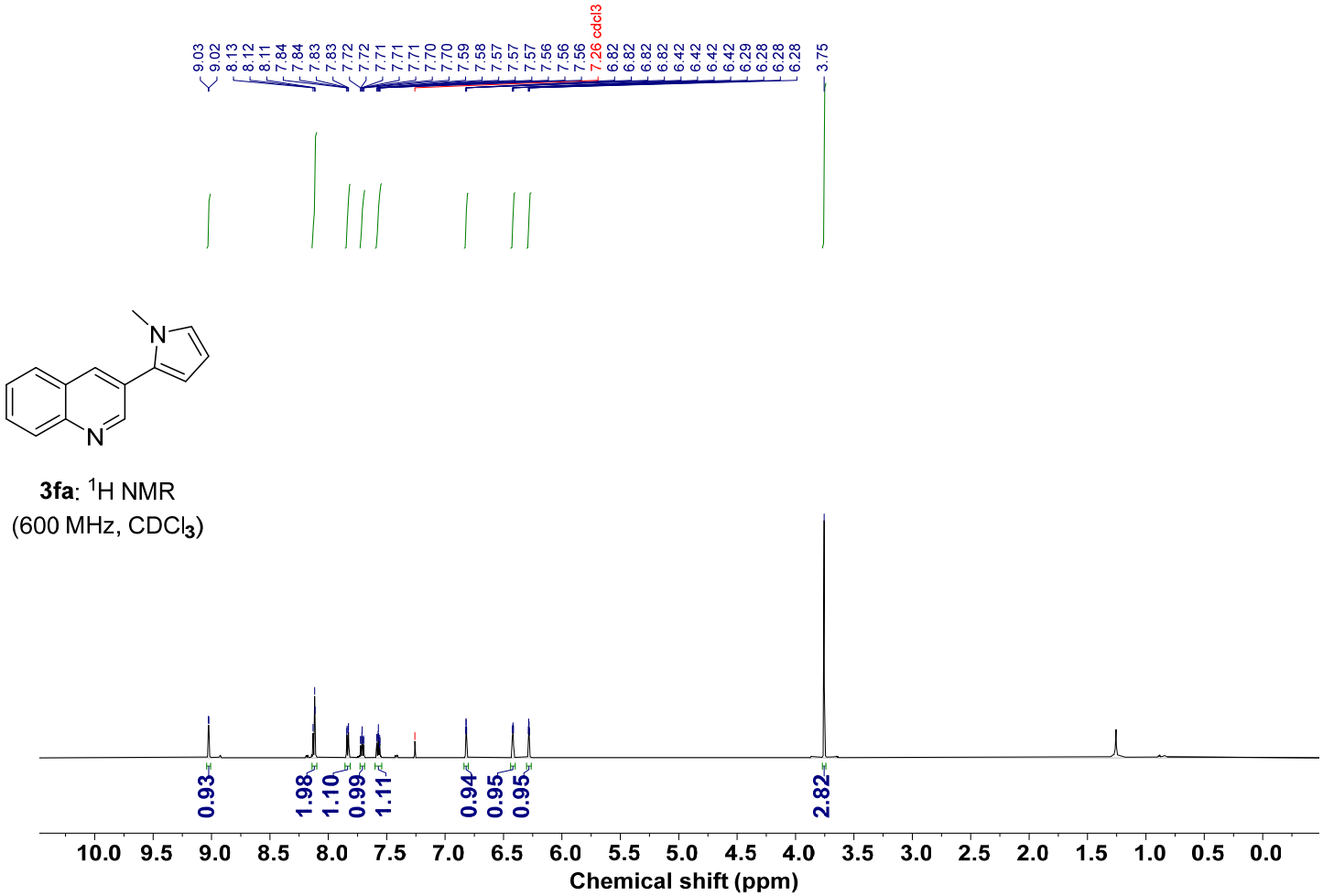

Supplementary Fig. 20 ^{1}H NMR (600 MHz, $CDCl_3$) spectrum of 3fa.

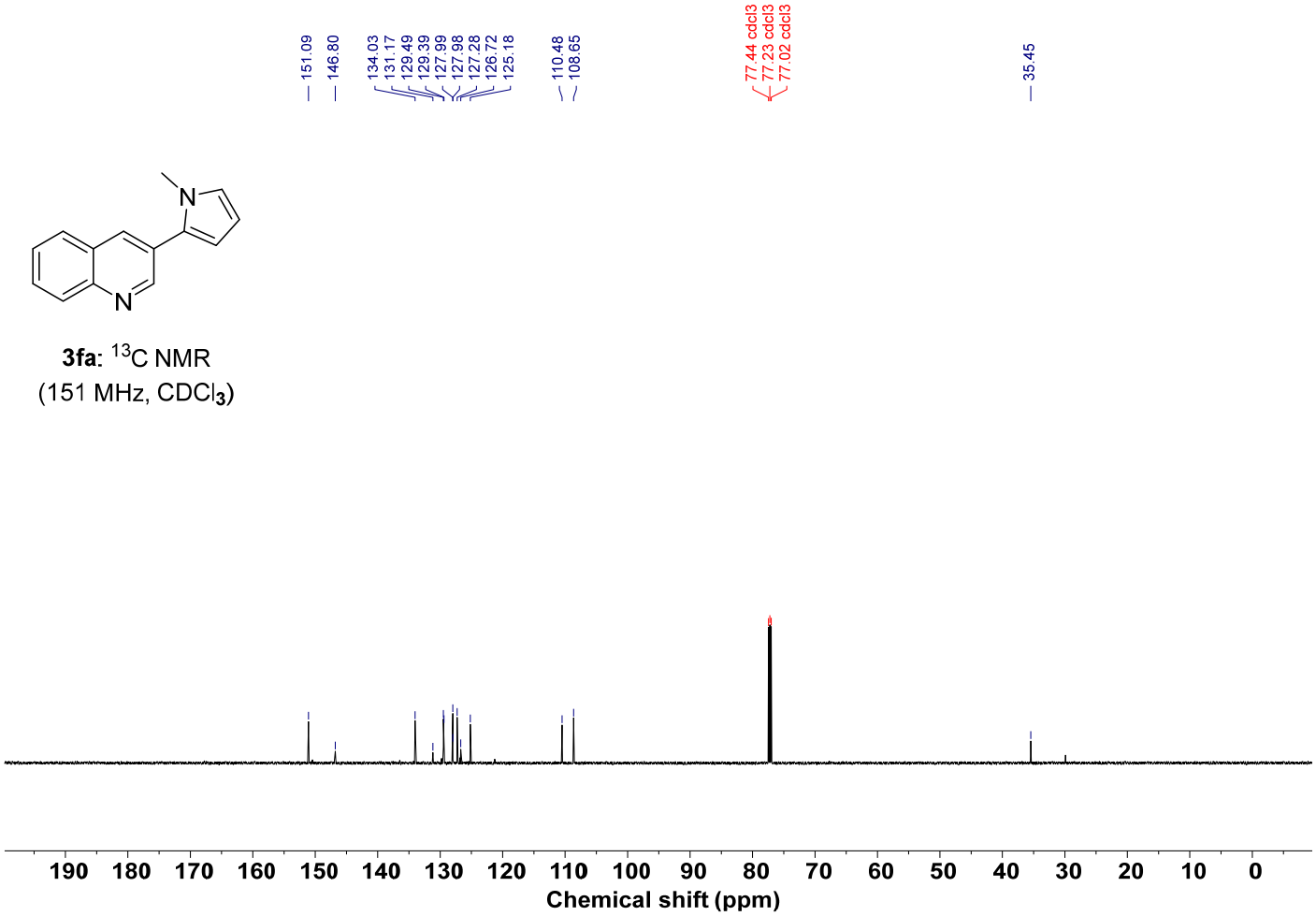

3fa: ^{13}C NMR
(151 MHz, $CDCl_3$)

Supplementary Fig. 21 $^{13}C\{^1H\}$ NMR (151 MHz, $CDCl_3$) spectrum of 3fa.

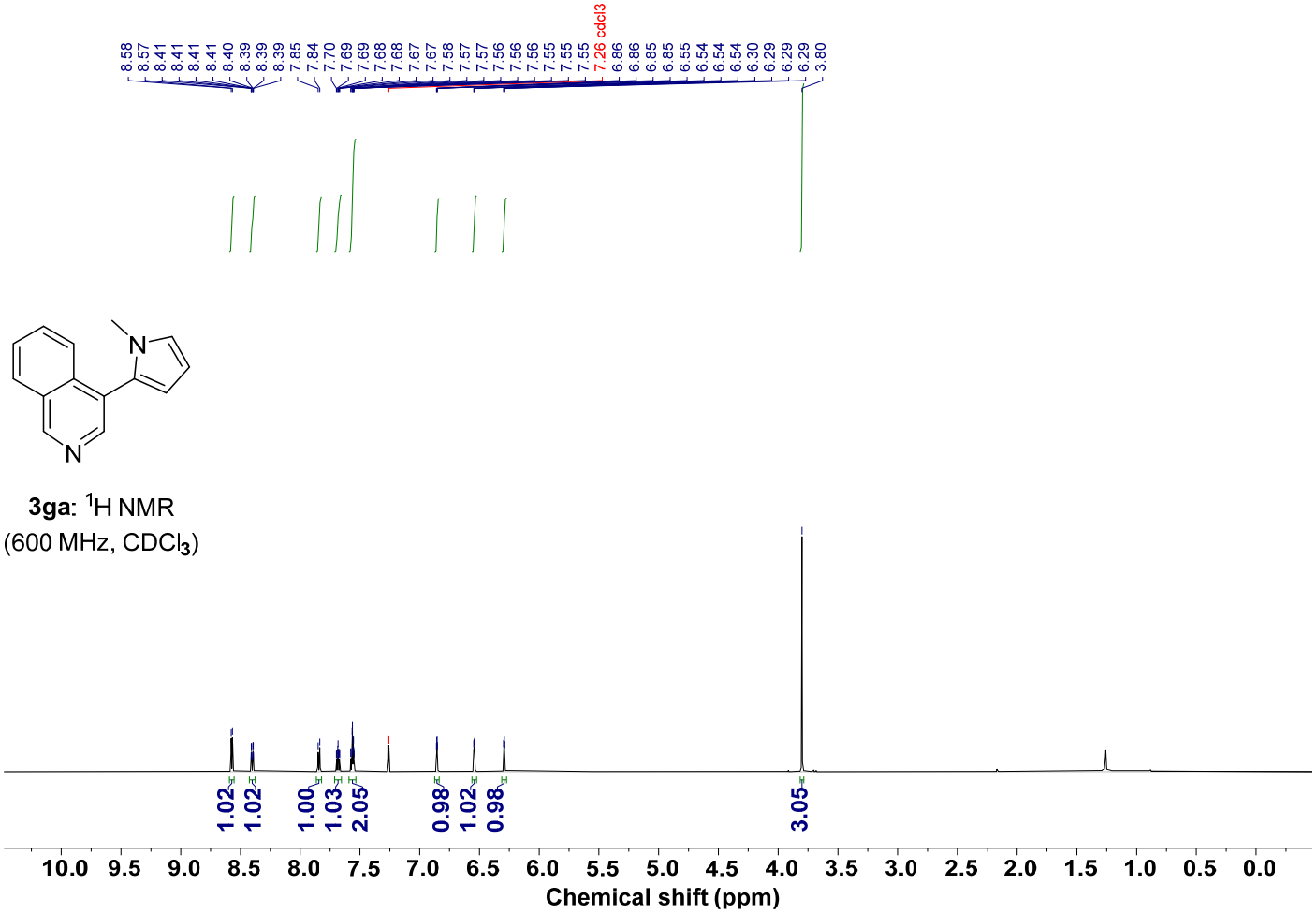

Supplementary Fig. 22 ^{1}H NMR (600 MHz, $CDCl_3$) spectrum of 3ga.

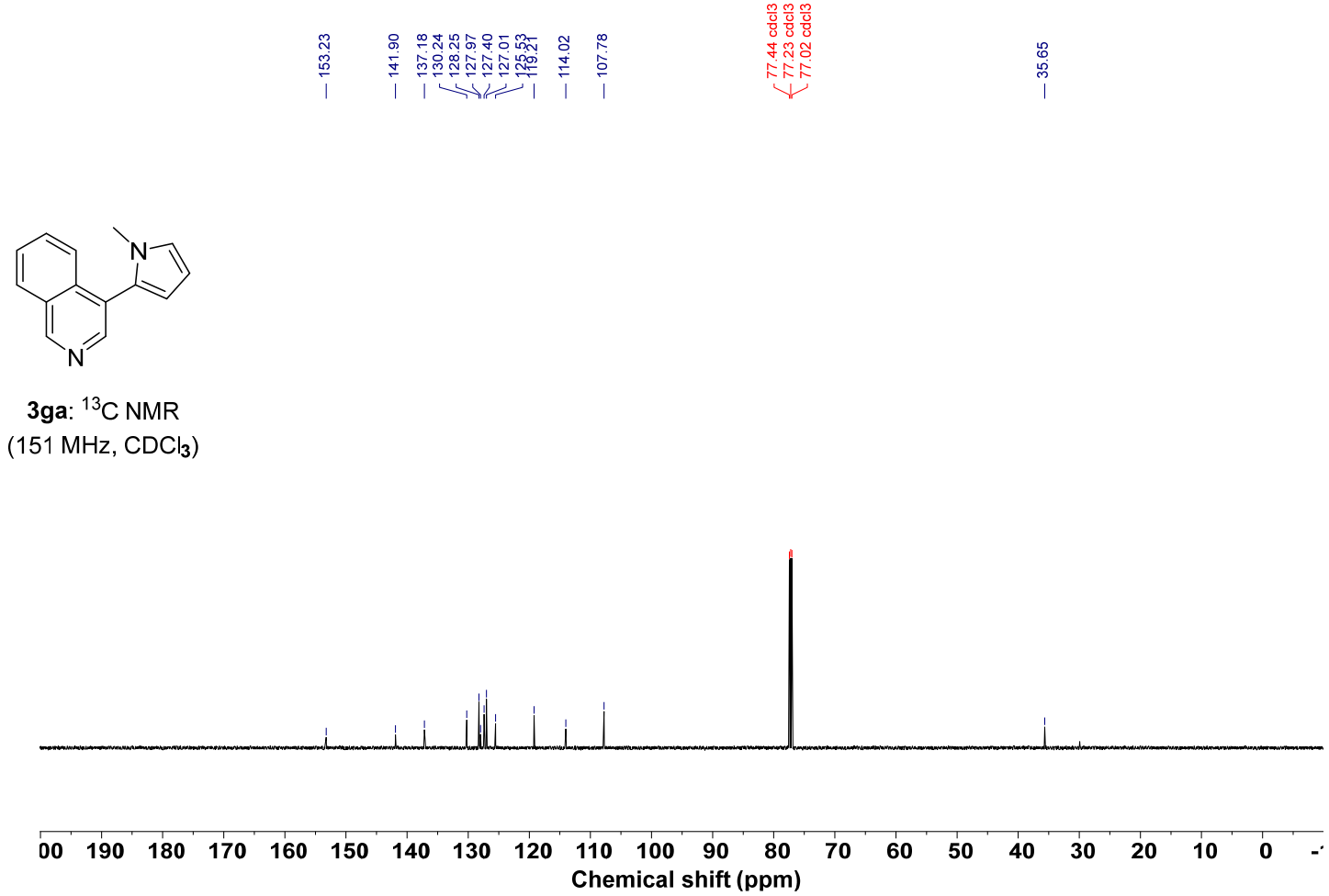

Supplementary Fig. 23 $^{13}C\{^{1}H\}$ NMR (151 MHz, $CDCl_3$) spectrum of 3ga.

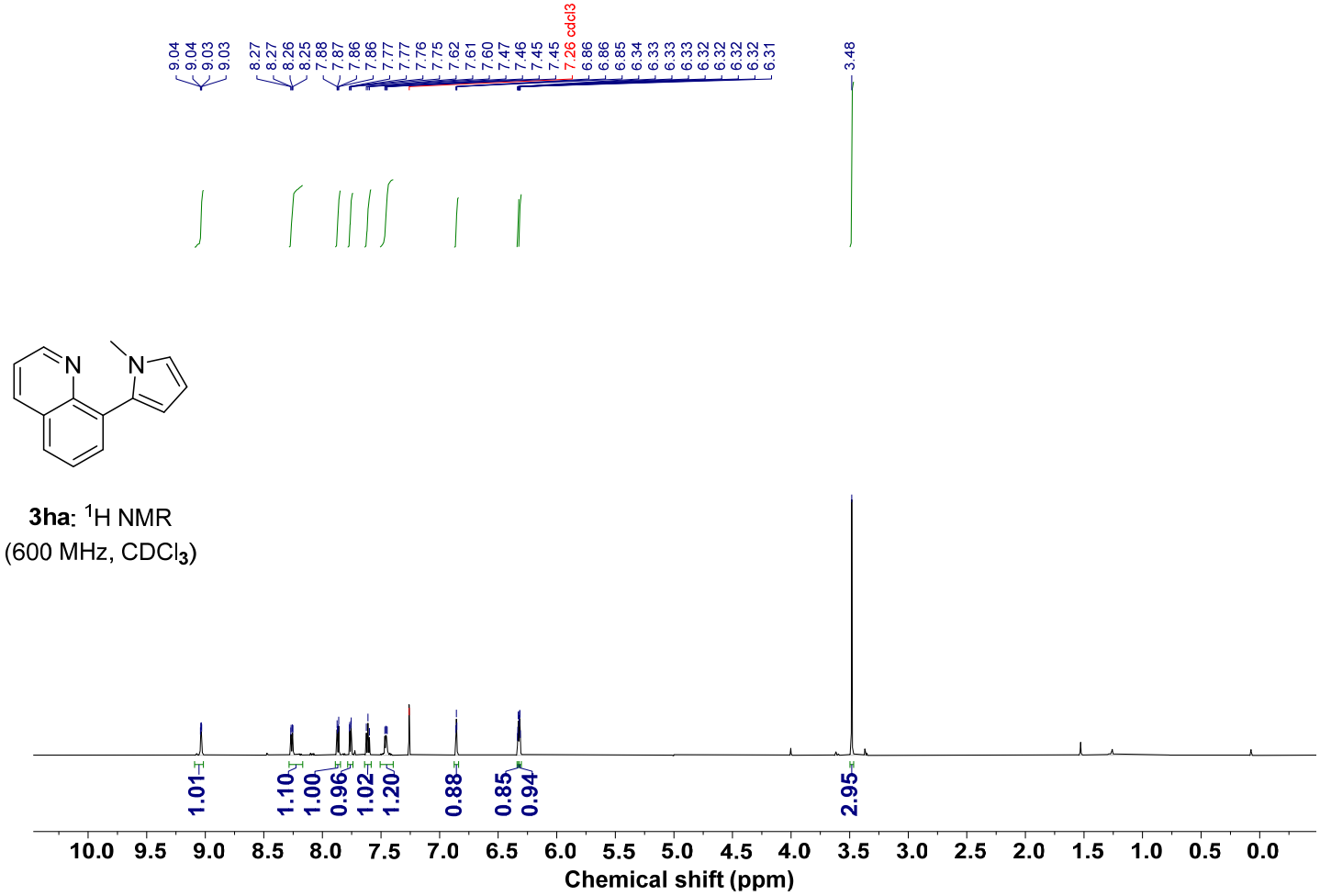

Supplementary Fig. 24 ^{1}H NMR (600 MHz, $CDCl_3$) spectrum of 3ha.

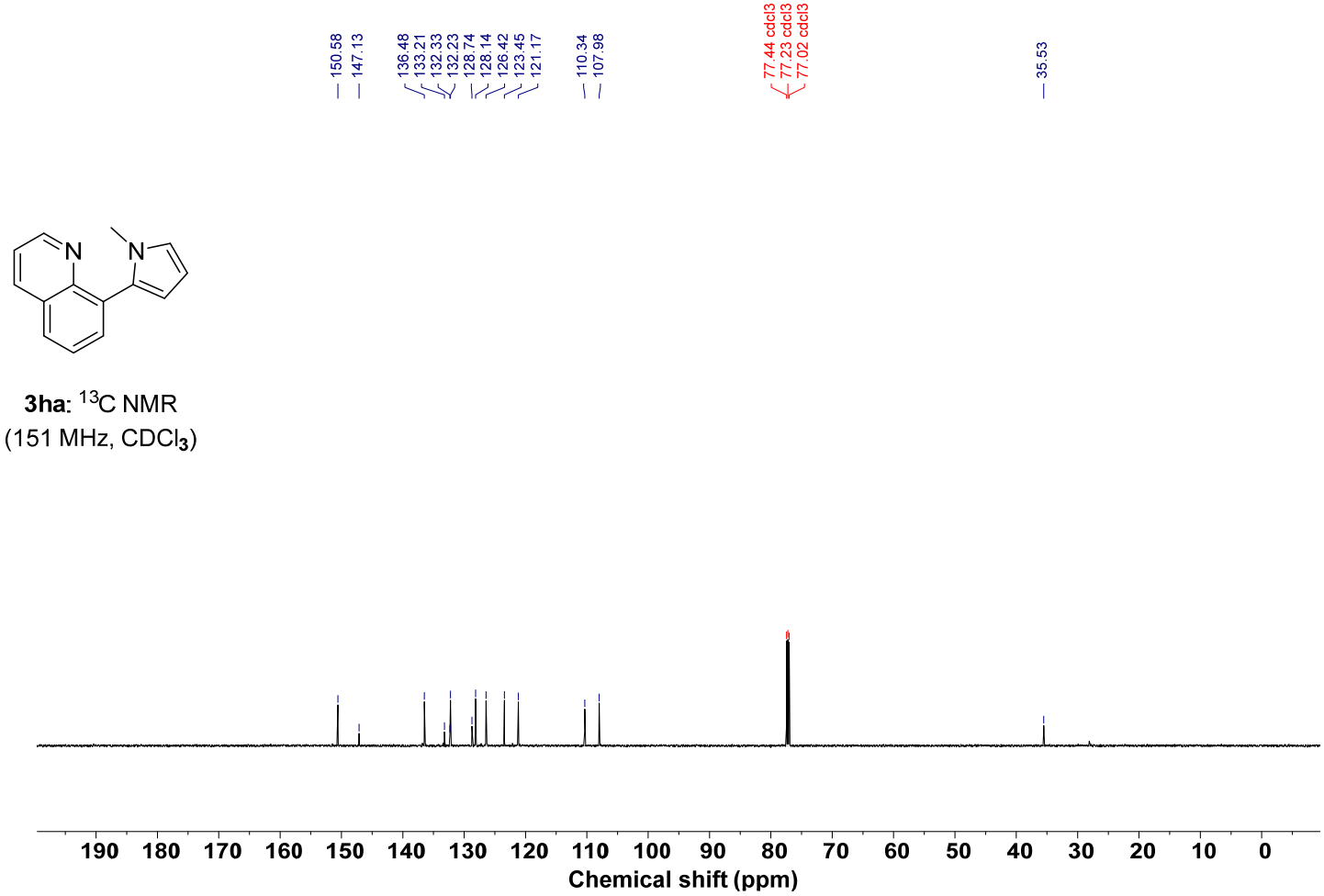

3ha: ^{13}C NMR
(151 MHz, $CDCl_3$)

Supplementary Fig. 25 $^{13}C\{^1H\}$ NMR (151 MHz, $CDCl_3$) spectrum of 3ha.

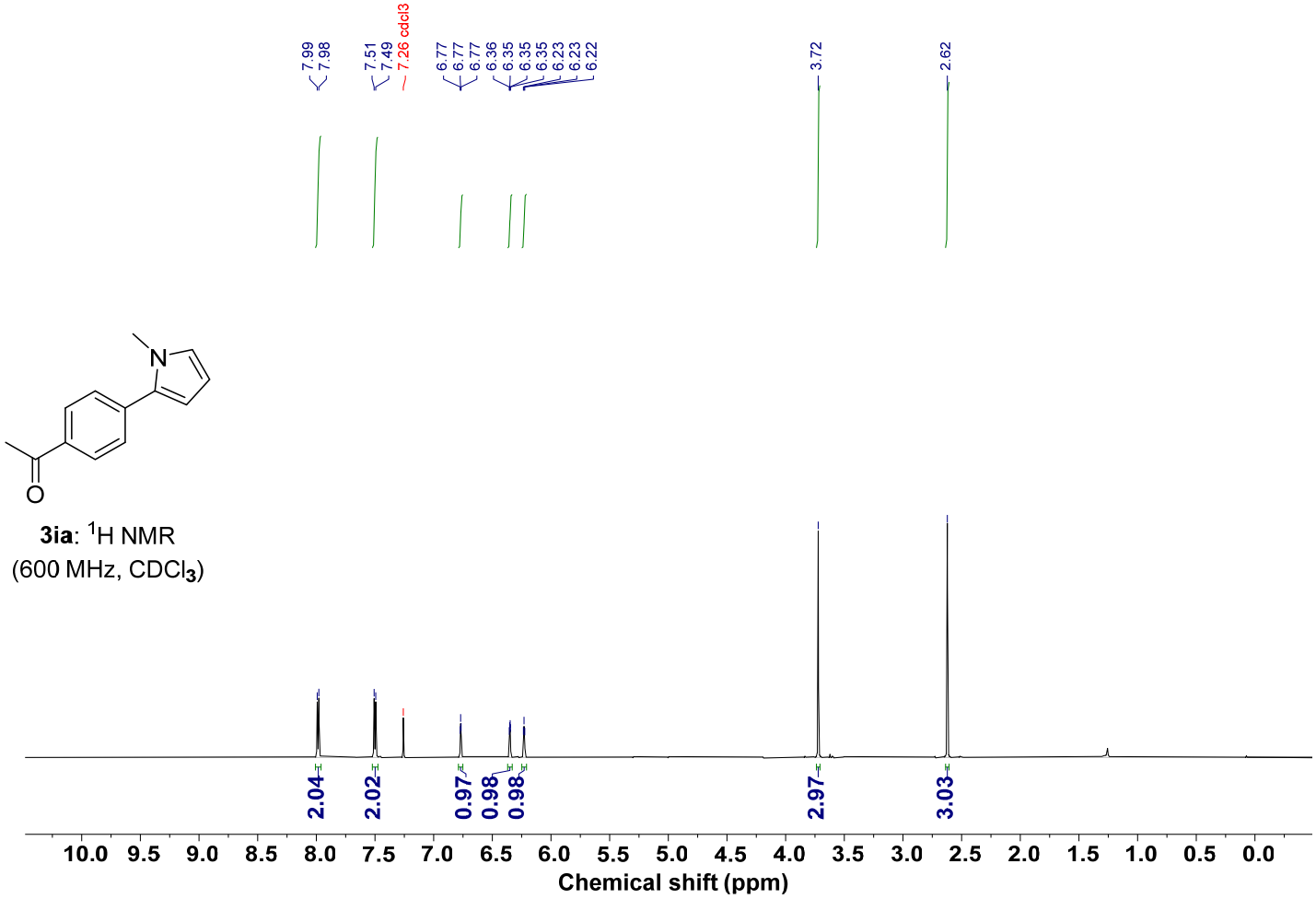

Supplementary Fig. 26 ^{1}H NMR (600 MHz, $CDCl_3$) spectrum of 3ia.

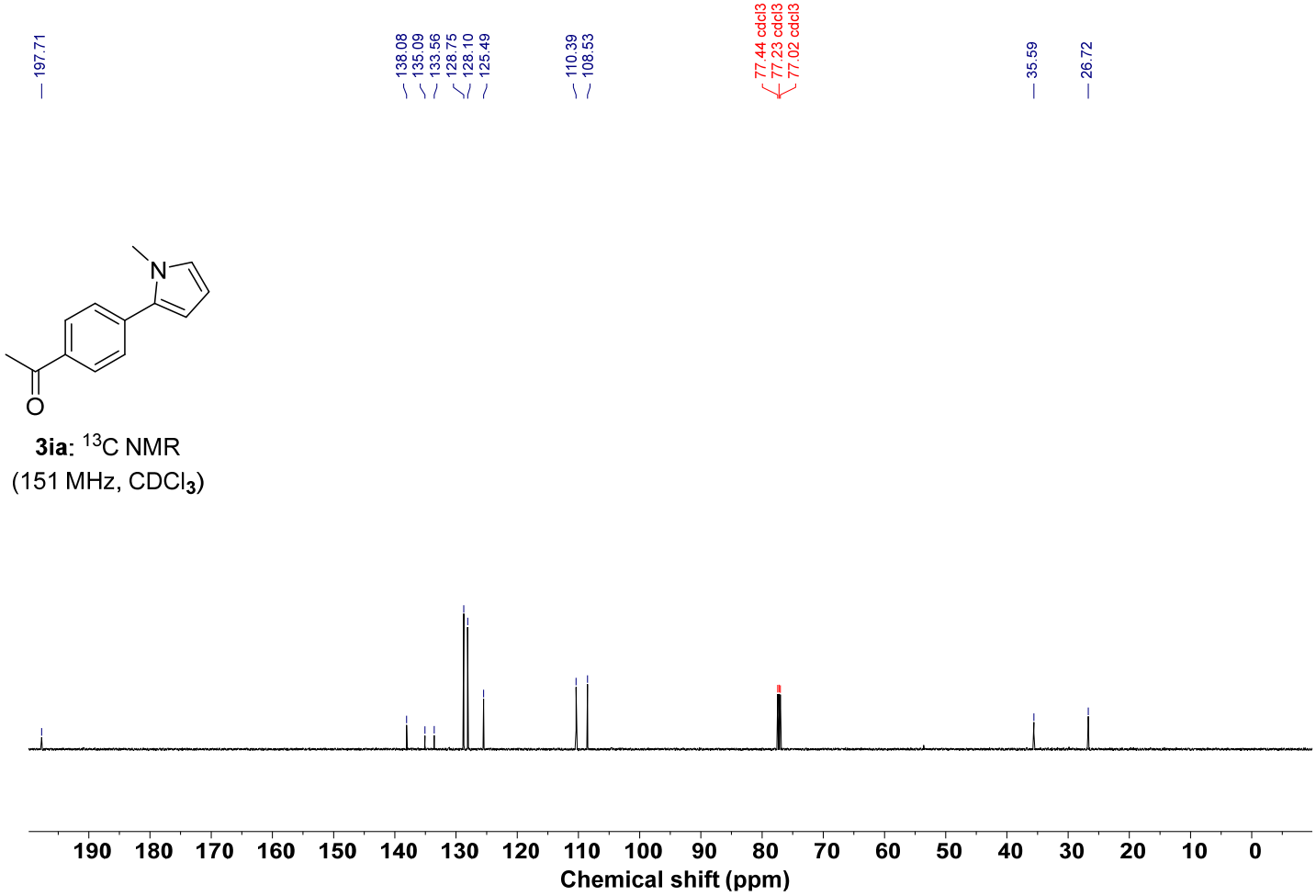

Supplementary Fig. 27 $^{13}C\{^{1}H\}$ NMR (151 MHz, $CDCl_3$) spectrum of 3ia.

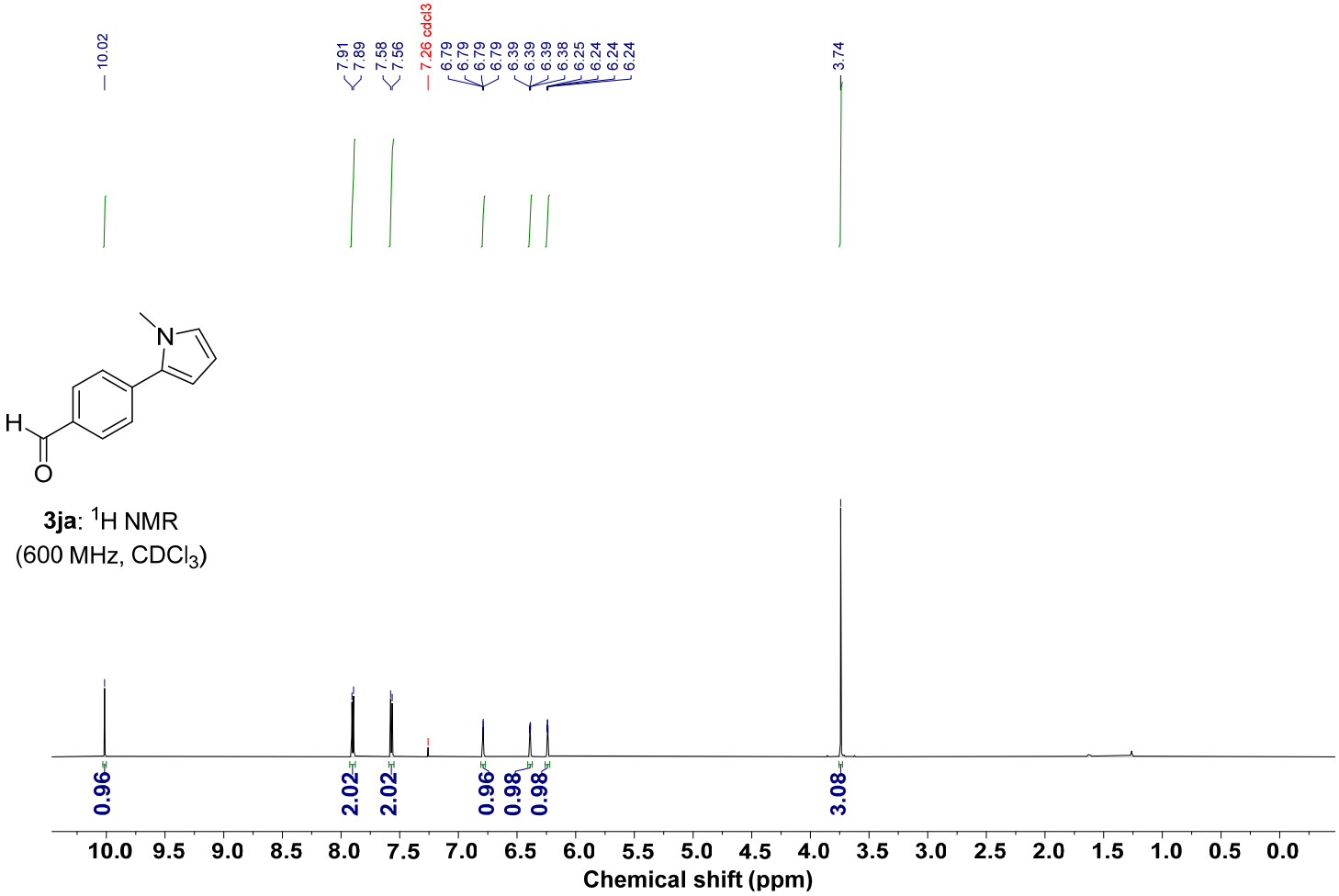

Supplementary Fig. 28 ^{1}H NMR (600 MHz, $CDCl_3$) spectrum of 3ja.

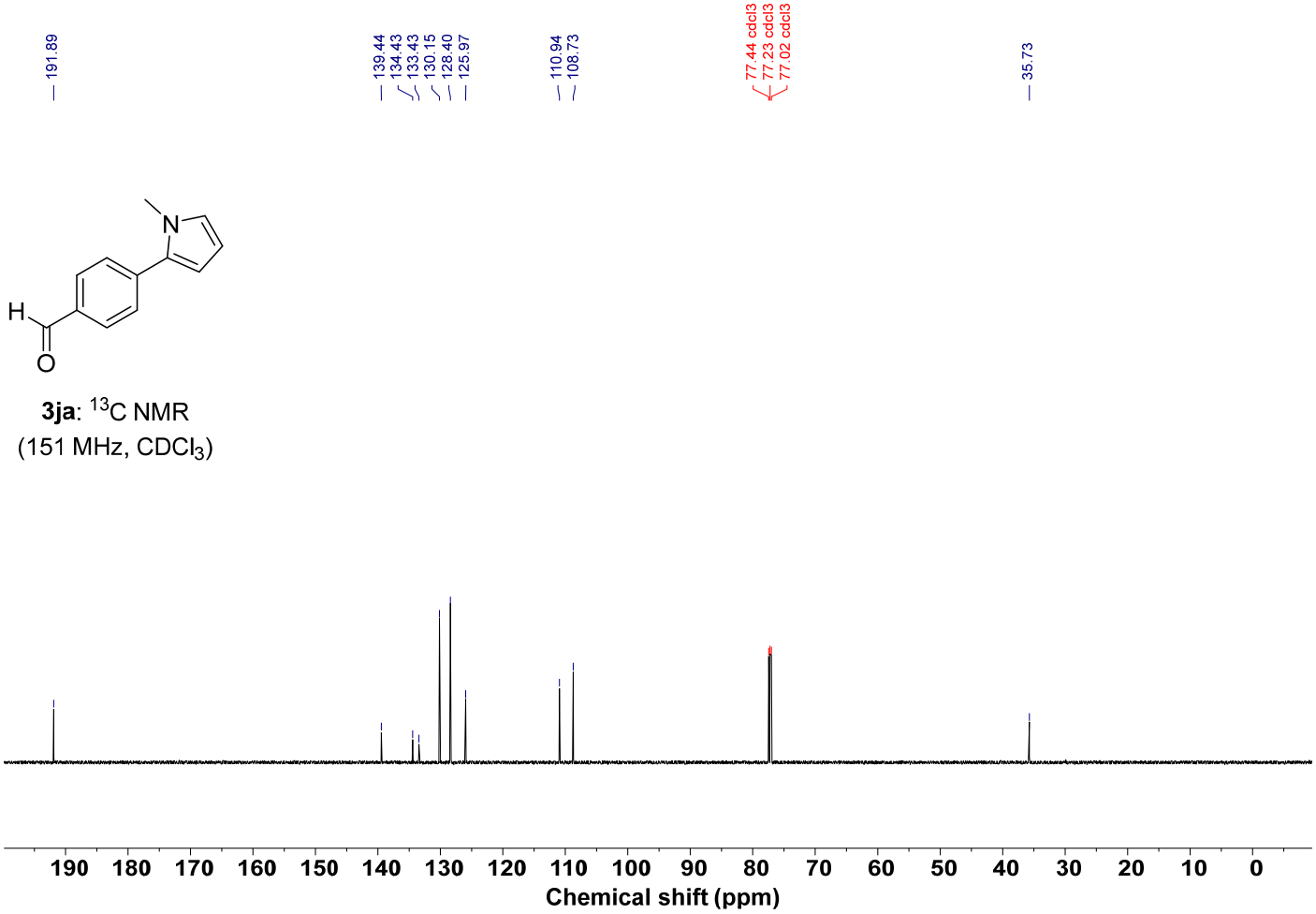

Supplementary Fig. 29 $^{13}C\{^{1}H\}$ NMR (151 MHz, $CDCl_3$) spectrum of 3ja.

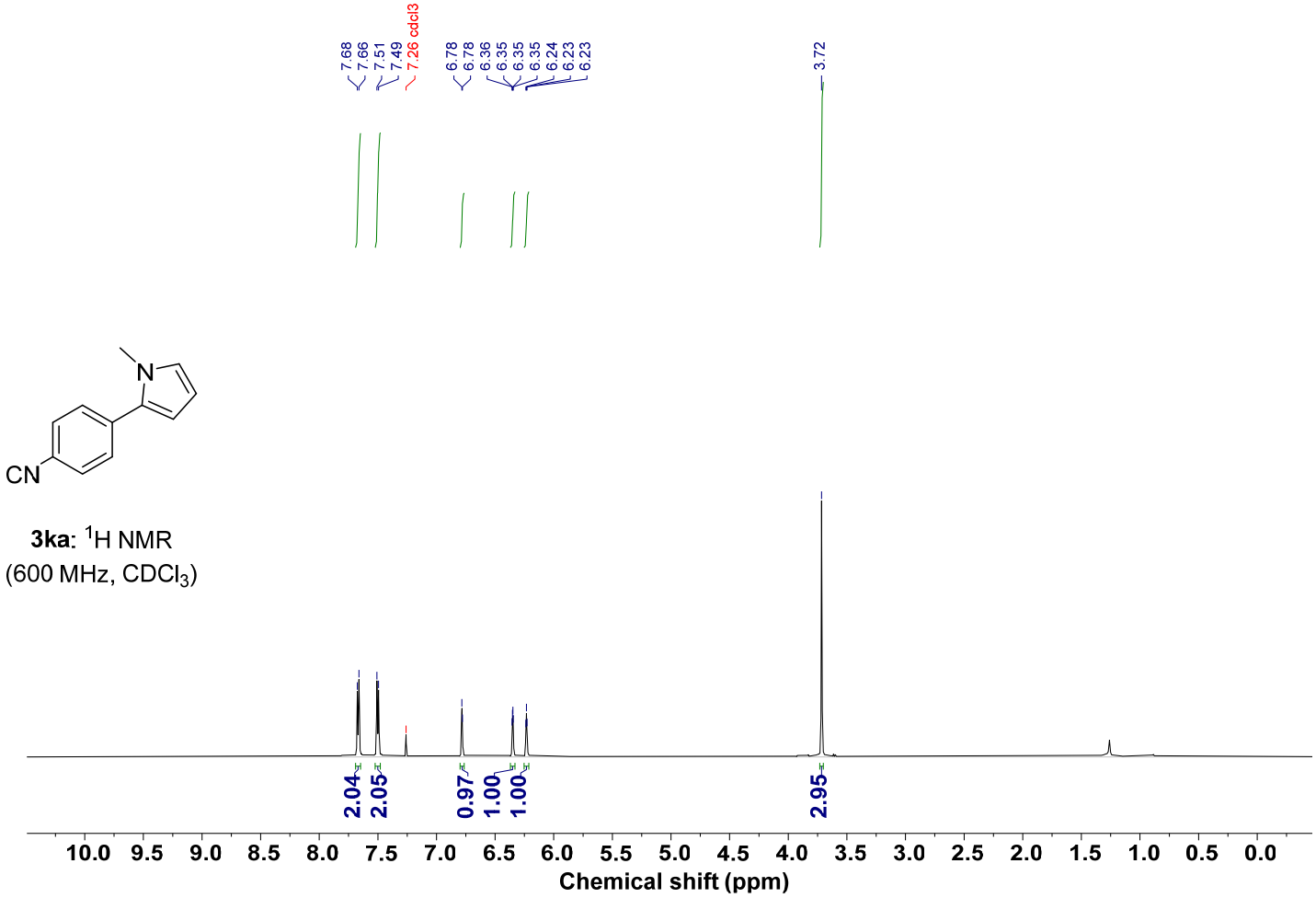

Supplementary Fig. 30 ^{1}H NMR (600 MHz, $CDCl_3$) spectrum of 3ka.

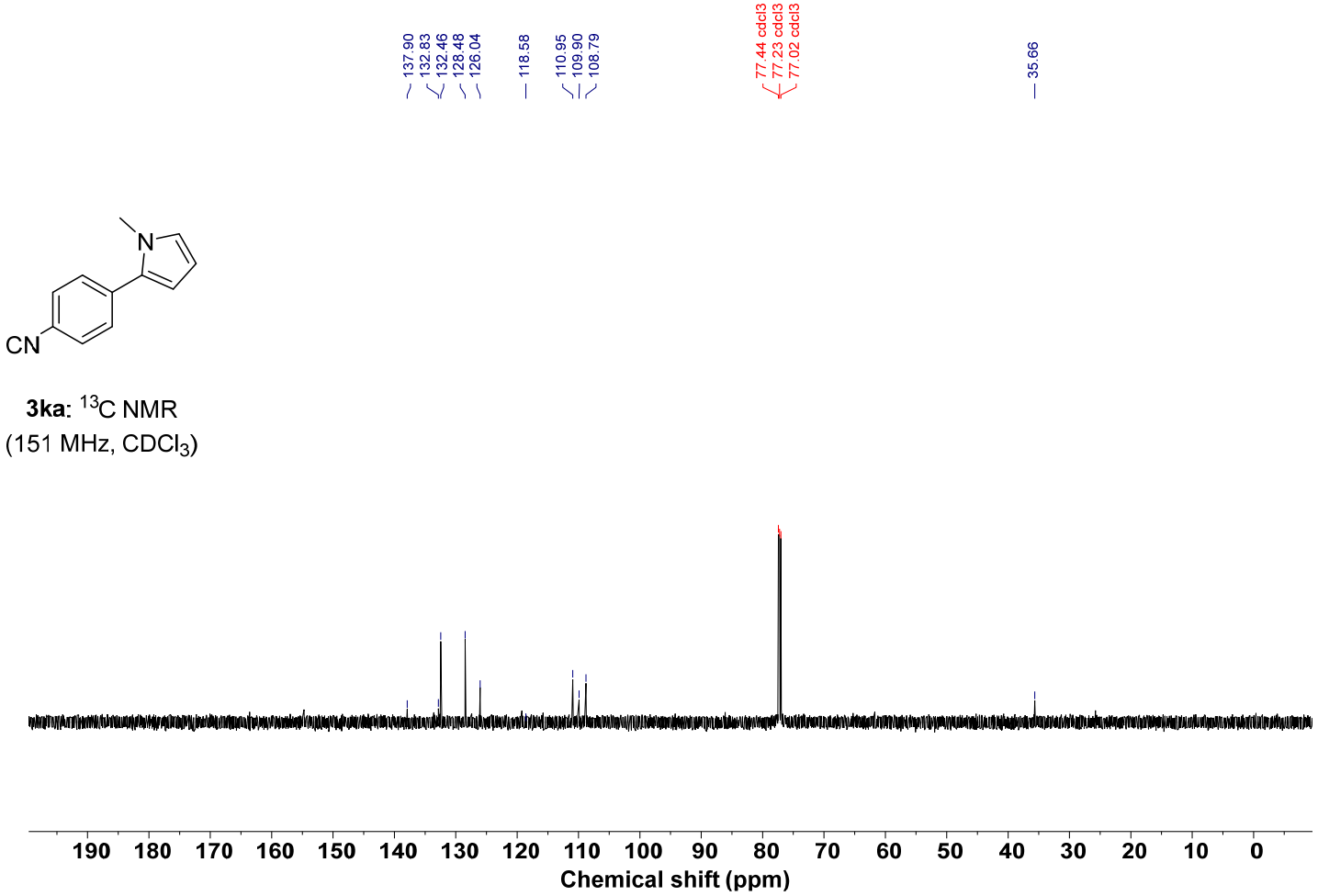

3ka: ^{13}C NMR
(151 MHz, $CDCl_3$)

Supplementary Fig. 31 $^{13}C\{^1H\}$ NMR (151 MHz, $CDCl_3$) spectrum of 3ka.

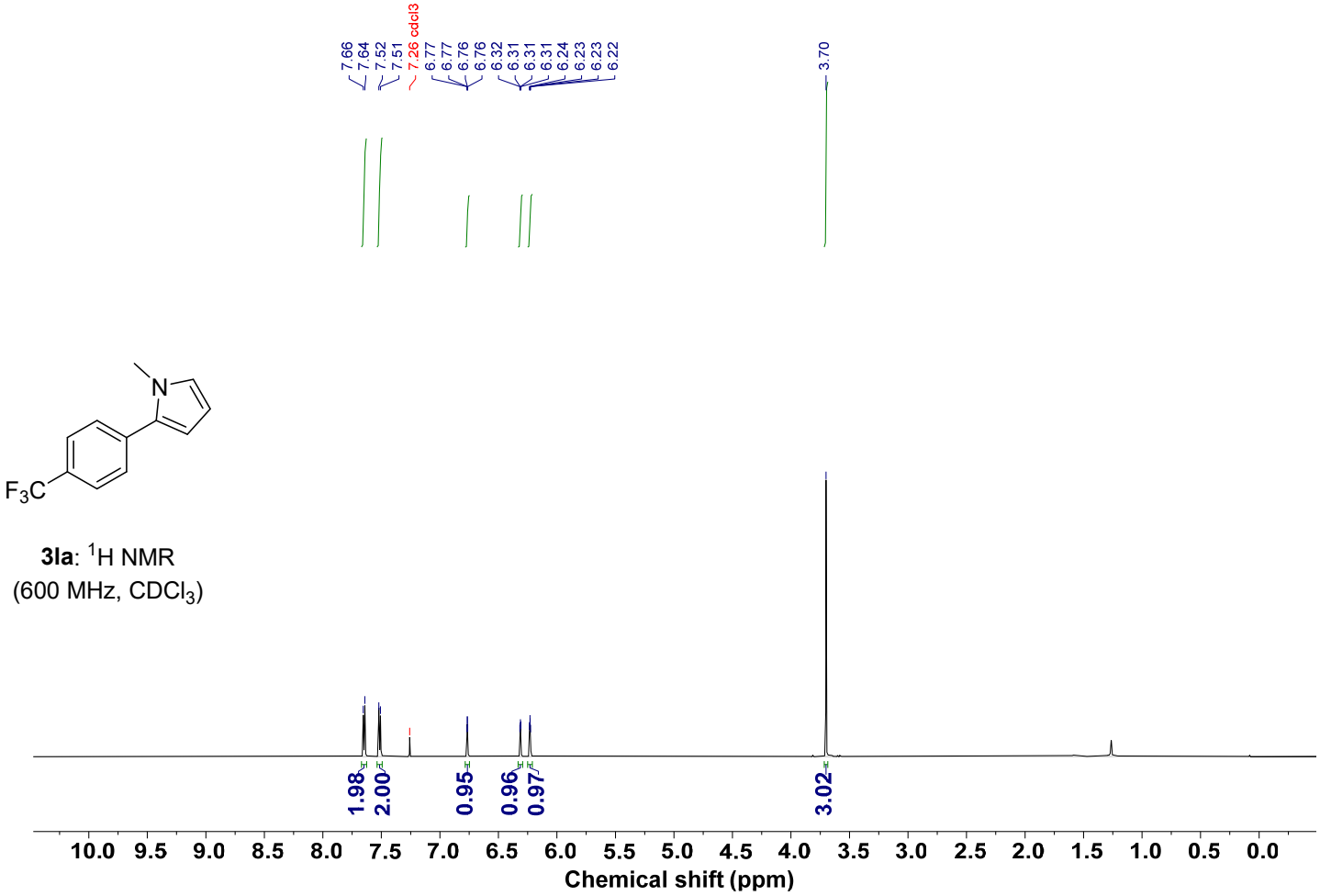

Supplementary Fig. 32 ^{1}H NMR (600 MHz, $CDCl_3$) spectrum of 3la.

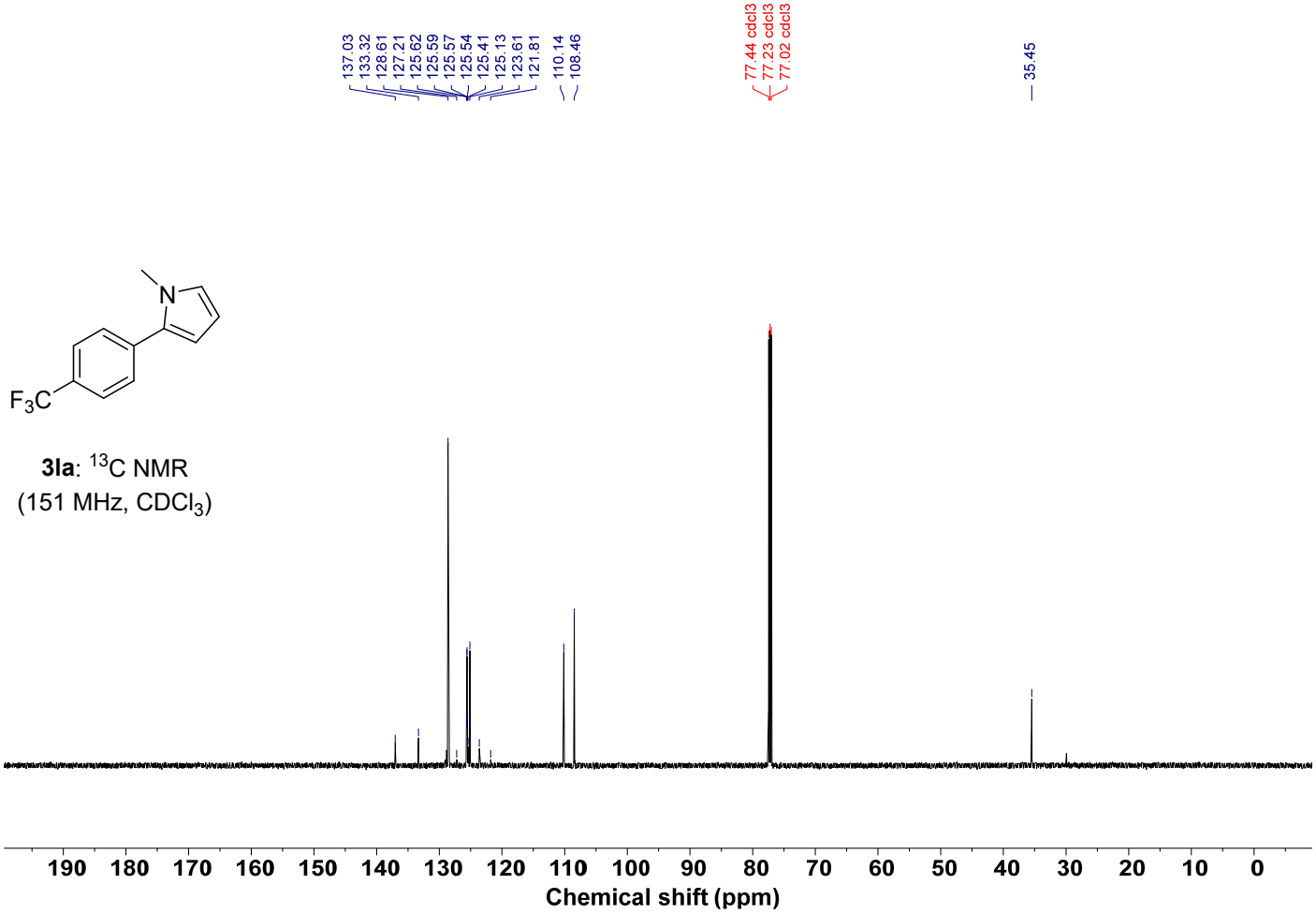

Supplementary Fig. 33 $^{13}C\{^{1}H\}$ NMR (151 MHz, $CDCl_3$) spectrum of 3la.

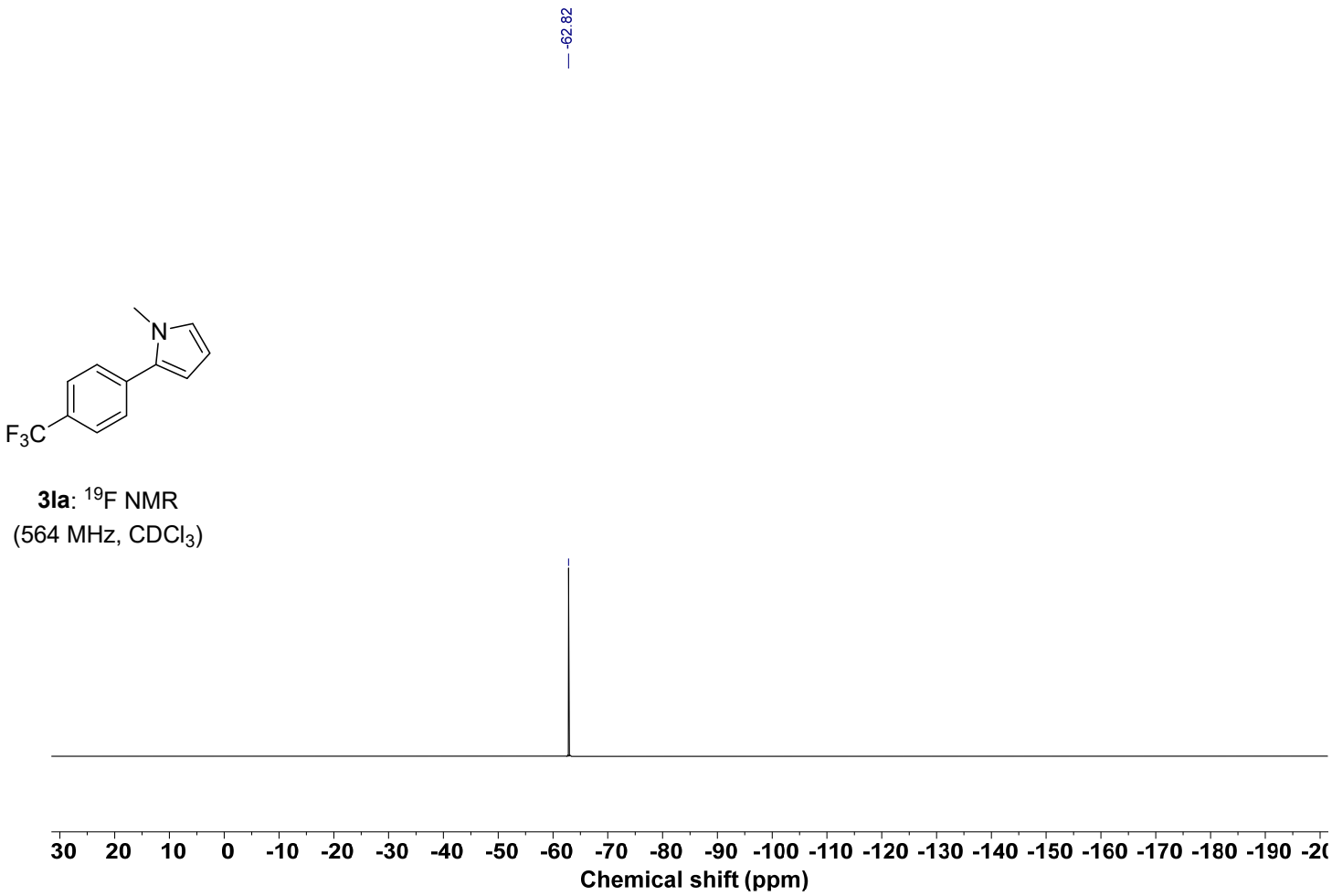

Supplementary Fig. 34 $^{19}F\{^{1}H\}$ NMR (564 MHz, $CDCl_3$) spectrum of 3la.

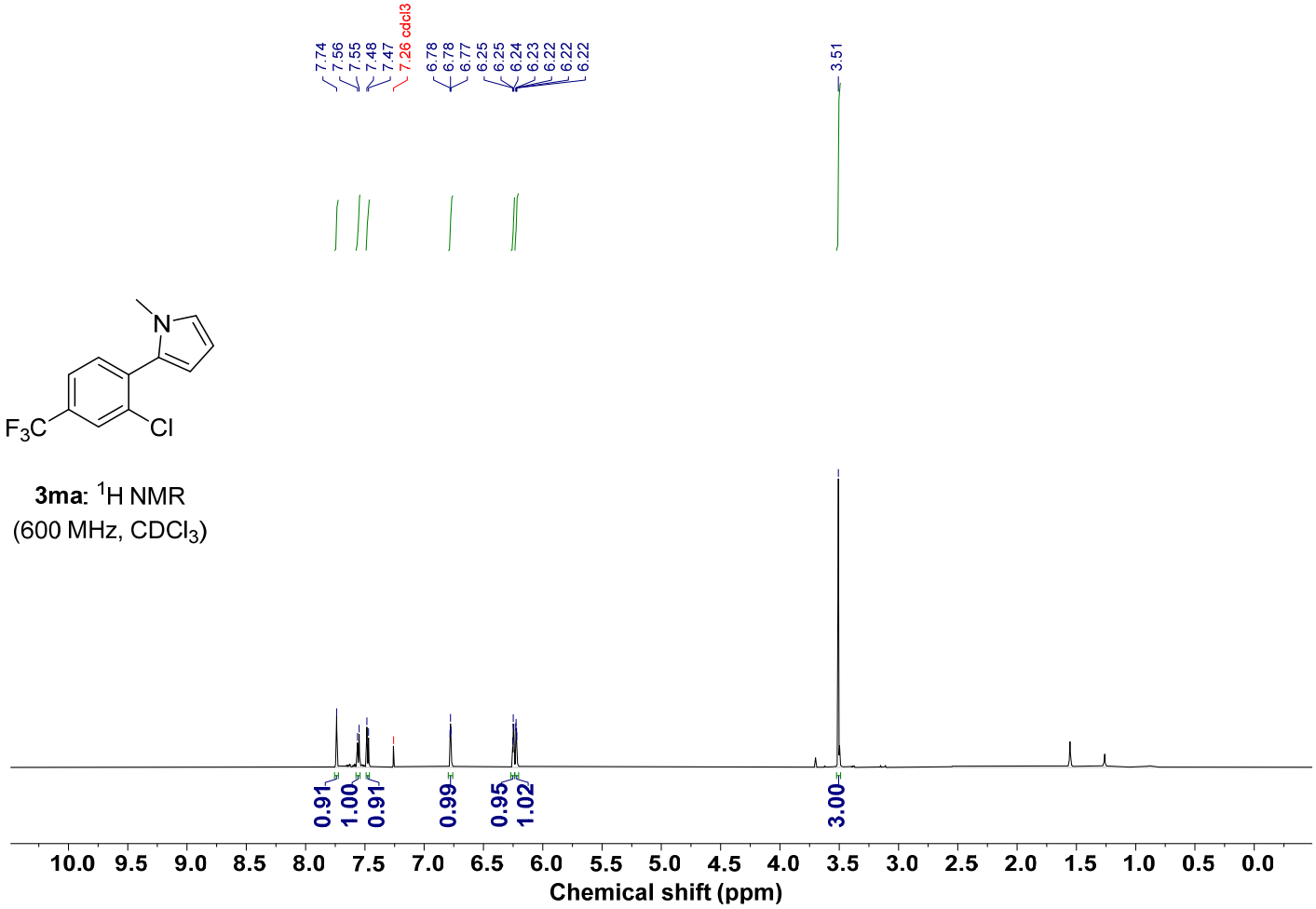

Supplementary Fig. 35 ^{1}H NMR (600 MHz, $CDCl_3$) spectrum of 3ma.

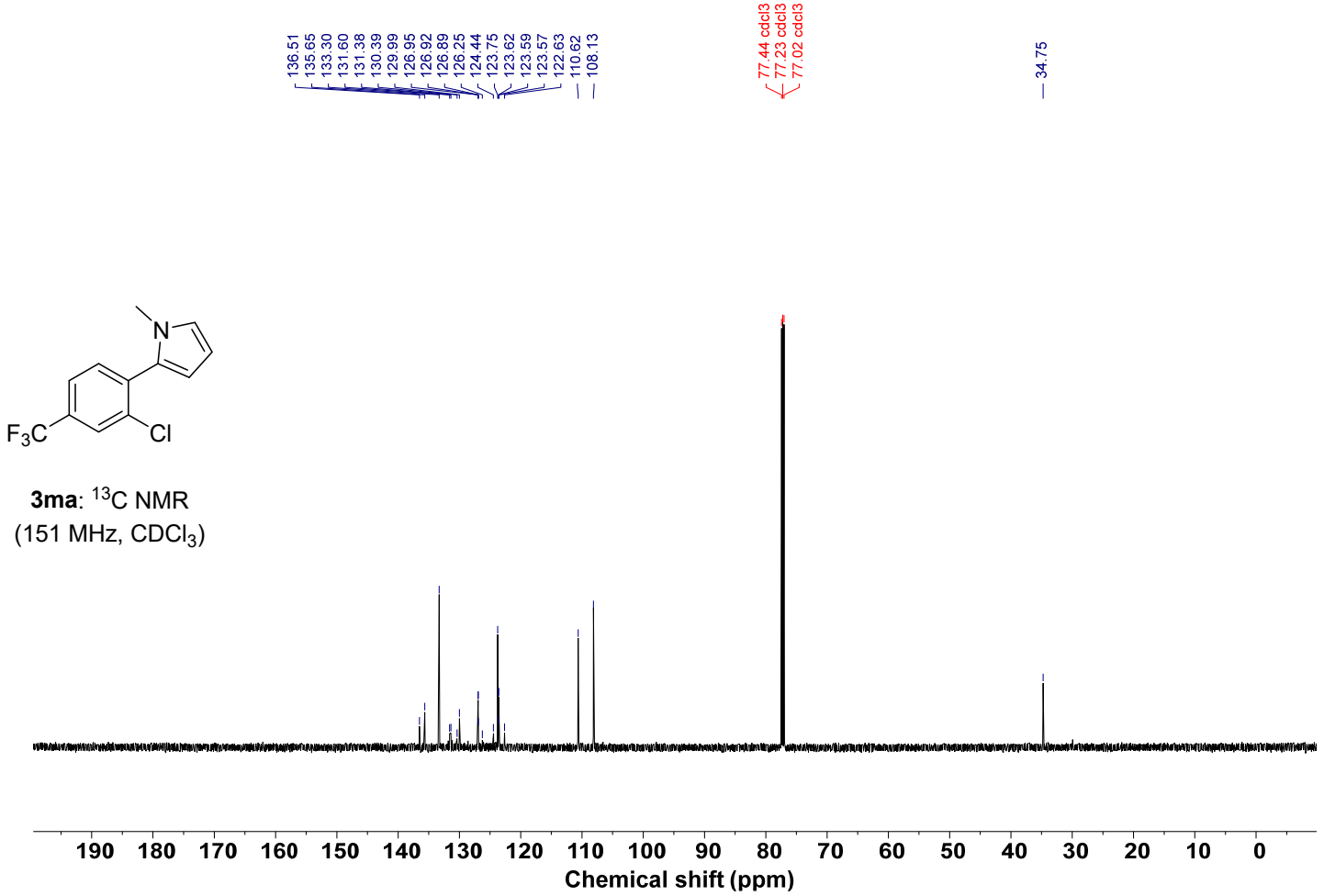

Supplementary Fig. 36 $^{13}C\{^{1}H\}$ NMR (151 MHz, $CDCl_3$) spectrum of 3ma.

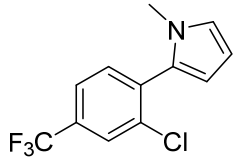

3ma: ^{19}F NMR
(564 MHz, $CDCl_3$)

Supplementary Fig. 37 $^{19}F\{^1H\}$ NMR (564 MHz, $CDCl_3$) spectrum of 3ma.

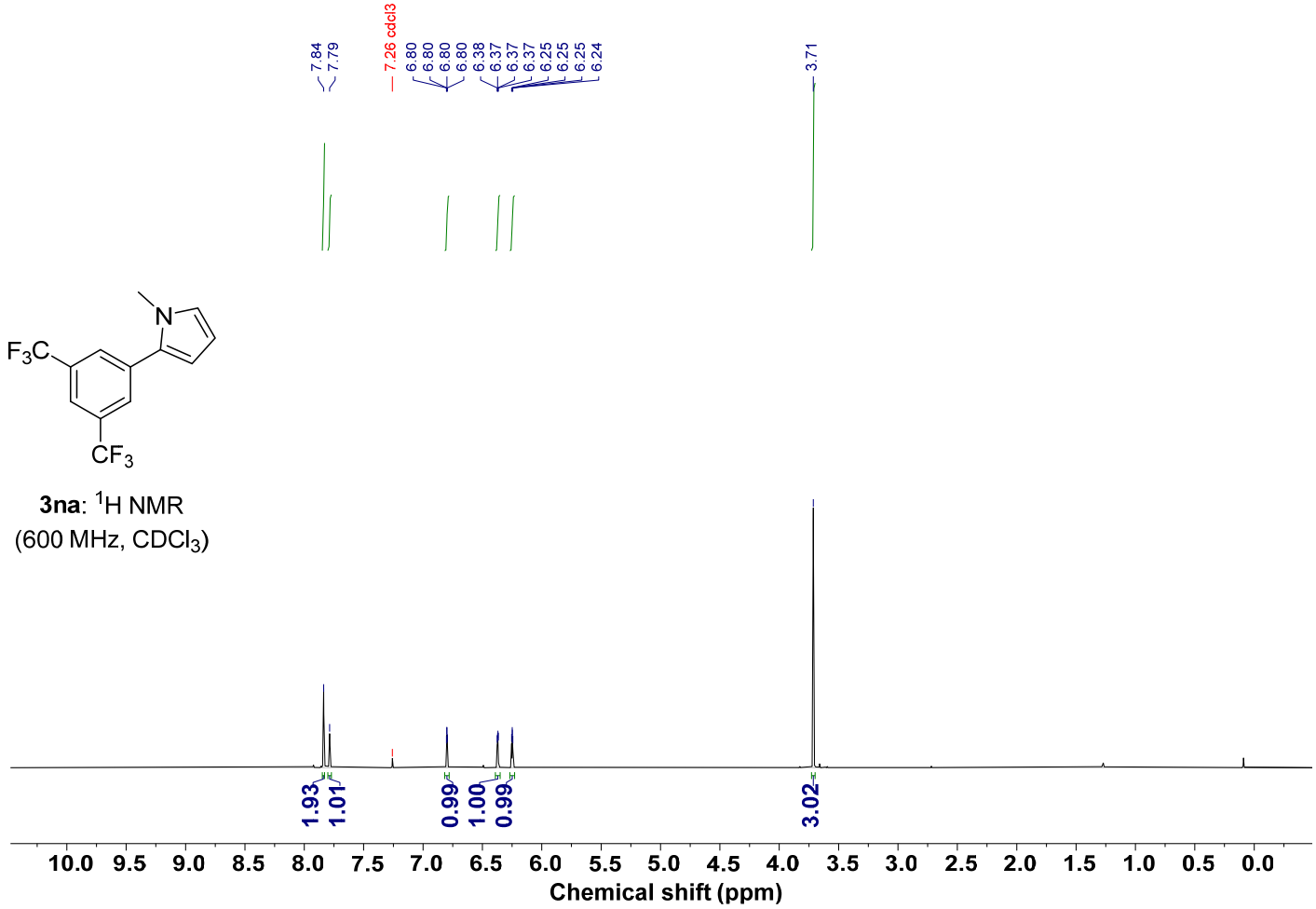

Supplementary Fig. 38 ^{1}H NMR (600 MHz, $CDCl_3$) spectrum of 3na.

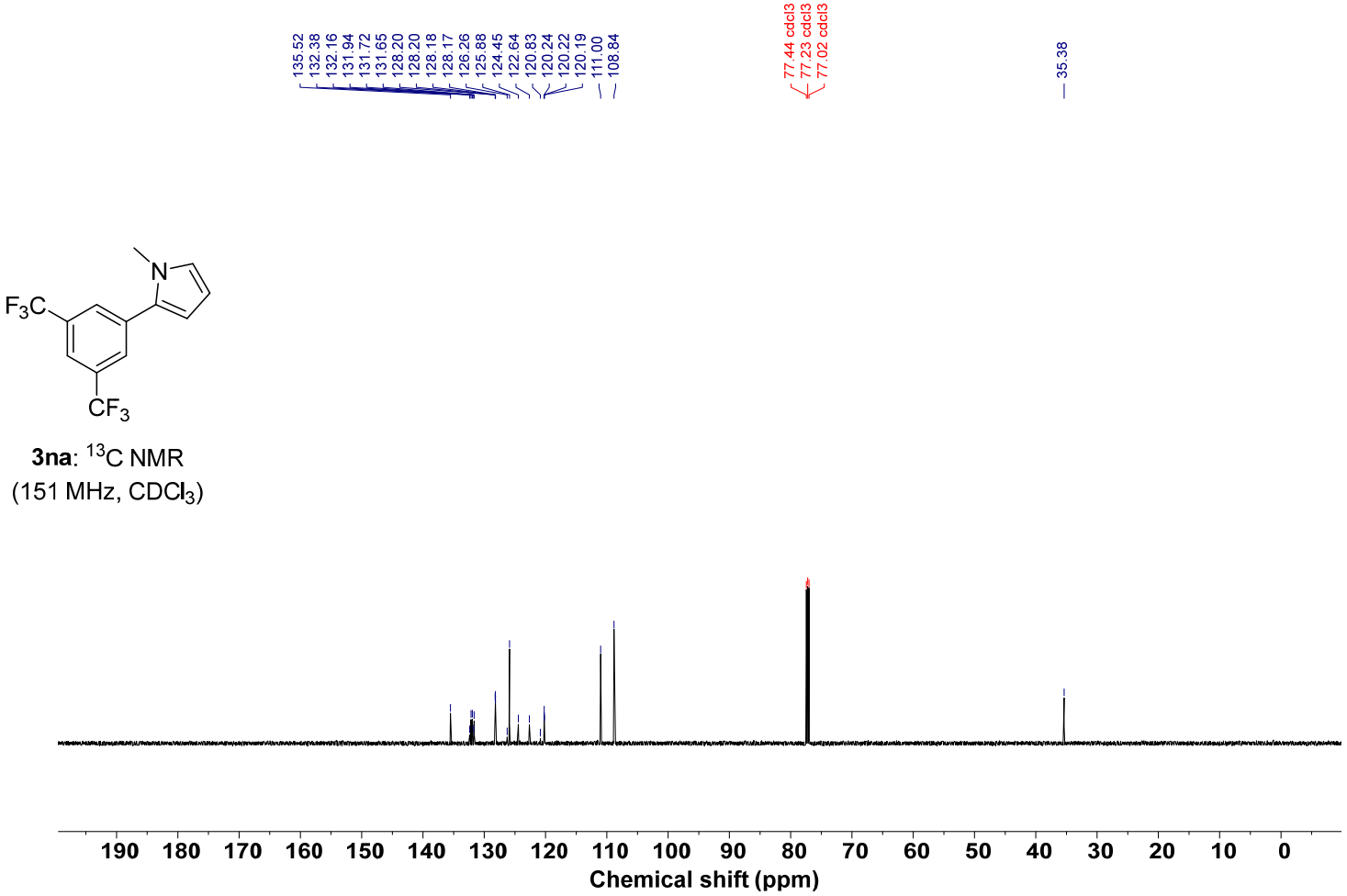

3na: ^{13}C NMR
(151 MHz, $CDCl_3$)

Supplementary Fig. 39 $^{13}C\{^1H\}$ NMR (151 MHz, $CDCl_3$) spectrum of 3na.

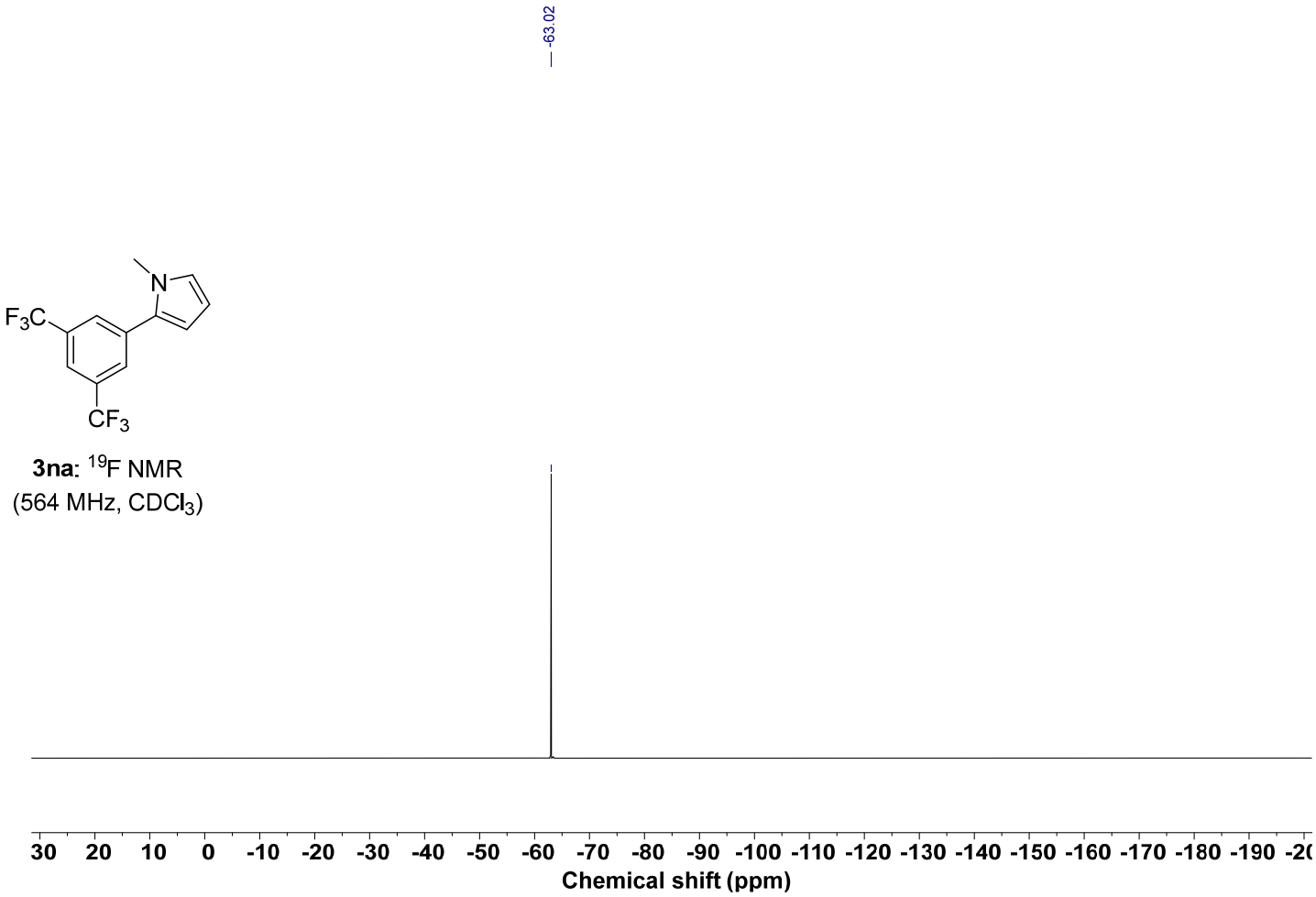

Supplementary Fig. 40 $^{19}F\{^{1}H\}$ NMR (564 MHz, $CDCl_3$) spectrum of 3na.

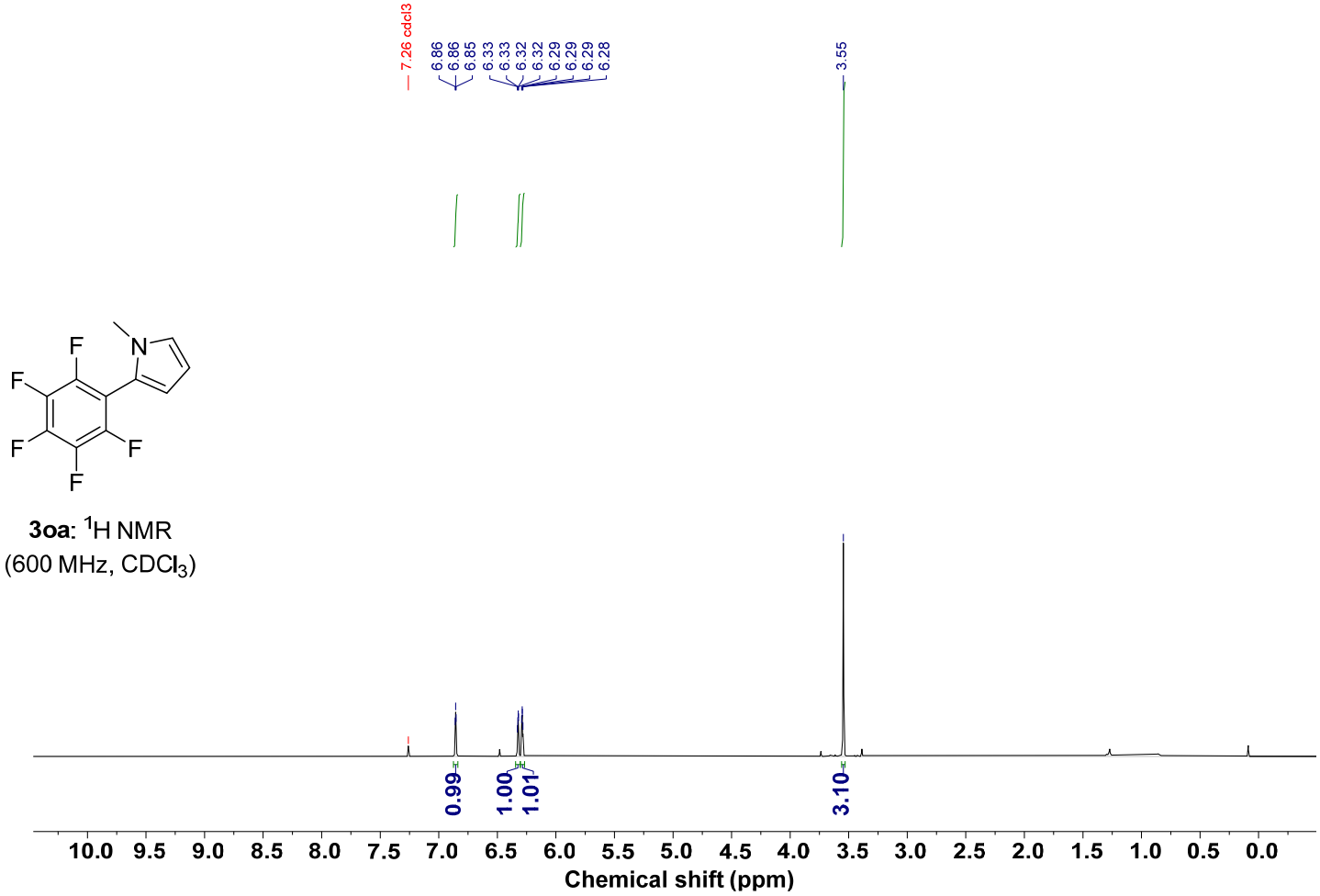

Supplementary Fig. 41 ^{1}H NMR (600 MHz, $CDCl_3$) spectrum of 3oa.

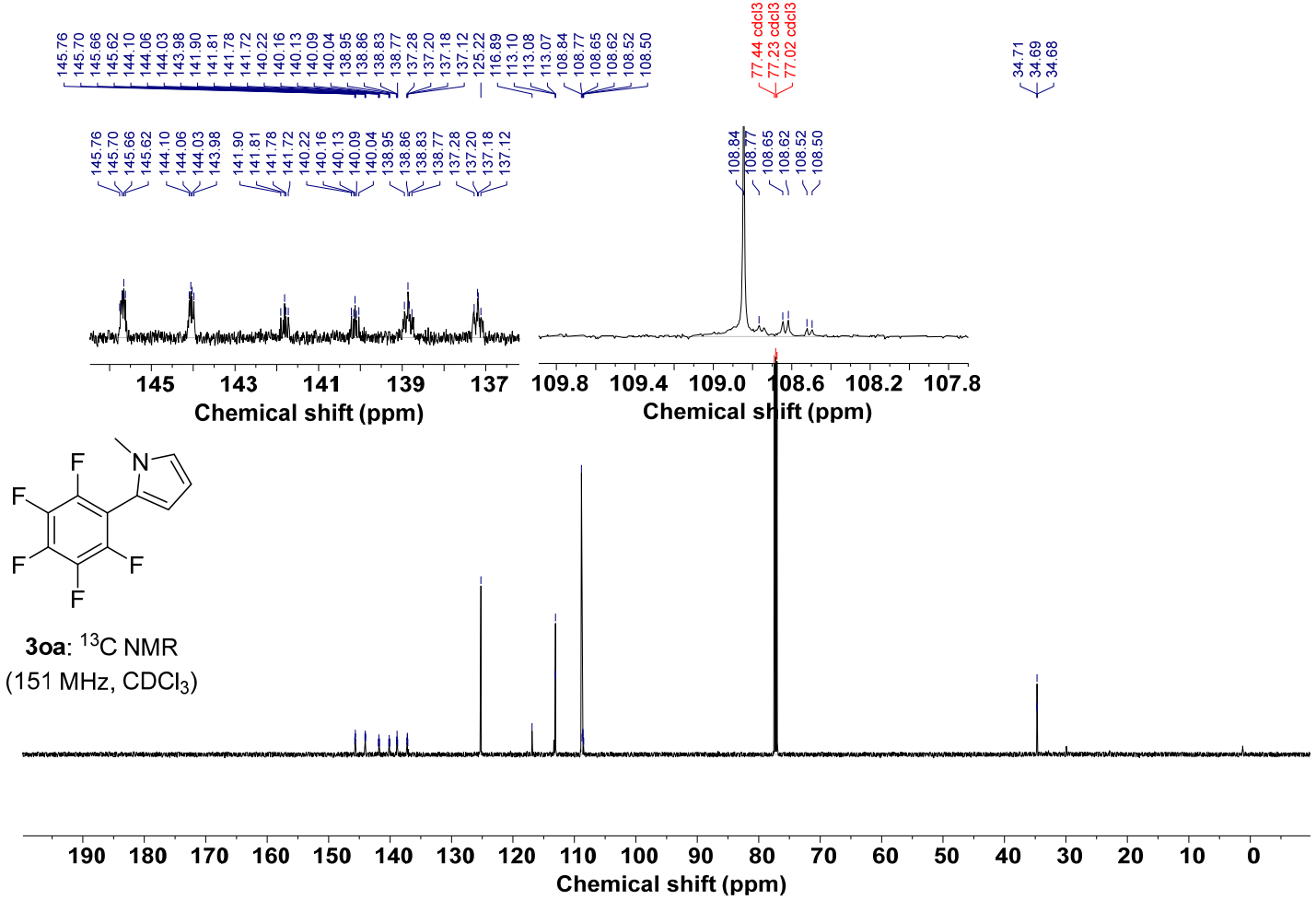

Supplementary Fig. 42 $^{13}C\{^{1}H\}$ NMR (151 MHz, $CDCl_3$) spectrum of 3oa.

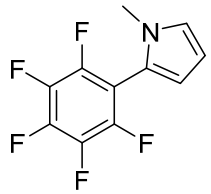

3oa: ^{19}F NMR
(564 MHz, $CDCl_3$)

Supplementary Fig. 43 $^{19}F\{^1H\}$ NMR (564 MHz, $CDCl_3$) spectrum of 3oa.

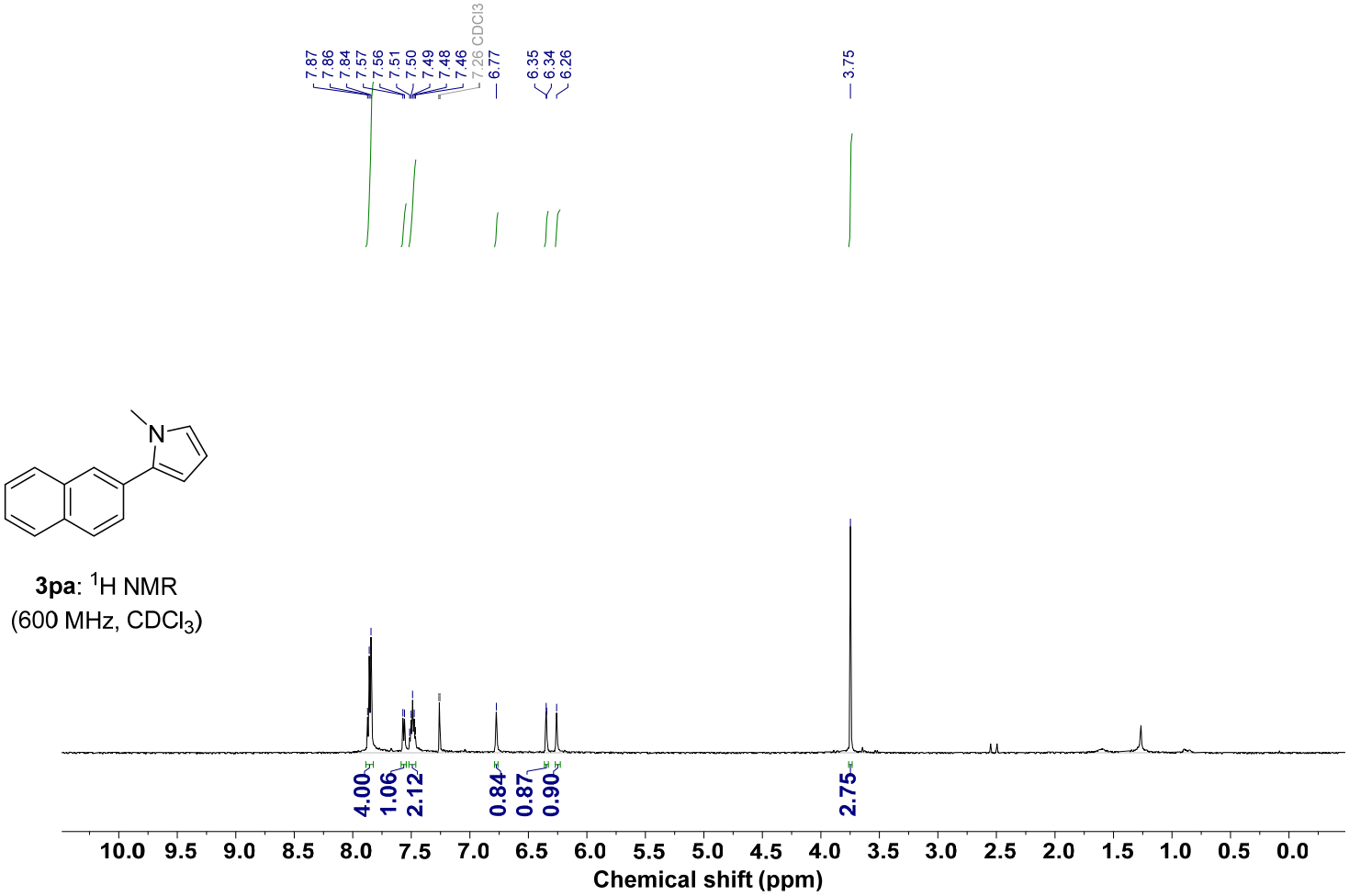

Supplementary Fig. 44 ^{1}H NMR (600 MHz, $CDCl_3$) spectrum of 3pa.

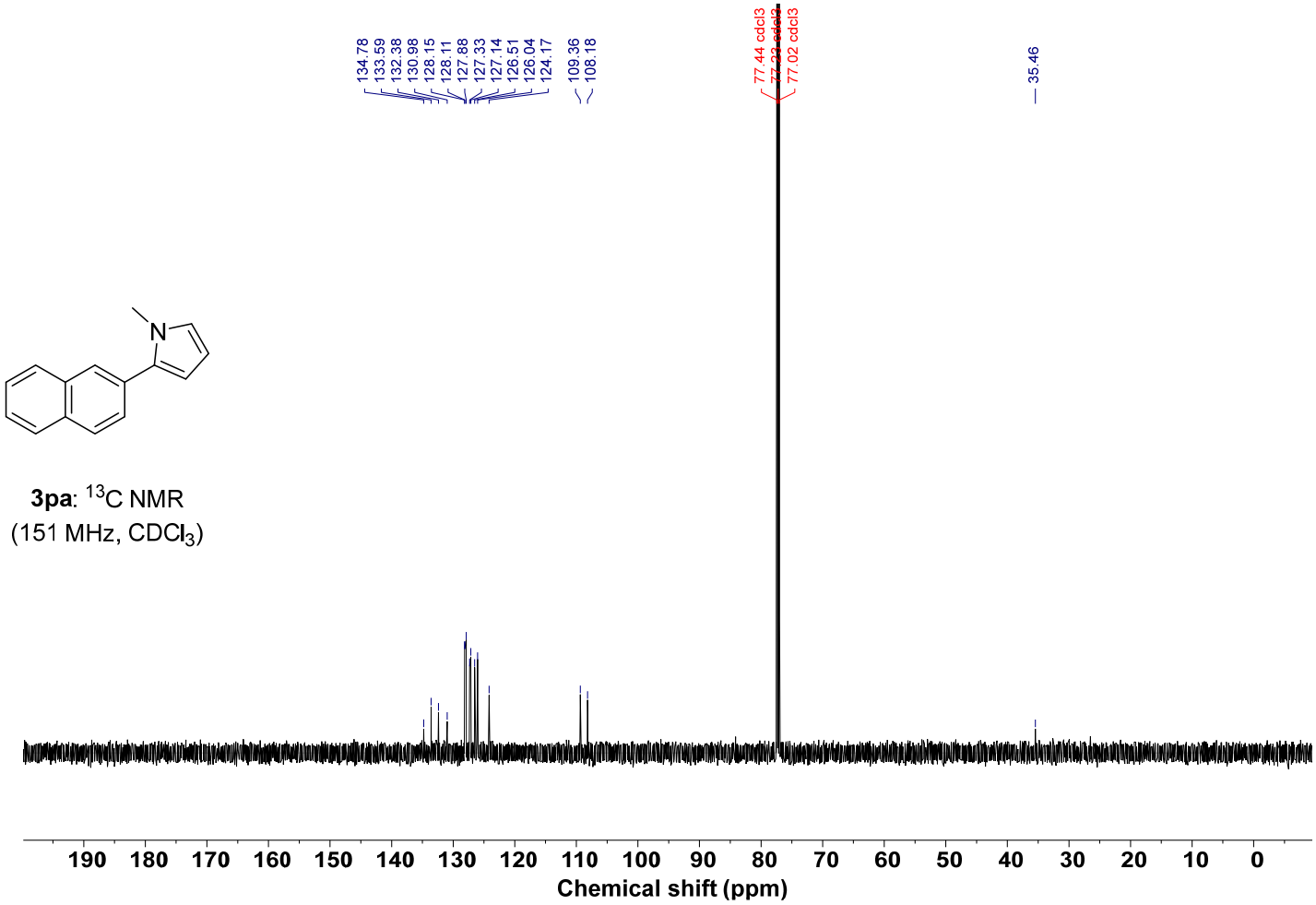

Supplementary Fig. 45 $^{13}C\{^{1}H\}$ NMR (151 MHz, $CDCl_3$) spectrum of 3pa.

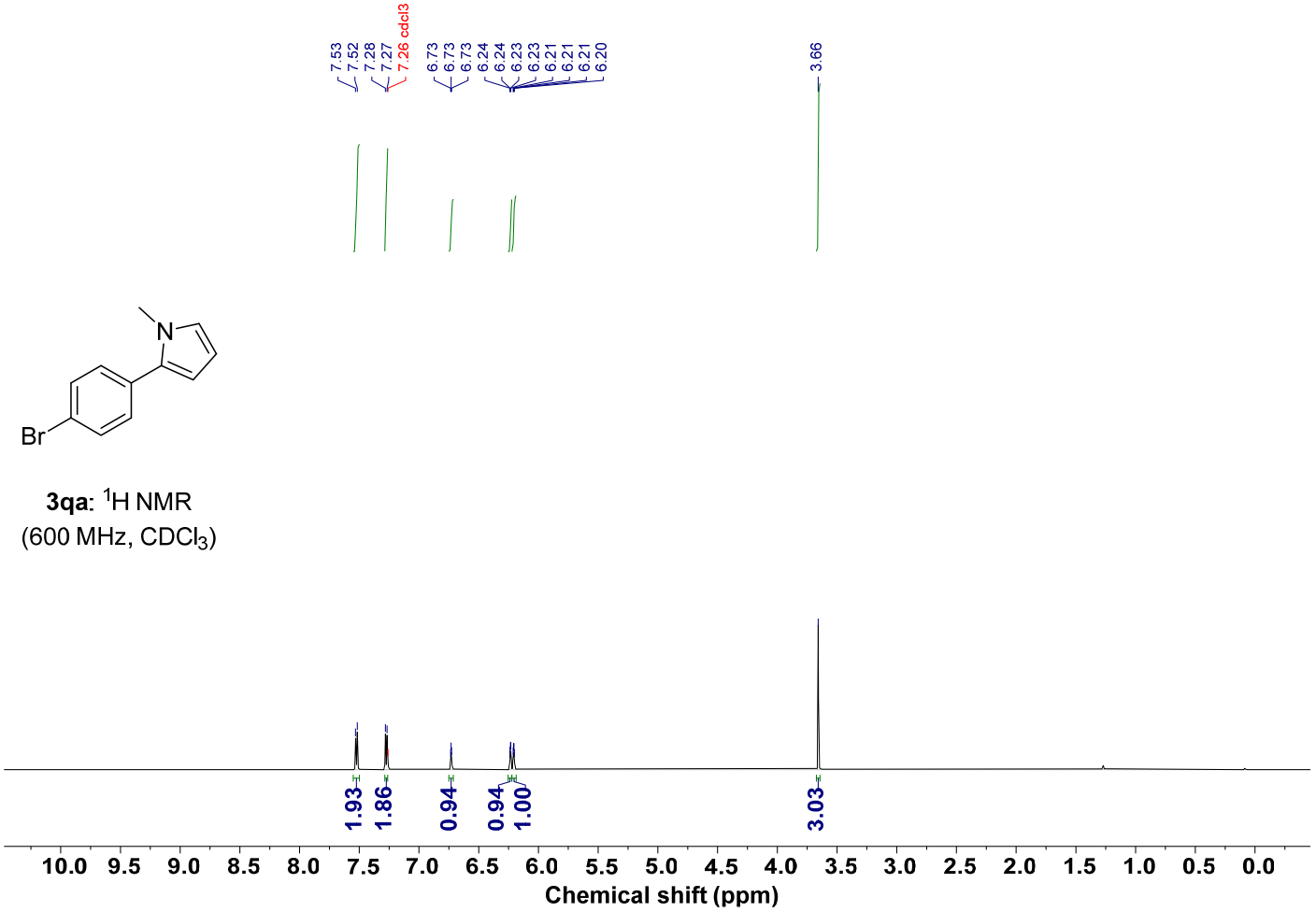

Supplementary Fig. 46 ^{1}H NMR (600 MHz, $CDCl_3$) spectrum of 3qa.

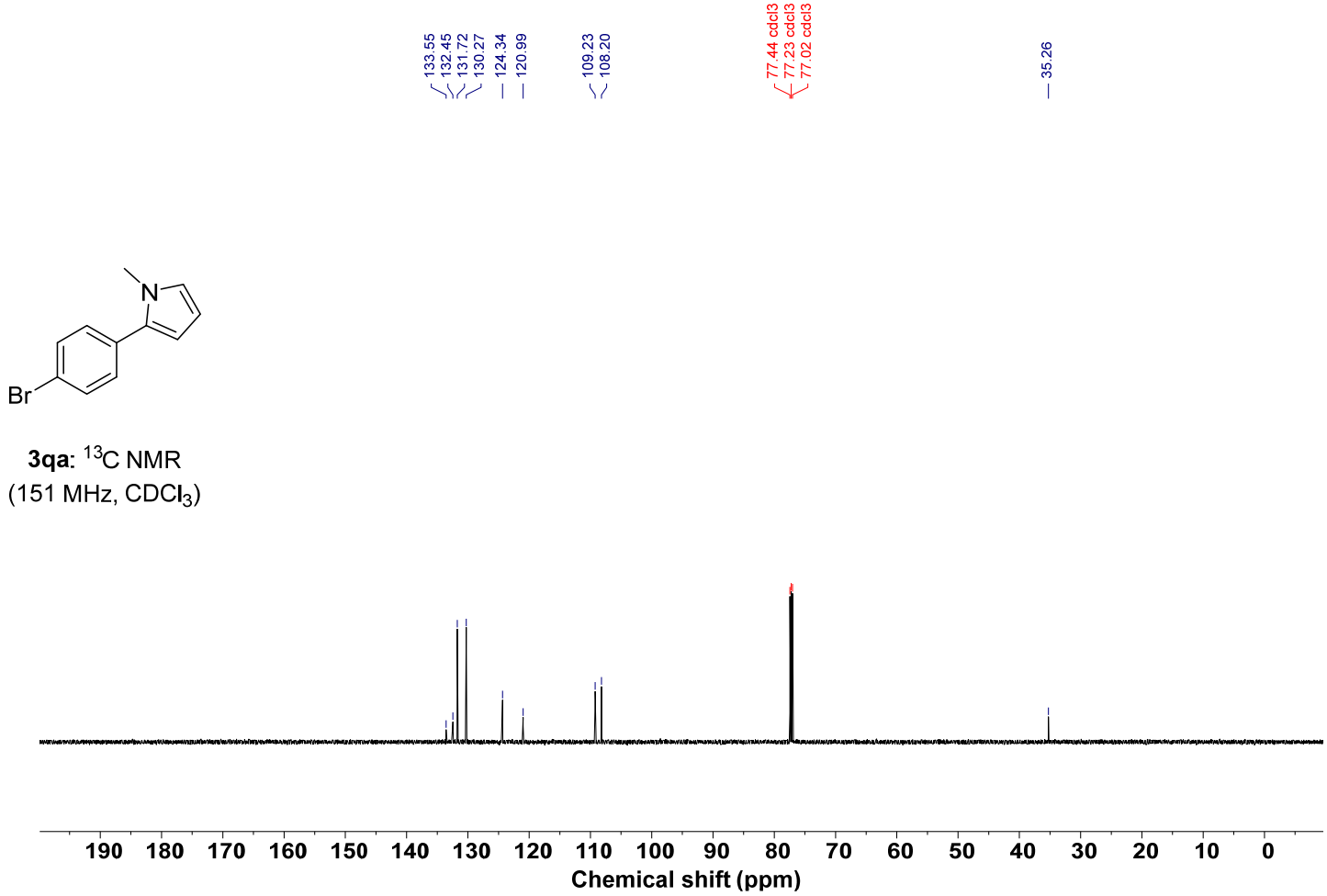

3qa: ^{13}C NMR
(151 MHz, $CDCl_3$)

Supplementary Fig. 47 $^{13}C\{^1H\}$ NMR (151 MHz, $CDCl_3$) spectrum of 3qa.

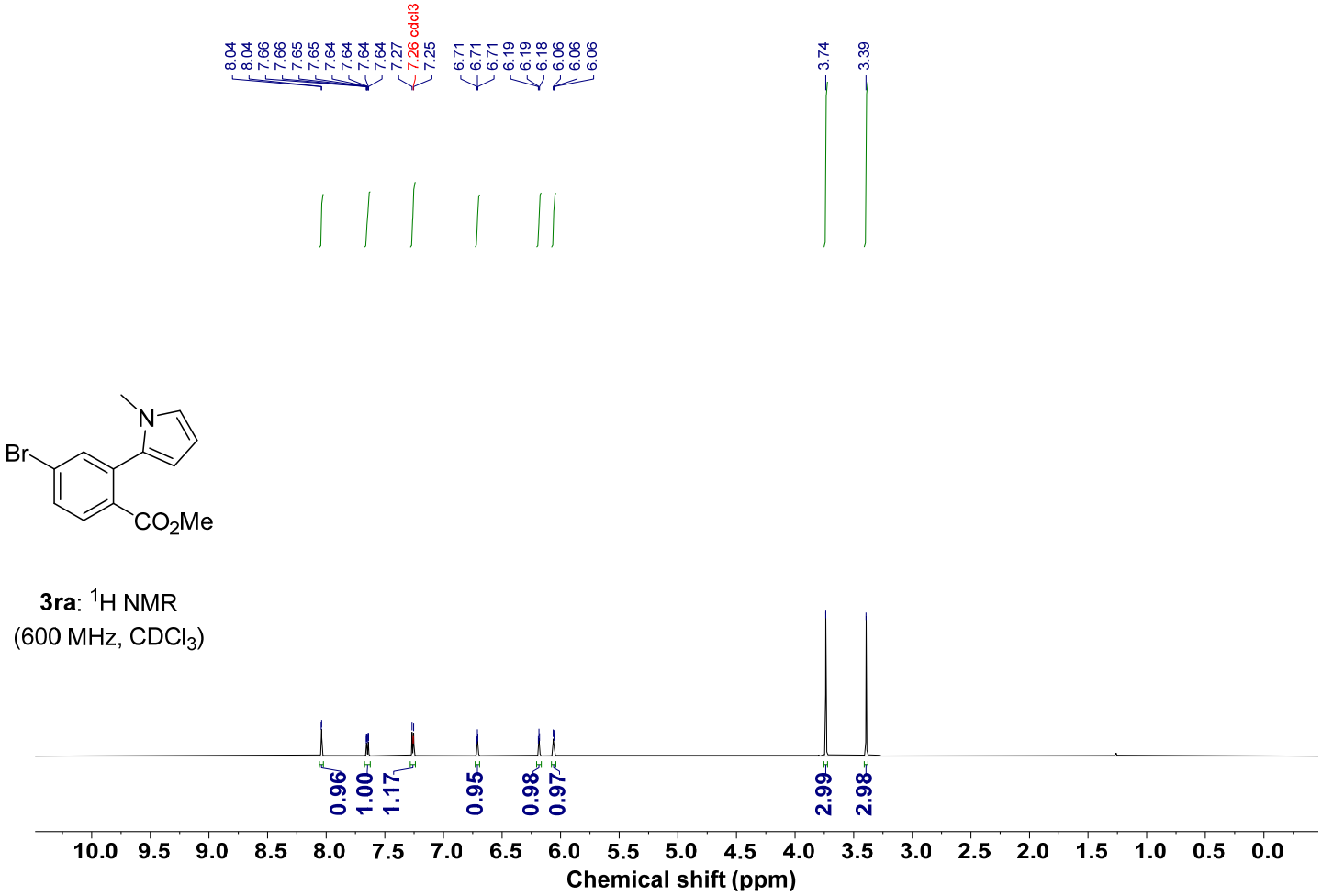

Supplementary Fig. 48 ^{1}H NMR (600 MHz, $CDCl_3$) spectrum of 3ra.

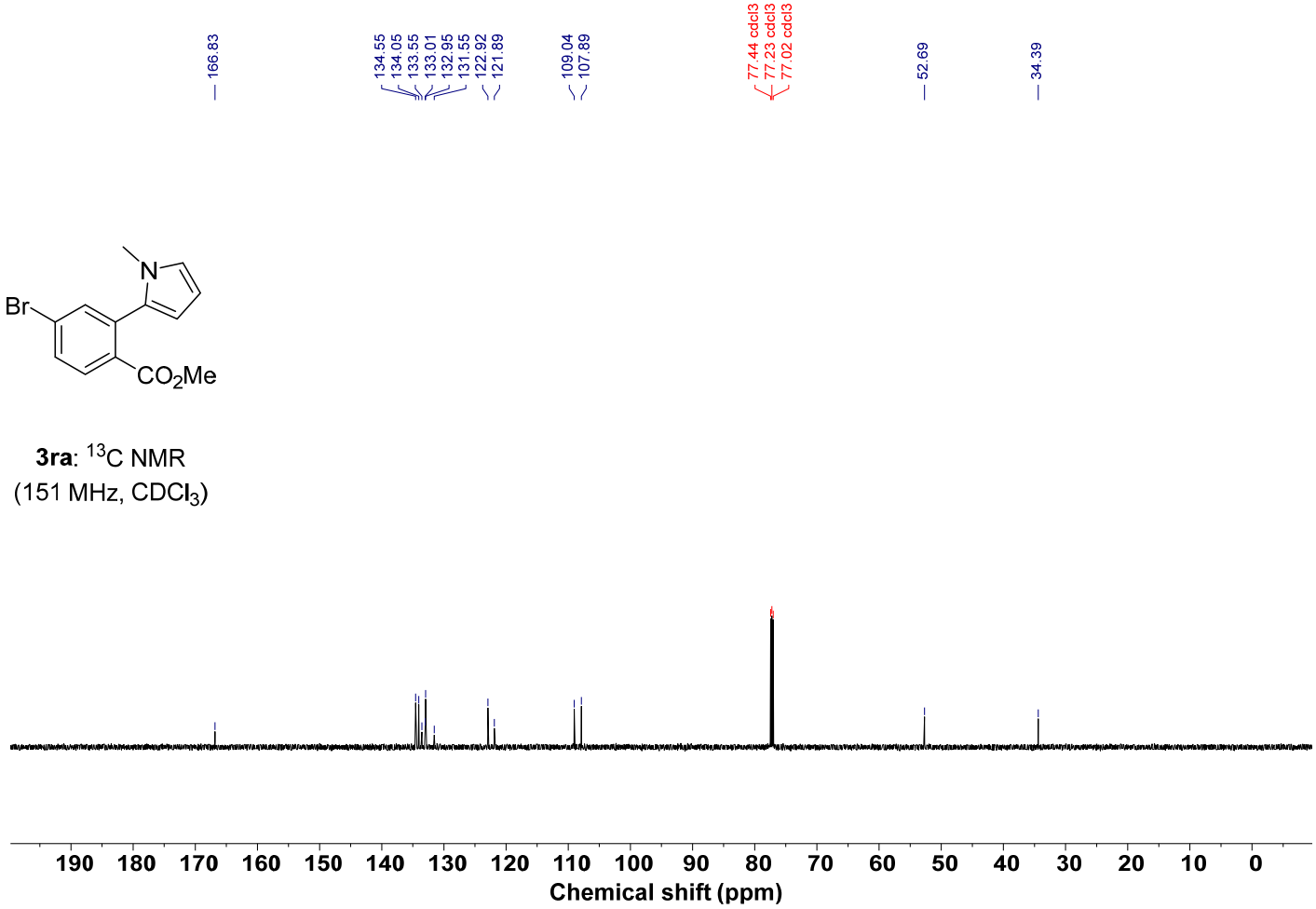

Supplementary Fig. 49 $^{13}C\{^{1}H\}$ NMR (151 MHz, $CDCl_3$) spectrum of 3ra.

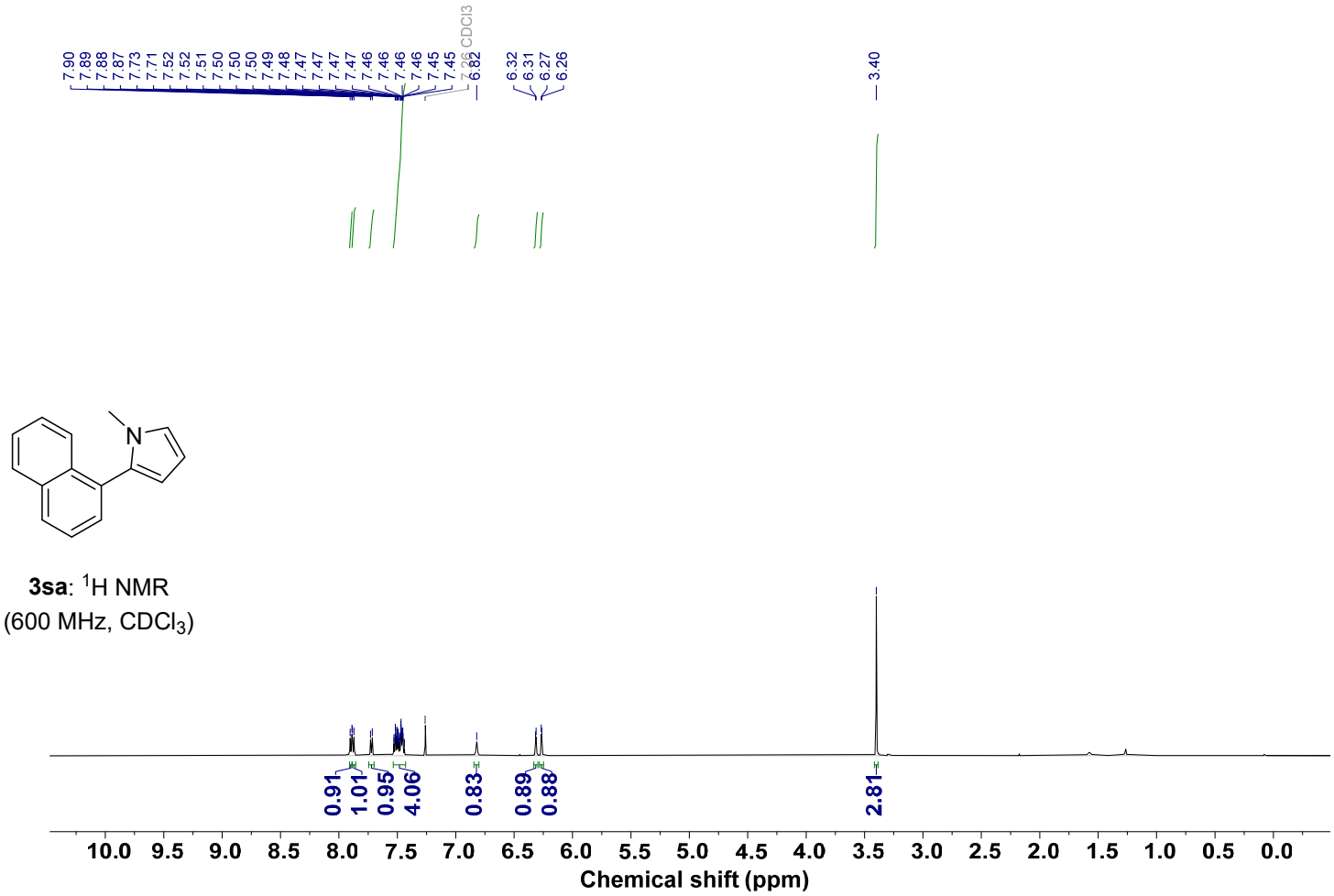

3sa: ^{1}H NMR
(600 MHz, $CDCl_3$)

Supplementary Fig. 50 ^{1}H NMR (600 MHz, $CDCl_3$) spectrum of 3sa.

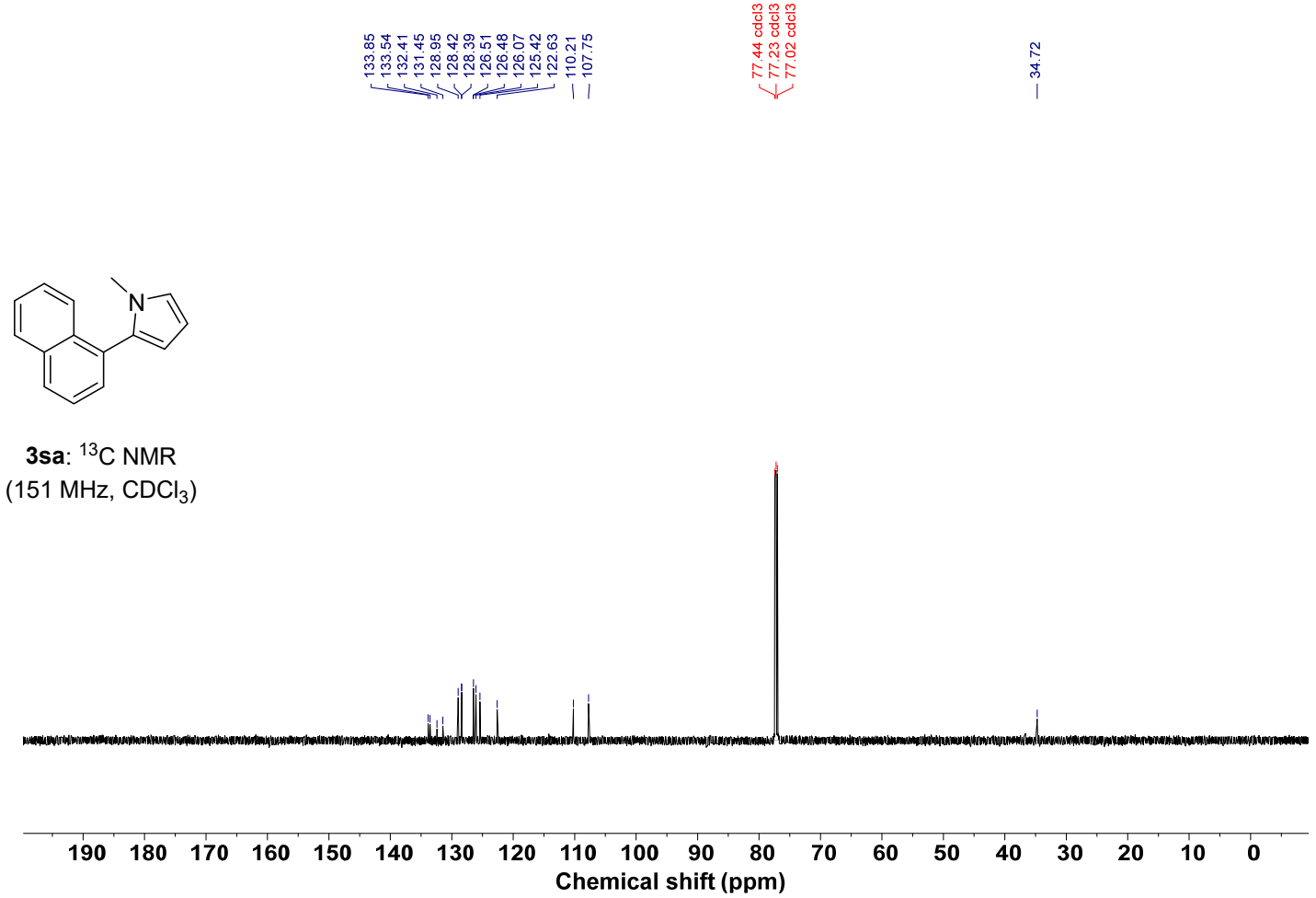

Supplementary Fig. 51 $^{13}C\{^{1}H\}$ NMR (151 MHz, $CDCl_3$) spectrum of 3sa.

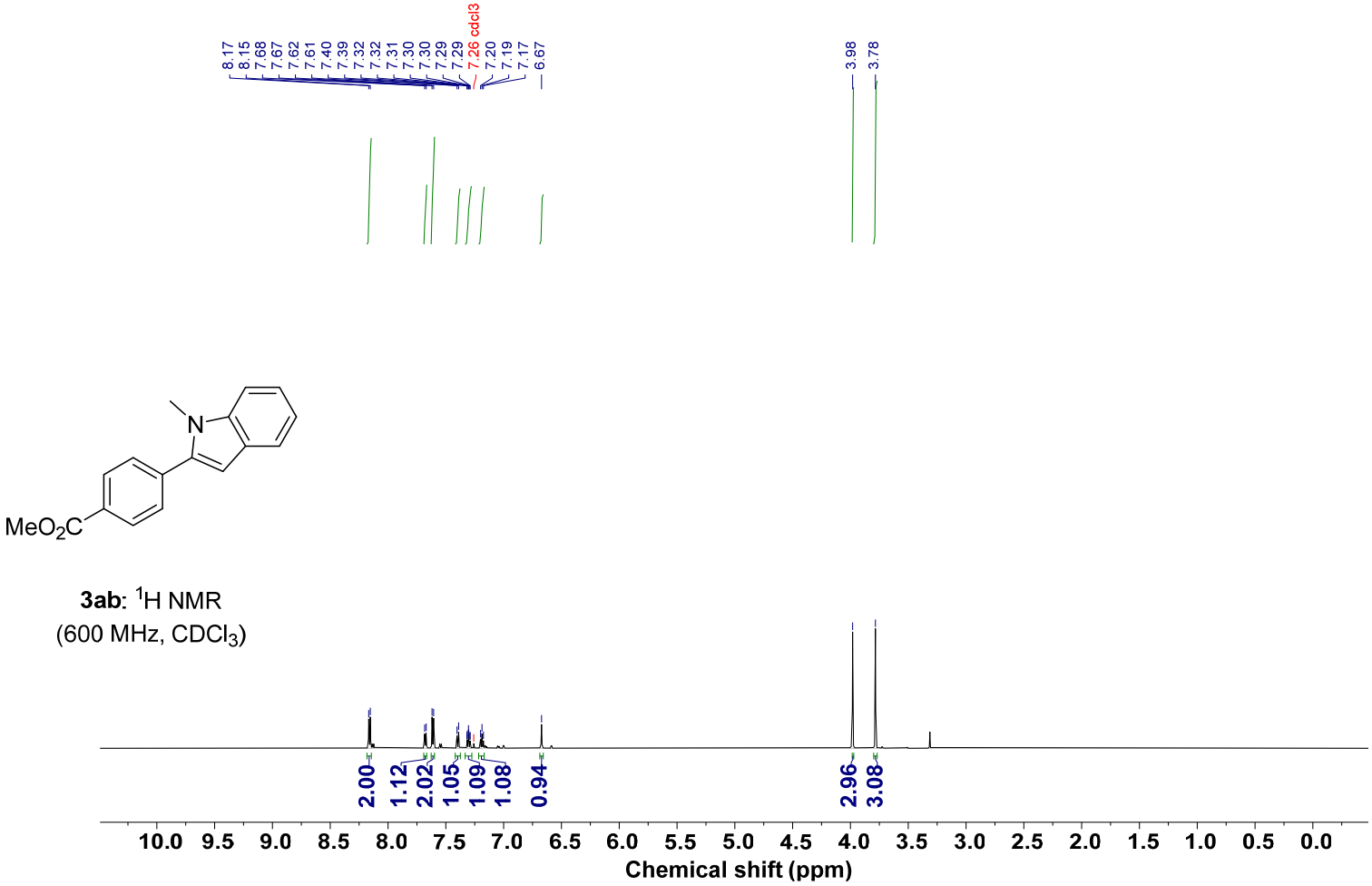

Supplementary Fig. 52 ^{1}H NMR (600 MHz, $CDCl_3$) spectrum of 3ab.

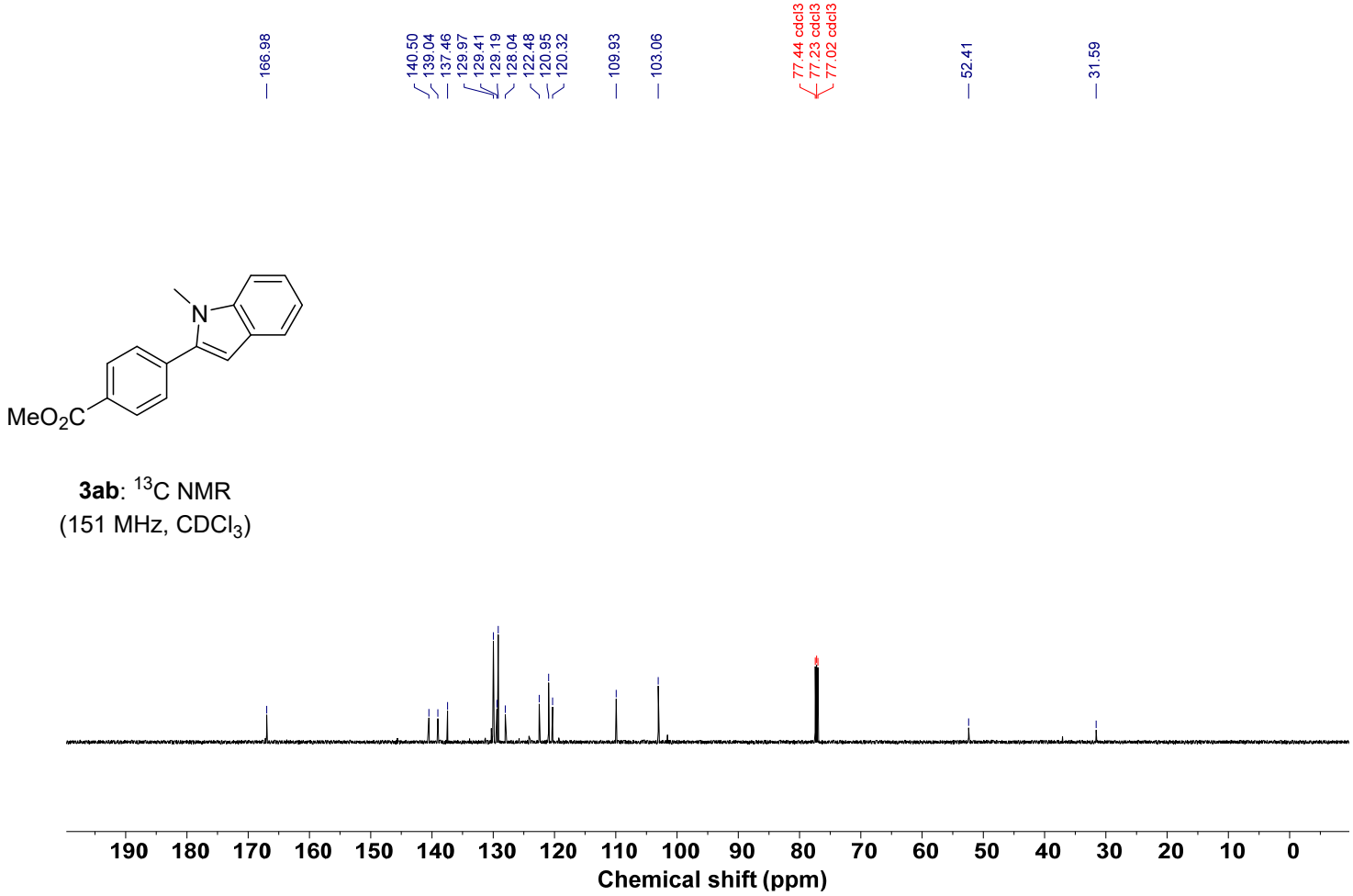

3ab: ^{13}C NMR
(151 MHz, $CDCl_3$)

Supplementary Fig. 53 $^{13}C\{^1H\}$ NMR (151 MHz, $CDCl_3$) spectrum of 3ab.

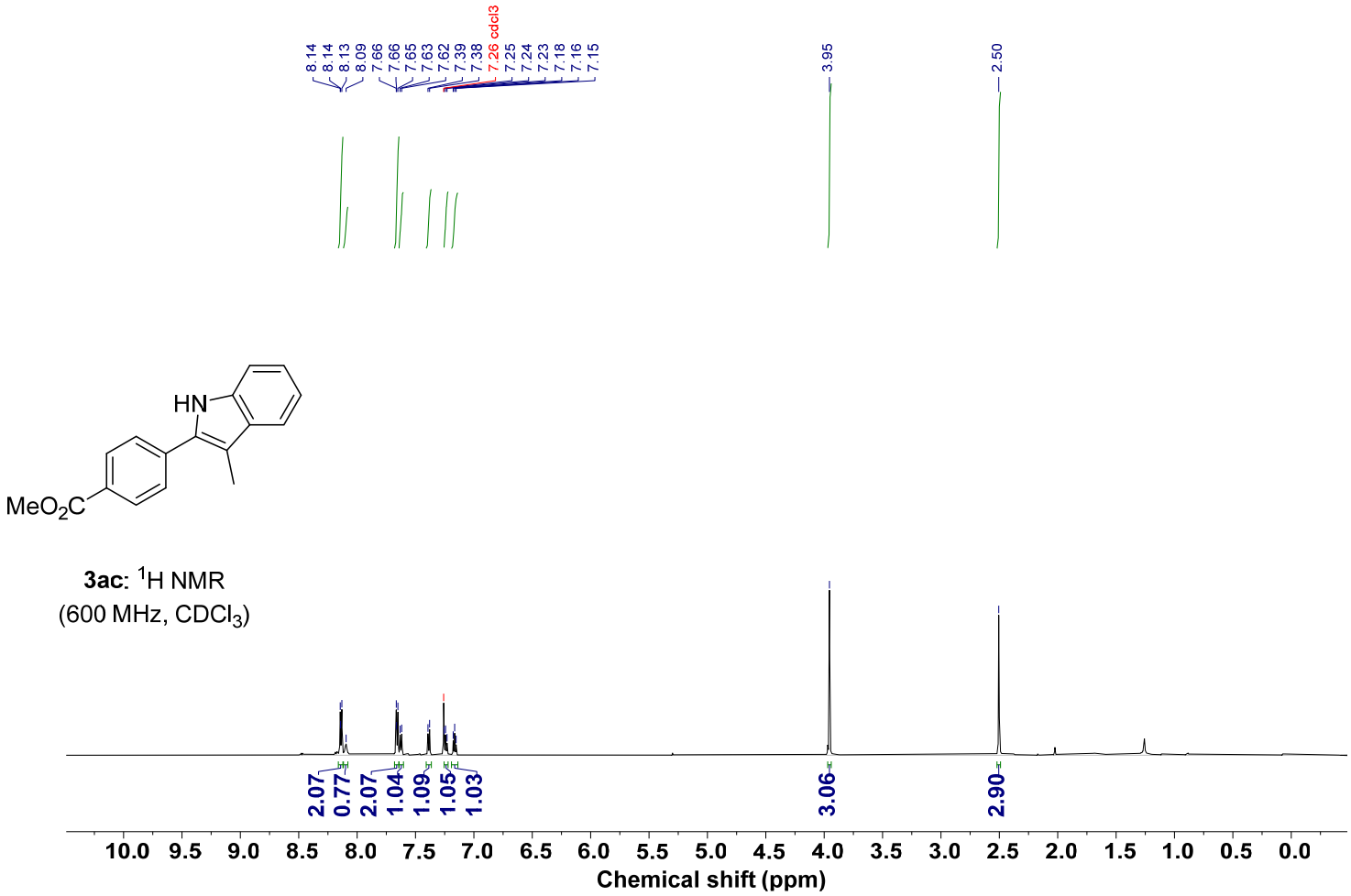

Supplementary Fig. 54 ^{1}H NMR (600 MHz, $CDCl_3$) spectrum of 3ac.

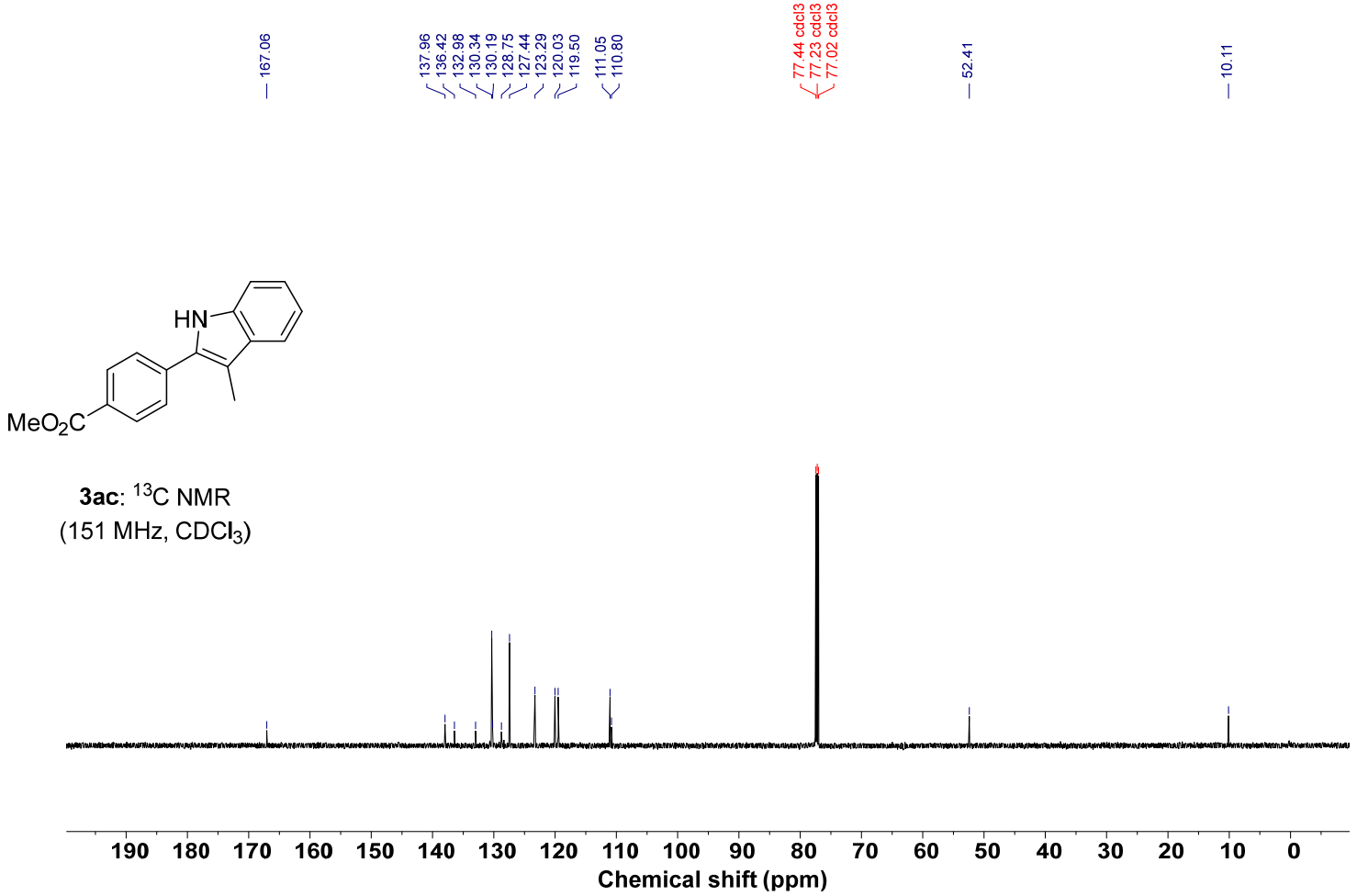

Supplementary Fig. 55 $^{13}C\{^{1}H\}$ NMR (151 MHz, $CDCl_3$) spectrum of 3ac.

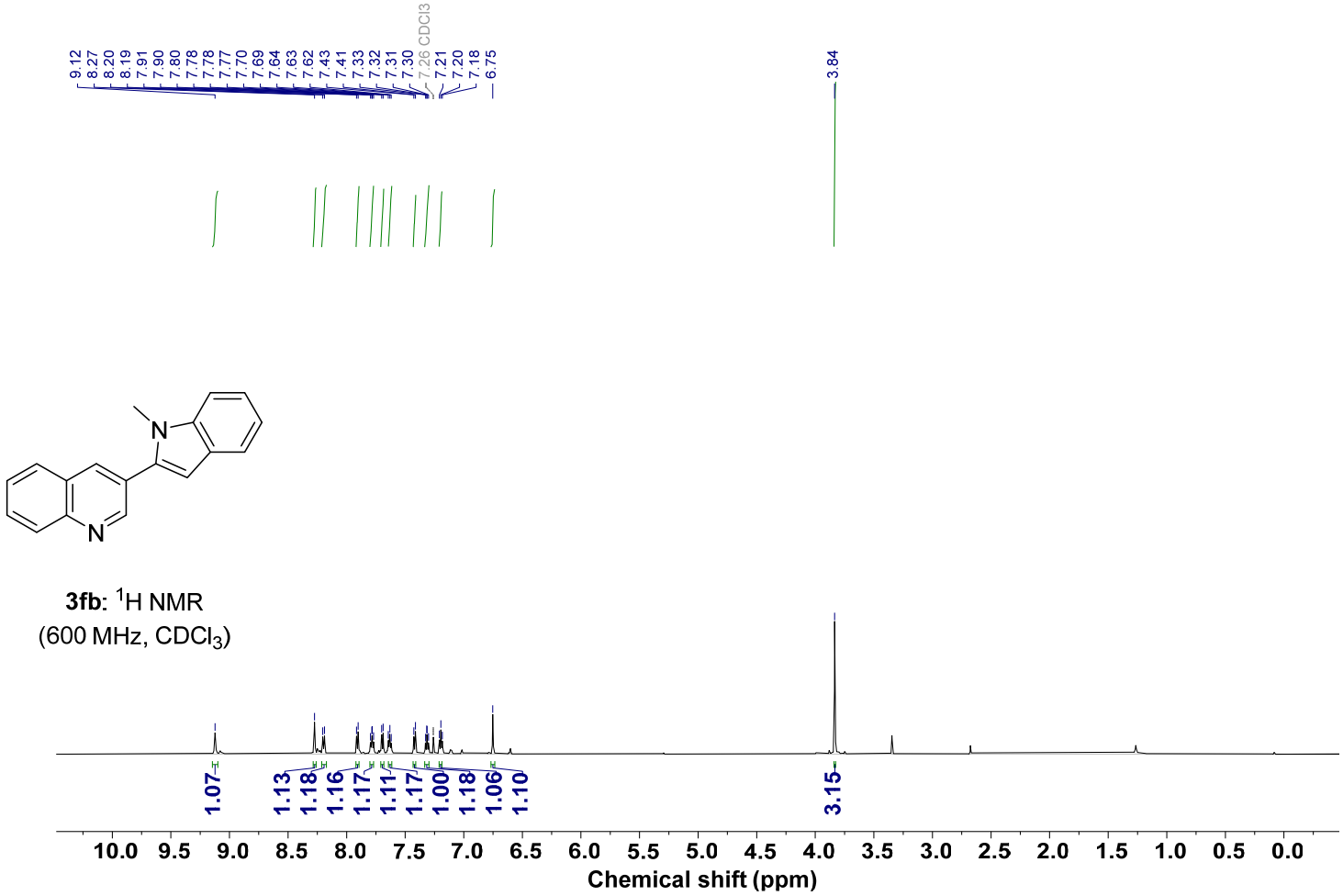

Supplementary Fig. 56 ^{1}H NMR (600 MHz, $CDCl_3$) spectrum of 3fb.

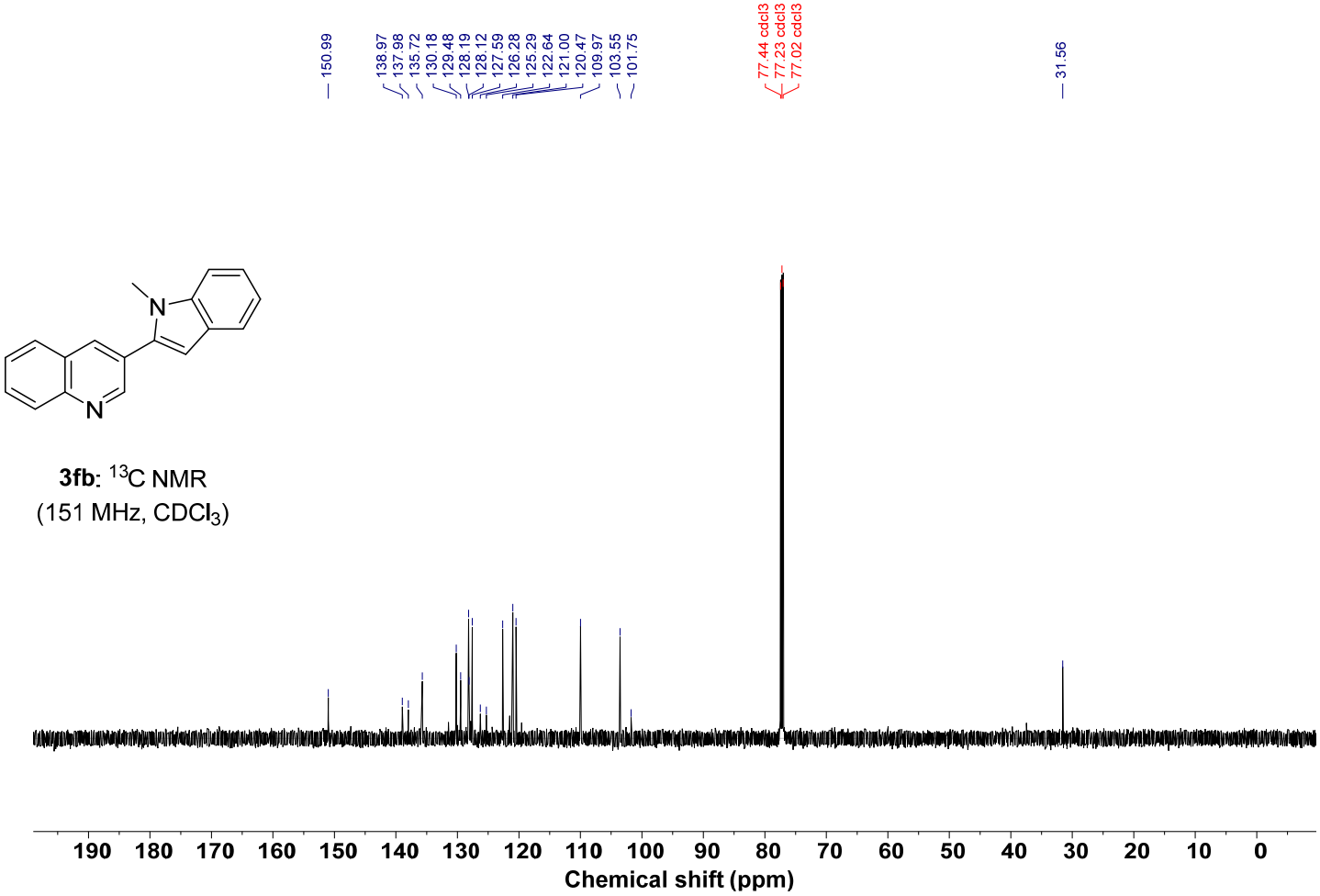

Supplementary Fig. 57 $^{13}C\{^{1}H\}$ NMR (151 MHz, $CDCl_3$) spectrum of 3fb.

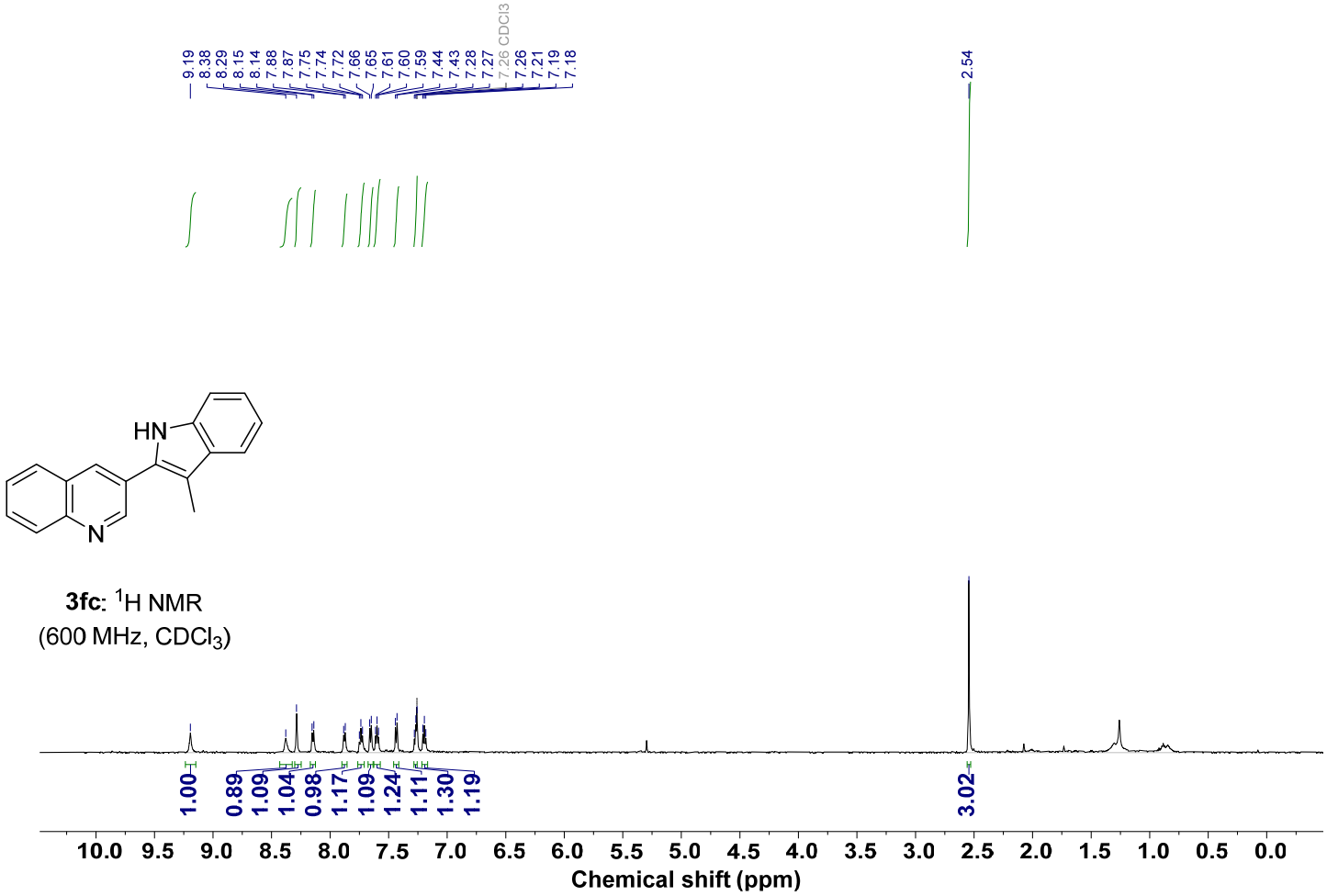

Supplementary Fig. 58 ^{1}H NMR (600 MHz, $CDCl_3$) spectrum of 3fc.

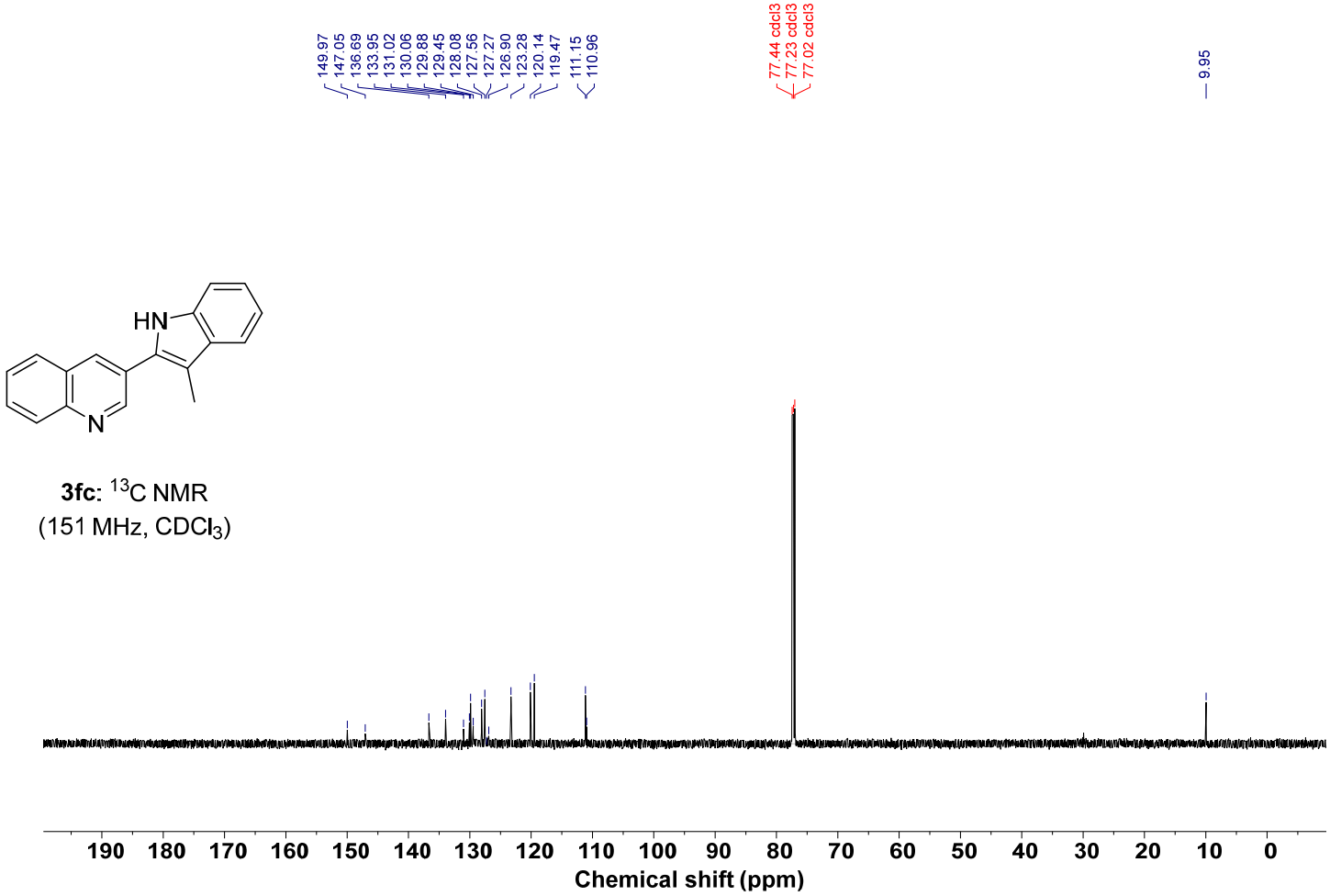

Supplementary Fig. 59 $^{13}C\{^{1}H\}$ NMR (151 MHz, $CDCl_3$) spectrum of 3fc.

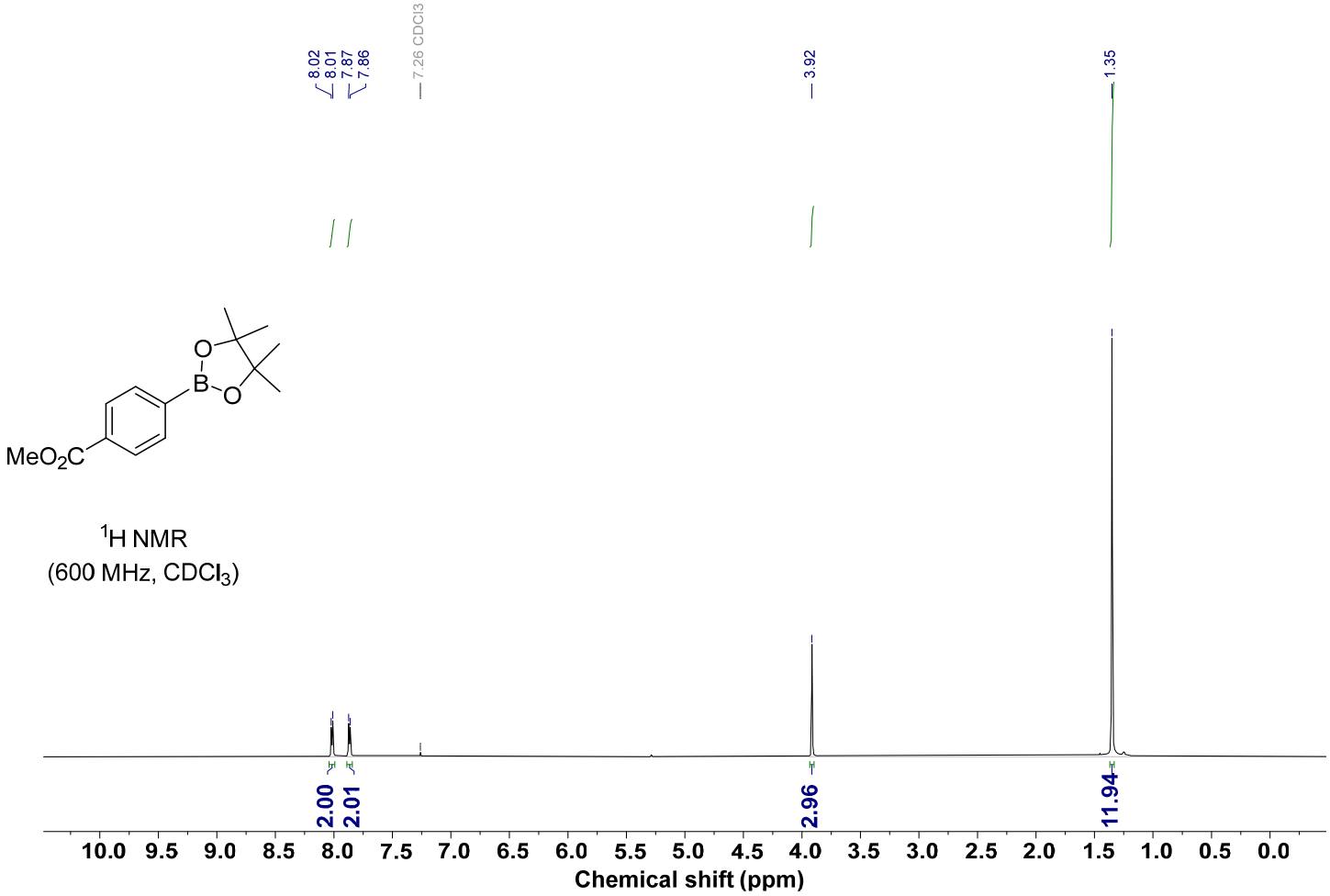

Supplementary Fig. 60 ^{1}H NMR (600 MHz, $CDCl_3$) spectrum of methyl 4-(4,4,5,5,-tetramethyl-1,3,2,-dioxaborolan-2-yl)benzoate.

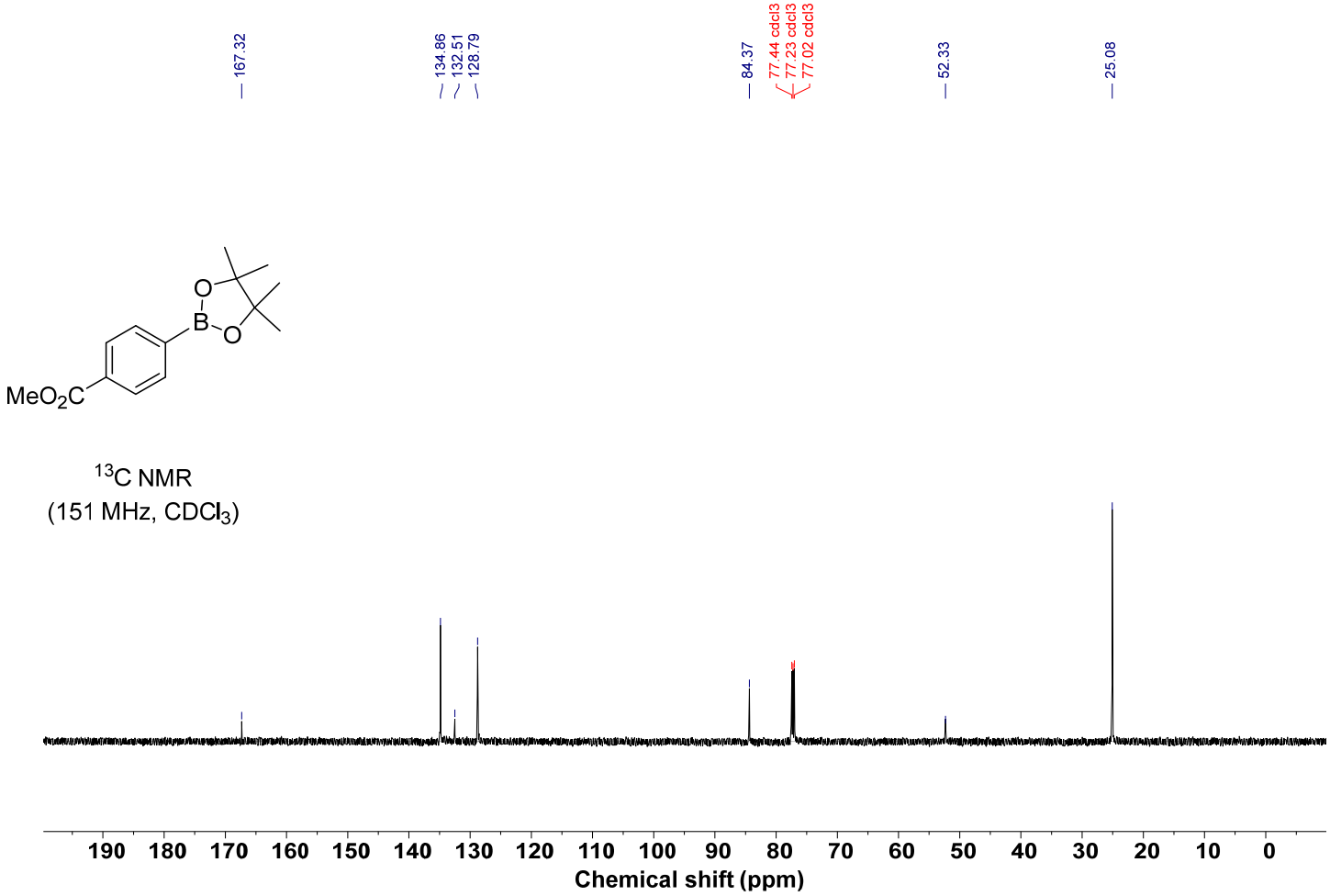

Supplementary Fig. 61 $^{13}C\{^{1}H\}$ NMR (151 MHz, $CDCl_3$) spectrum of methyl 4-(4,4,5,5,-tetramethyl-1,3,2,-dioxaborolan-2-yl)benzoate.

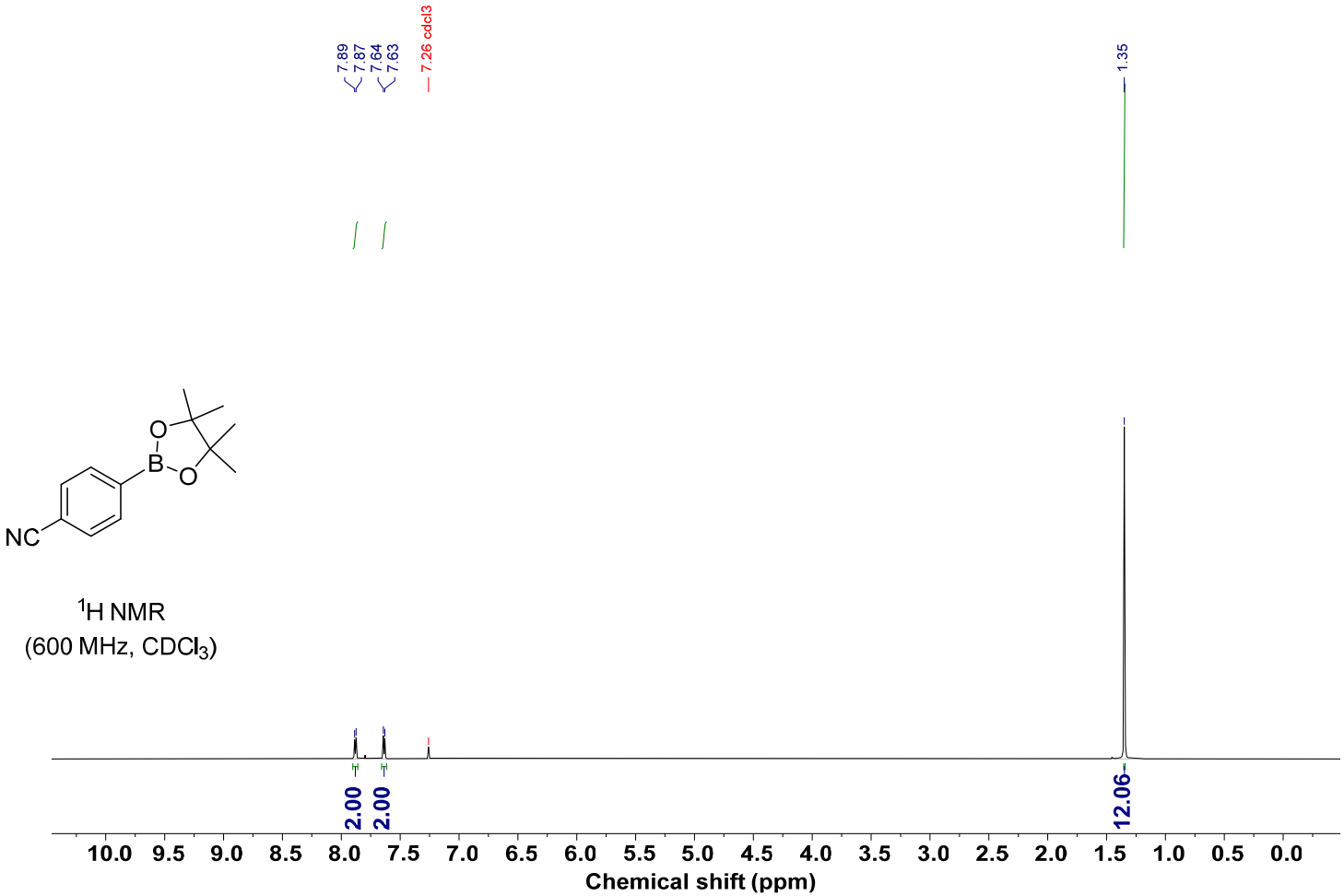

Supplementary Fig. 62 ^{1}H NMR (600 MHz, $CDCl_3$) spectrum of 4-(4-(4,4,5,5-tetramethyl-1,3,2-dioxaborolan-2-yl)phenyl)benzonitrile.

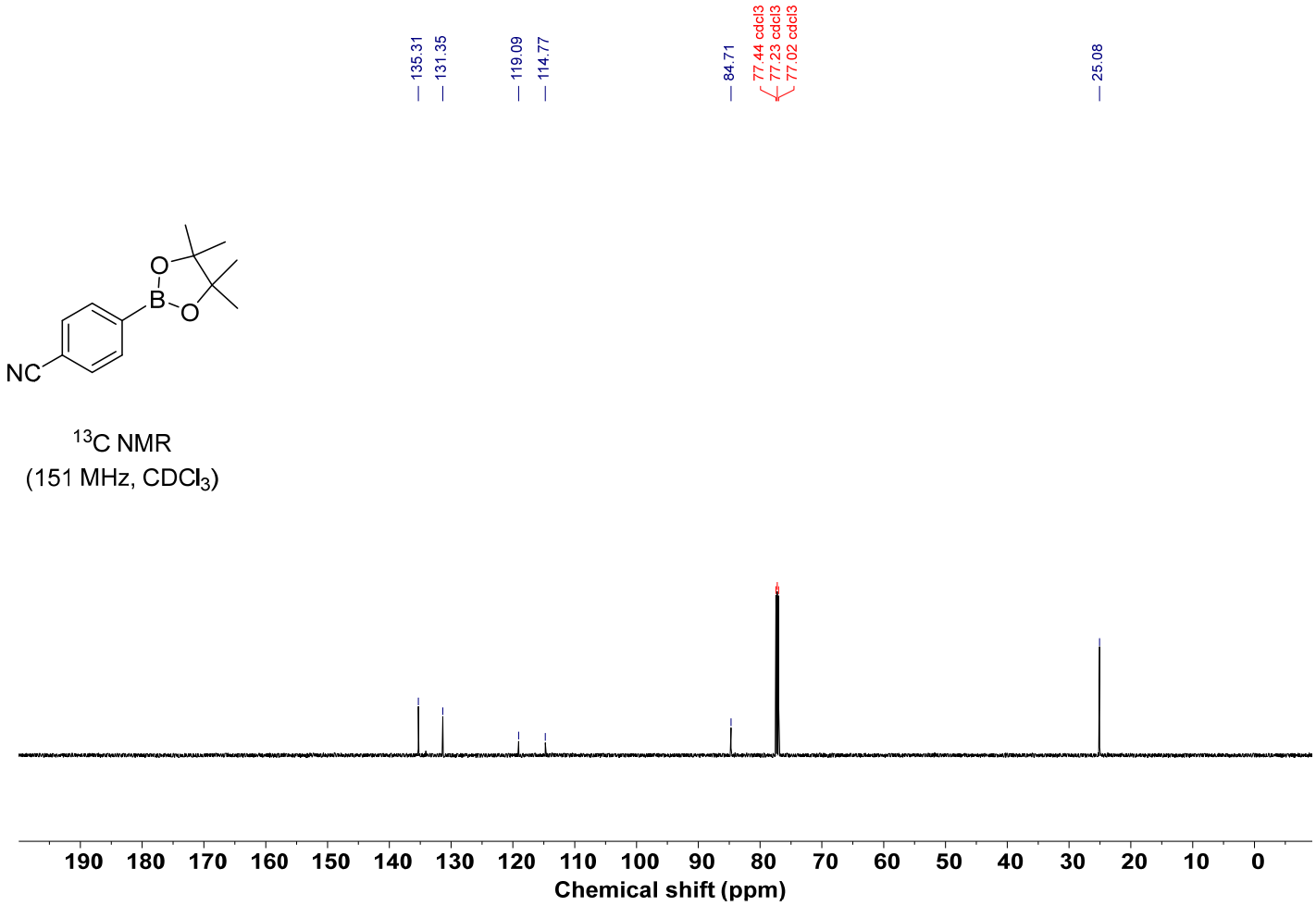

Supplementary Fig. 63 $^{13}C\{^{1}H\}$ NMR (151 MHz, $CDCl_3$) spectrum of 4-(4-(4,4,5,5-tetramethyl-1,3,2-dioxaborolan-2-yl)phenyl)benzonitrile.

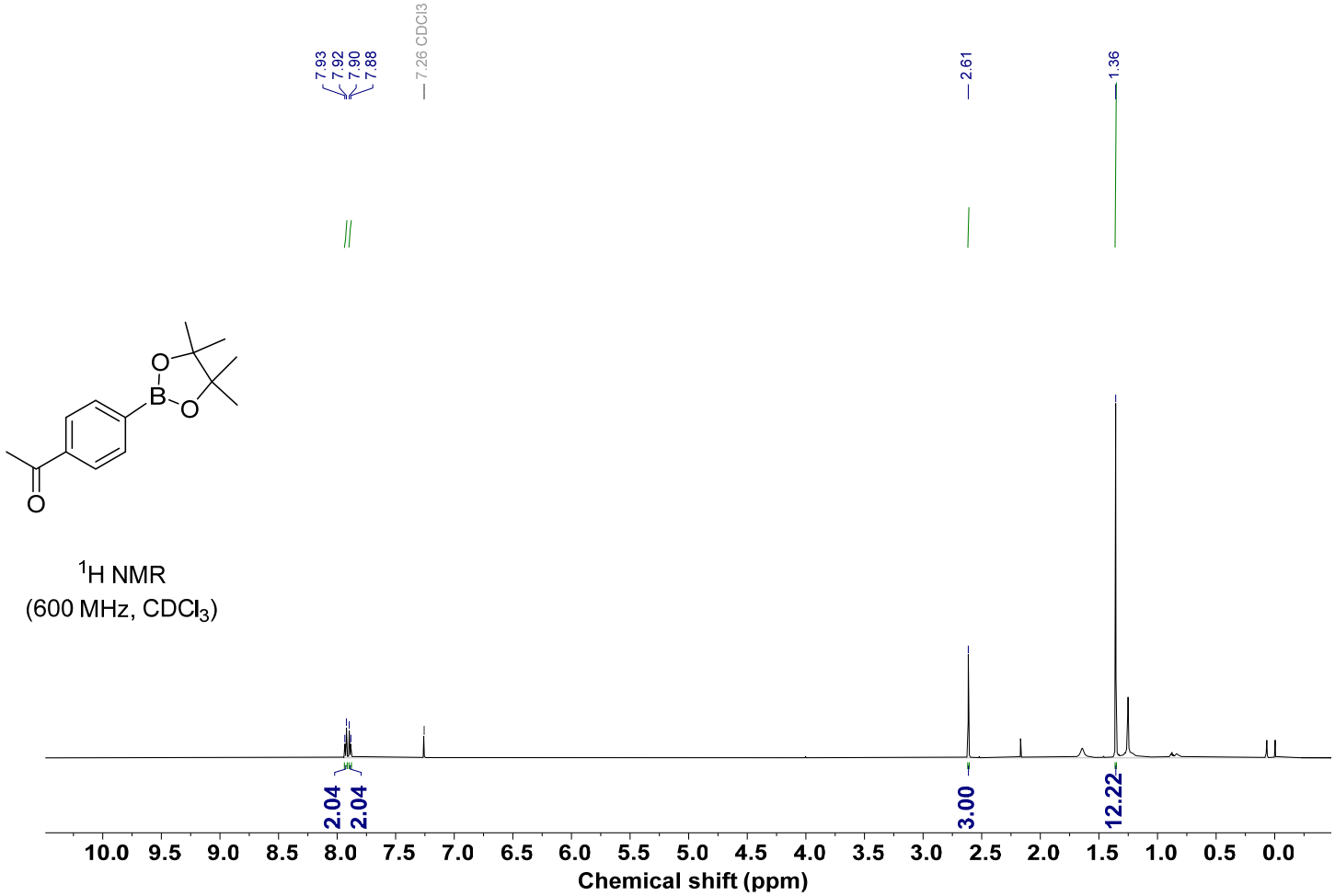

Supplementary Fig. 64 ^{1}H NMR (600 MHz, $CDCl_3$) spectrum of 1-(4-(4,4,5,5-tetramethyl-1,3,2-dioxaborolan-2-yl)phenyl)ethan-1-one.

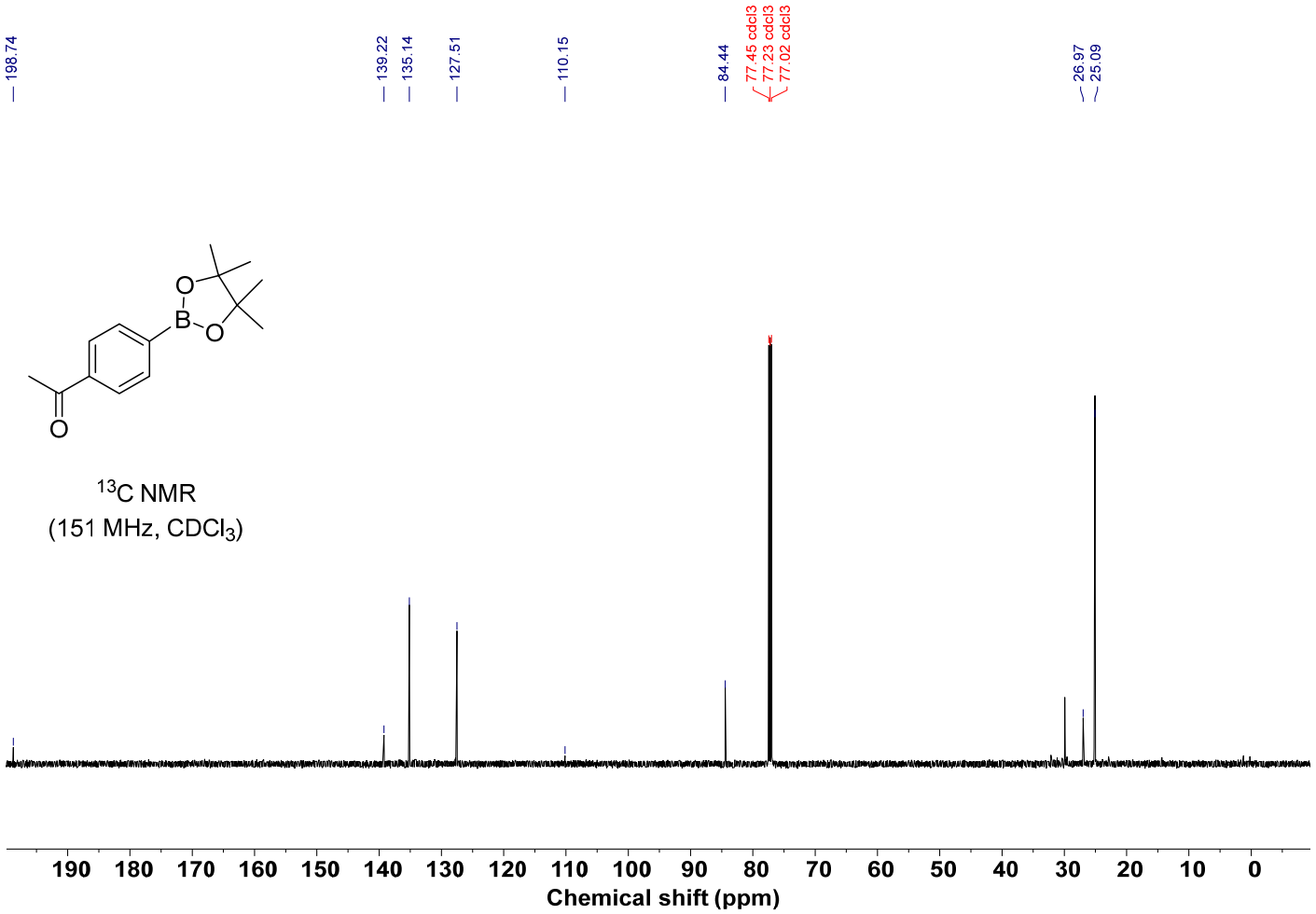

Supplementary Fig. 65 $^{13}C\{^{1}H\}$ NMR (151 MHz, $CDCl_3$) spectrum of 1-(4-(4,4,5,5-tetramethyl-1,3,2-dioxaborolan-2-yl)phenyl)ethan-1-one.

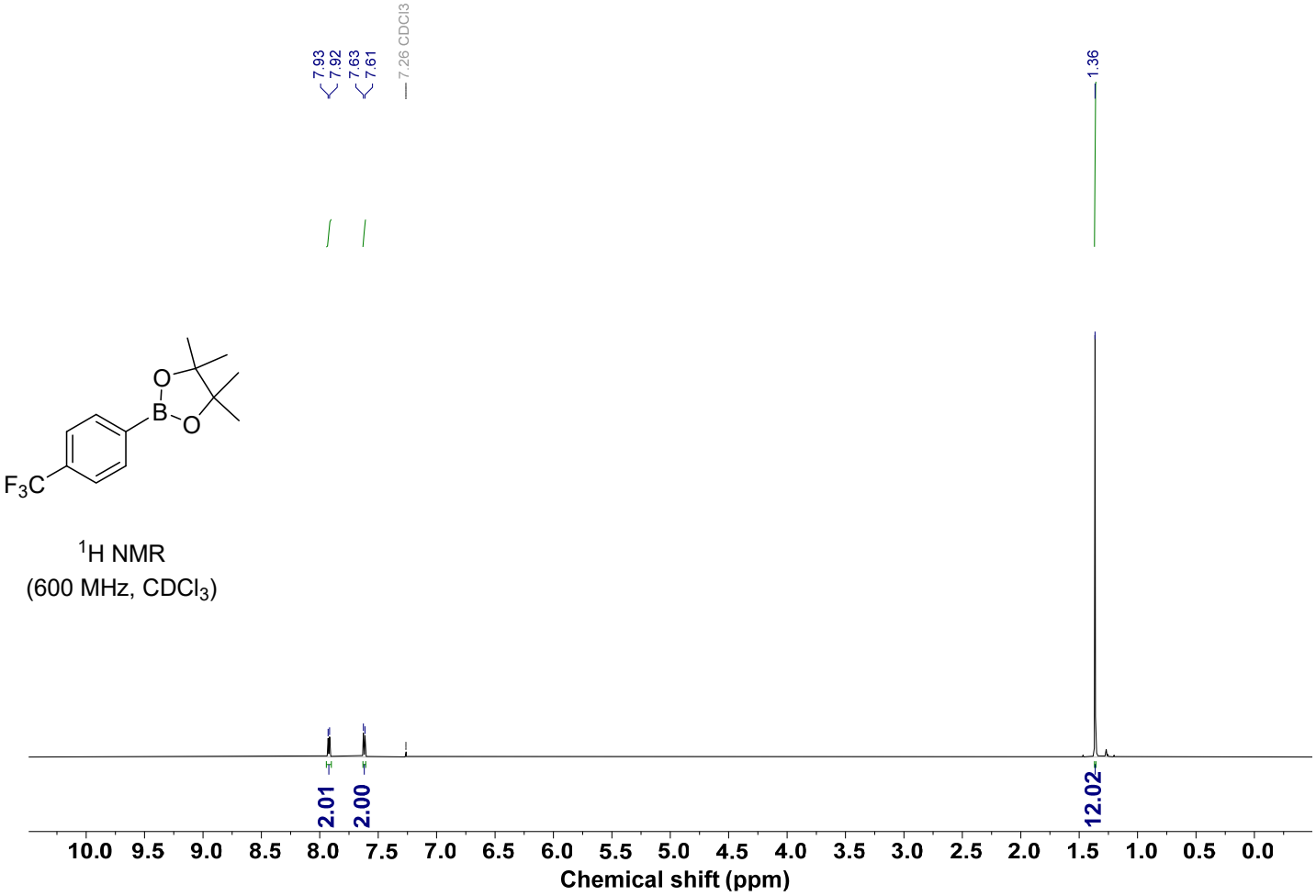

Supplementary Fig. 66 ^{1}H NMR (600 MHz, $CDCl_3$) spectrum of 4,4,5,5,-tetramethyl-2-(4-(trifluoromethyl)phenyl)-1,3,2-dioxaborolane.

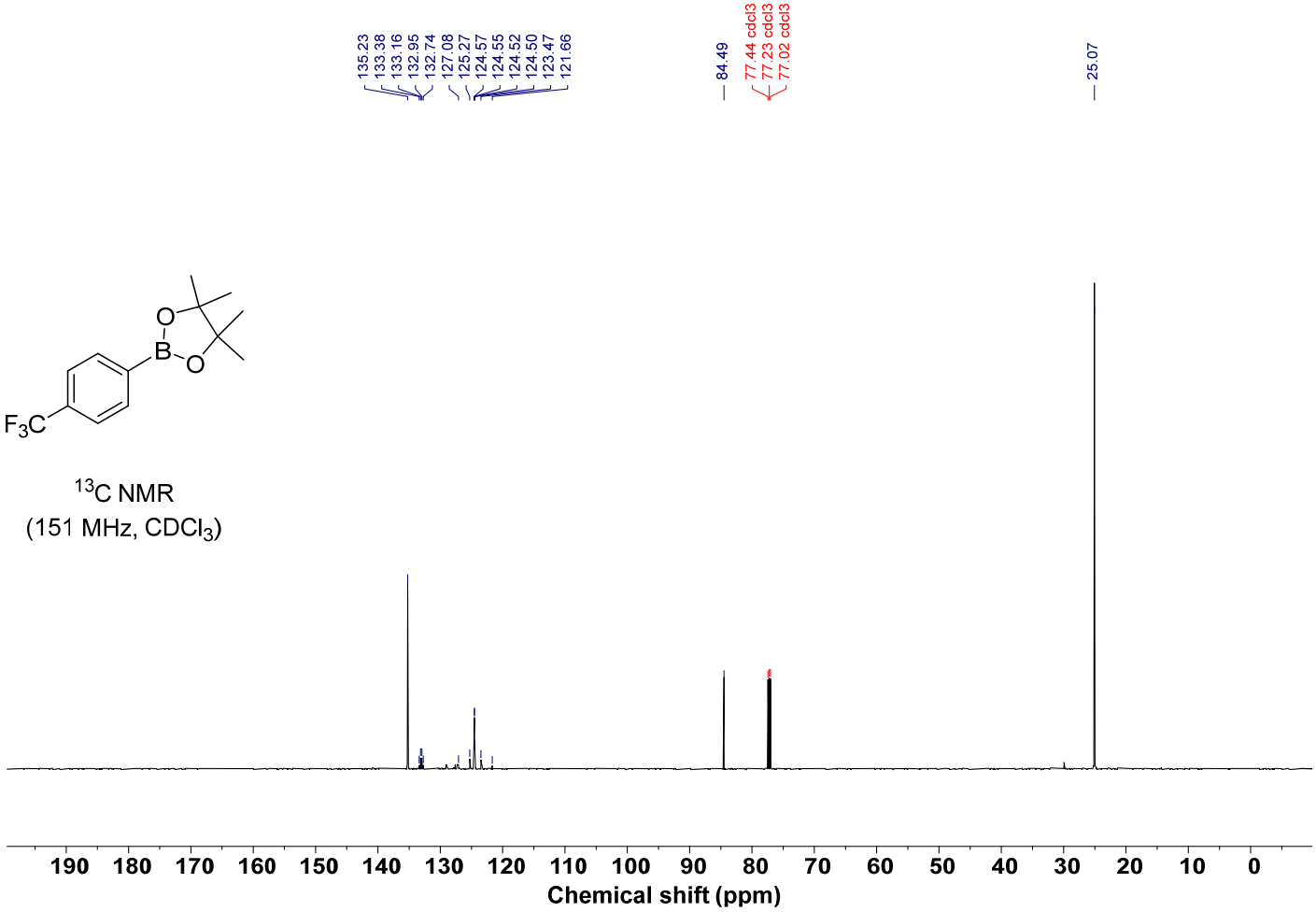

Supplementary Fig. 67 $^{13}C\{^{1}H\}$ NMR (151 MHz, $CDCl_3$) spectrum of 4,4,5,5,-tetramethyl-2-(4-(trifluoromethyl)phenyl)-1,3,2-dioxaborolane.

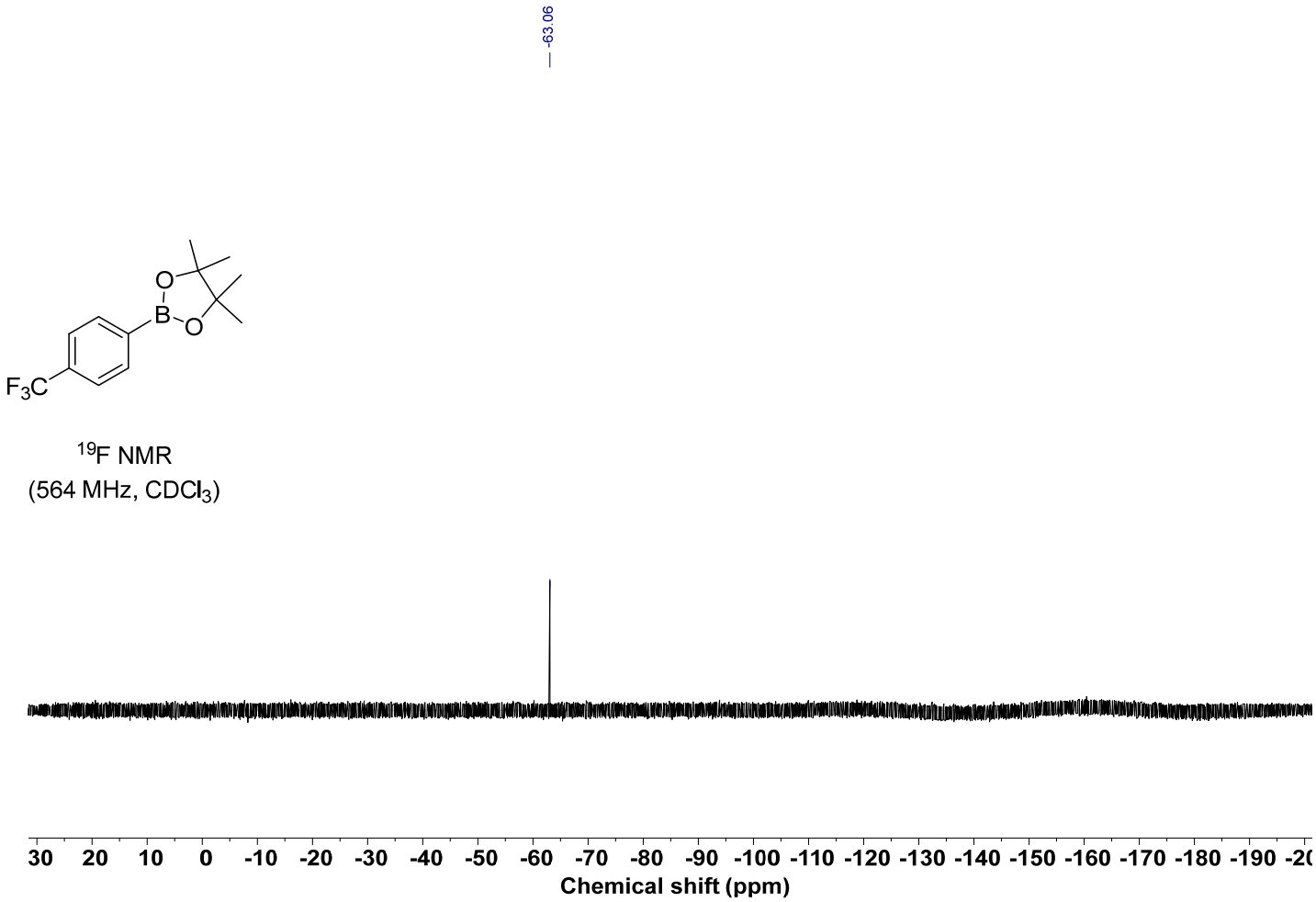

Supplementary Fig. 68 $^{19}F\{^{1}H\}$ NMR (564 MHz, $CDCl_3$) spectrum of 4,4,5,5,-tetramethyl-2-(4-(trifluoromethyl)phenyl)-1,3,2-dioxaborolane.

References

1 Heo, S., Jhun, B. H., Woo, S., Kim, H. S., Kim, I., Kim, J., Son, W. J., Jung, Y., Kim, K. & Cho, J. Improving Electroluminescence of Two-Coordinate Au (I) Complexes: Insights into Steric and Electronic Control. *Adv. Opt. Mater.*, 2302148 (2023).

2 Heinrich, G., Schoof, S. & Gusten, H. 9, 10-diphenylanthracene as a fluorescence quantum yield standard. *J. Photochem.* **3**, 315-320 (1974).

3 Kim, S., Park, G., Cho, E. J. & You, Y. Coreactant strategy for the photoredox catalytic generation of trifluoromethyl radicals under low-energy photoirradiation. *J. Org. Chem.* **81**, 7072-7079 (2016).

4 Shen, T., Zhao, Z.-G., Yu, Q. & Xu, H.-J. Photosensitized reduction of benzil by heteroatom-containing anthracene dyes. *J. Photochem. Photobiol. A.* **47**, 203-212 (1989).

5 Yasui, S., Tsujimoto, M., Itoh, K. & Ohno, A. Quenching of a photosensitized dye through single-electron transfer from trivalent phosphorus compounds. *J. Org. Chem.* **65**, 4715-4720 (2000).

6 Speckmeier, E., Fischer, T. G. & Zeitler, K. A toolbox approach to construct broadly applicable metal-free catalysts for photoredox chemistry: deliberate tuning of redox potentials and importance of halogens in donor–acceptor cyanoarenes. *J. Am. Chem. Soc.* **140**, 15353-15365 (2018).

7 Rillema, D. P., Allen, G., Meyer, T. & Conrad, D. Redox properties of ruthenium (II) tris chelate complexes containing the ligands 2, 2'-bipyrazine, 2, 2'-bipyridine, and 2, 2'-bipyrimidine. *Inorg. Chem.* **22**, 1617-1622 (1983).

8 Crutchley, R. & Lever, A. Ruthenium (II) tris (bipyrazyl) dication-a new photocatalyst. *J. Am. Chem. Soc.* **102**, 7128-7129 (1980).

9 Juris, A., Balzani, V., Belser, P. & von Zelewsky, A. Characterization of the excited state properties of some new photosensitizers of the ruthenium (polypyridine) family. *Helv. Chim. Acta* **64**, 2175-2182 (1981).

10 Young, R. C., Meyer, T. J. & Whitten, D. G. Electron transfer quenching of excited states of metal complexes. *J. Am. Chem. Soc.* **98**, 286-287 (1976).

11 Slinker, J. D., Gorodetsky, A. A., Lowry, M. S., Wang, J., Parker, S., Rohl, R., Bernhard, S. & Malliaras, G. G. Efficient yellow electroluminescence from a single layer of a cyclometalated iridium complex. *J. Am. Chem. Soc.* **126**, 2763-2767 (2004).

12 Kern, J.-M. & Sauvage, J.-P. Photoassisted C–C coupling via electron transfer to benzylic halides by a bis (di-imine) copper (I) complex. *Journal of the Chemical Society, Chemical Communications*, 546-548 (1987).

13 Flamigni, L., Barbieri, A., Sabatini, C., Ventura, B. & Barigelletti, F. Photochemistry and photophysics of coordination compounds: iridium. *Topics in Current Chemistry* **281**, 143-203

(2007).

14 Fukuzumi, S., Kotani, H., Ohkubo, K., Ogo, S., Tkachenko, N. V. & Lemmetyinen, H. Electron-transfer state of 9-mesityl-10-methylacridinium ion with a much longer lifetime and higher energy than that of the natural photosynthetic reaction center. *J. Am. Chem. Soc.* **126**, 1600-1601 (2004).

15 Xiang, M., Xin, Z.-K., Chen, B., Tung, C.-H. & Wu, L.-Z. Exploring the reducing ability of organic dye (Acr+-Mes) for fluorination and oxidation of benzylic C (sp3)–H bonds under visible light irradiation. *Org. Lett.* **19**, 3009-3012 (2017).

16 Sinha, N., Wegeberg, C., Häussinger, D., Prescimone, A. & Wenger, O. S. Photoredox-active Cr (0) luminophores featuring photophysical properties competitive with Ru (II) and Os (II) complexes. *Nat. Chem.*, 1-7 (2023).

17 Guo, X., Okamoto, Y., Schreier, M. R., Ward, T. R. & Wenger, O. S. Enantioselective synthesis of amines by combining photoredox and enzymatic catalysis in a cyclic reaction network. *Chem. Sci.* **9**, 5052-5056 (2018).

18 Pfund, B. r., Steffen, D. M., Schreier, M. R., Bertrams, M.-S., Ye, C., Börjesson, K., Wenger, O. S. & Kerzig, C. UV light generation and challenging photoreactions enabled by upconversion in water. *J. Am. Chem. Soc.* **142**, 10468-10476 (2020).

19 Lamansky, S., Djurovich, P., Murphy, D., Abdel-Razzaq, F., Kwong, R., Tsyba, I., Bortz, M., Mui, B., Bau, R. & Thompson, M. E. Synthesis and characterization of phosphorescent cyclometalated iridium complexes. *Inorg. Chem.* **40**, 1704-1711 (2001).

20 Radwan, Y. K., Maity, A. & Teets, T. S. Manipulating the excited states of cyclometalated iridium complexes with β-ketoiminate and β-diketiminate ligands. *Inorg. Chem.* **54**, 7122-7131 (2015).

21 Shon, J.-H. & Teets, T. S. Potent bis-cyclometalated iridium photoreductants with β-diketiminate ancillary ligands. *Inorg. Chem.* **56**, 15295-15303 (2017).

22 Shon, J.-H., Kim, D., Rathnayake, M. D., Sittel, S., Weaver, J. & Teets, T. S. Photoredox catalysis on unactivated substrates with strongly reducing iridium photosensitizers. *Chem. Sci.* **12**, 4069-4078 (2021).

23 Shon, J.-H., Kim, D., Gray, T. G. & Teets, T. S. β-Diketiminate-supported iridium photosensitizers with increased excited-state reducing power. *Inorg. Chem. Front.* **8**, 3253-3265 (2021).

24 Li, K., Wan, Q., Yang, C., Chang, X. Y., Low, K. H. & Che, C. M. Air-Stable Blue Phosphorescent Tetradentate Platinum (II) Complexes as Strong Photo-Reductant. *Angew. Chem., Int. Ed.* **57**, 14129 (2018).

25 Choi, W. J., Choi, S., Ohkubo, K., Fukuzumi, S., Cho, E. J. & You, Y. Mechanisms and applications of cyclometalated Pt (II) complexes in photoredox catalytic trifluoromethylation. *Chem. Sci.* **6**, 1454-1464 (2015).

26 Minozzi, C., Caron, A., Grenier-Petel, J. C., Santandrea, J. & Collins, S. K. Heteroleptic Copper (I)-Based Complexes for Photocatalysis: Combinatorial Assembly, Discovery, and Optimization. *Angew. Chem., Int. Ed.* **57**, 5477-5481 (2018).

27 Büldt, L. A., Guo, X., Prescimone, A. & Wenger, O. S. A Molybdenum (0) Isocyanide Analogue of Ru (2, 2′-Bipyridine) 32+: A Strong Reductant for Photoredox Catalysis. *Angew. Chem., Int. Ed.* **55**, 11247-11250 (2016).

28 Herr, P., Glaser, F., Büldt, L. A., Larsen, C. B. & Wenger, O. S. Long-lived, strongly emissive, and highly reducing excited states in Mo (0) complexes with chelating isocyanides. *J. Am. Chem. Soc.* **141**, 14394-14402 (2019).

29 Yin, H., Carroll, P. J., Manor, B. C., Anna, J. M. & Schelter, E. J. Cerium photosensitizers: structure–function relationships and applications in photocatalytic aryl coupling reactions. *J. Am. Chem. Soc.* **138**, 5984-5993 (2016).

30 Qiao, Y., Cheisson, T., Manor, B. C., Carroll, P. J. & Schelter, E. J. A strategy to improve the performance of cerium (III) photocatalysts. *Chem. Commun.* **55**, 4067-4070 (2019).

31 Muniz, C. N., Archer, C. A., Applebaum, J. S., Alagaratnam, A., Schaab, J., Djurovich, P. I. & Thompson, M. E. Two-Coordinate Coinage Metal Complexes as Solar Photosensitizers. *J. Am. Chem. Soc.* (2023).

32 MacKenzie, I. A., Wang, L., Onuska, N. P., Williams, O. F., Begam, K., Moran, A. M., Dunietz, B. D. & Nicewicz, D. A. Discovery and characterization of an acridine radical photoreductant. *Nature* **580**, 76-80 (2020).

33 Louvel, D., Chelagha, A., Rouillon, J., Payard, P. A., Khrouz, L., Monnereau, C. & Tlili, A. Metal-Free Visible-Light Synthesis of Arylsulfonyl Fluorides: Scope and Mechanism. *Chem. –Eur. J.* **27**, 8704-8708 (2021).

34 Tlili, A. & Lakhdar, S. Acridinium salts and cyanoarenes as powerful photocatalysts: opportunities in organic synthesis. *Angew. Chem., Int. Ed.* **60**, 19526-19549 (2021).

35 Mateos, J., Rigodanza, F., Vega-Peñaloza, A., Sartorel, A., Natali, M., Bortolato, T., Pelosi, G., Companyó, X., Bonchio, M. & Dell'Amico, L. Naphthochromenones: organic bimodal photocatalysts engaging in both oxidative and reductive quenching processes. *Angew. Chem., Int. Ed.* **59**, 1302-1312 (2020).

36 Mei, L., Veleta, J. M. & Gianetti, T. L. Helical carbenium ion: A versatile organic photoredox catalyst for red-light-mediated reactions. *J. Am. Chem. Soc.* **142**, 12056-12061 (2020).

37 de Souza, A. A., Silva, N. S., Müller, A. V., Polo, A. S., Brocksom, T. J. & de Oliveira, K. T. Porphyrins as photoredox catalysts in Csp2–H arylations: batch and continuous flow approaches. *J. Org. Chem.* **83**, 15077-15086 (2018).

38 Mandal, T., Das, S. & De Sarkar, S. Nickel (II) Tetraphenylporphyrin as an efficient photocatalyst featuring visible light promoted dual redox activities. *Adv. Synth. Cat.* **361**, 3200-3209 (2019).

39 Zhao, Y., Gong, H., Jiang, K., Yan, S., Lin, J. & Chen, M. Organocatalyzed photoredox polymerization from aromatic sulfonyl halides: Facilitating graft from aromatic C–H bonds. *Macromolecules* **51**, 938-946 (2018).

40 Liu, D., Jiao, M.-J., Feng, Z.-T., Wang, X.-Z., Xu, G.-Q. & Xu, P.-F. Design, synthesis, and application of highly reducing organic visible-light photocatalysts. *Org. Lett.* **20**, 5700-5704 (2018).

41 Zidan, M., Rohe, S., McCallum, T. & Barriault, L. Recent advances in mono and binuclear gold photoredox catalysis. *Cat. Sci. Tech.* **8**, 6019-6028 (2018).

42 Srivastava, V., Singh, P. K. & Singh, P. P. Recent advances of visible-light photocatalysis in the functionalization of organic compounds. *J. Photochem. Photobiol. C: Photochem. Rev.* **50**, 100488 (2022).

43 Luo, J. & Zhang, J. Donor–Acceptor Fluorophores for Visible-Light-Promoted Organic Synthesis: Photoredox/Ni Dual Catalytic $C(sp^3)$–$C(sp^2)$ Cross-Coupling. *ACS Catal.* **6**, 873-877 (2016).

44 Ishimatsu, R., Matsunami, S., Kasahara, T., Mizuno, J., Edura, T., Adachi, C. Nakano, K. & Imato, T. Electrogenerated Chemiluminescence of Donor–Acceptor Molecules with Thermally Activated Delayed Fluorescence. *Angew. Chem., Int. Ed.* **53**, 6993-6996 (2014).

45 Tilby, M. J., Dewez, D. F., Pantaine, L. R. E., Hall, A., Martinez-Lamenca, C. & Willis, M. C. Photocatalytic Late-Stage Functionalization of Sulfonamides via Sulfonyl Radical Intermediates. *ACS Catal.* **12**, 6060-6067 (2022).

46 Prentice, C., Morrison, J., Smith, A. D. & Zysman-Colman, E. Multi-Resonant Thermally Activated Delayed Fluorescent (MR-TADF) Compounds as Photocatalysts. *Chem. -Eur. J.* **29**, e202202998 (2023).

47 Bryden. M. A., Milward, F., Matulaitis, T., Chen, D., Villa, M., Fermi, A., Cetin, S., Ceroni, P. & Zysman-Colman, E. Moving Beyond Cyanoarene Thermally Activated Delayed Fluorescence Compounds as Photocatalysts: An Assessment of the Performance of a Pyrimidyl Sulfone Photocatalyst in Comparison to 4CzIPN. *J. Org. Chem.* **88**, 6364-6373 (2023).

48 Bortolato, T., Dyguda, M., Vega-Peñaloza, A. & Dell'Amico, L. Properties and Synthetic Performances of Phenylamino Cyanoarenes under One-Photon Excitation Manifolds. *Synthesis* **54**, 3409-3413 (2022).

49 Sharma, S. & Sengupta, S. Twisted Organic TADF Triads Based on a Diindolocarbazole Donor for Efficient Photoisomerization of Stilbene and Photo-Arylation of Heteroarenes. *Org. Chem. Front.* **10**, 6087-6095 (2023).

50 Aranzaes, J. R., Daniel, M.-C. & Astruc, D. Metallocenes as references for the determination of

redox potentials by cyclic voltammetry Permethylated iron and cobalt sandwich complexes, inhibition by polyamine dendrimers, and the role of hydroxy-containing ferrocenes. *Can. J. Chem.* **84**, 288-299 (2006).

51 Charboneau, D. J., Huang, H., Barth, E. L., Germe, C. C., Hazari, N., Mercado, B. Q., Uehling, M. R. & Zultanski, S. L. Tunable and practical homogeneous organic reductants for cross-electrophile coupling. *J. Am. Chem. Soc.* **143**, 21024-21036 (2021).

52 Charboneau, D. J., Hazari, N., Huang, H., Uehling, M. R. & Zultanski, S. L. Homogeneous organic electron donors in nickel-catalyzed reductive transformations. *J. Org. Chem.* **87**, 7589-7609 (2022).

53 Connelly, N. G. & Geiger, W. E. Chemical redox agents for organometallic chemistry. *Chem. Rev.* **96**, 877-910 (1996).

54 Horsewill, S. J., Hierlmeier, G., Farasat, Z., Barham, J. P., Scott, D. J. Shining Fresh Light on Complex Photoredox Mechanisms through Isolation of Intermediate Radical Anions. *ACS Catal.* **13**, 9392-9403 (2023).